Geo-Bio Interfaces (2025), **2**, e6, 1–31
doi:10.1180/gbi.2024.9

CAMBRIDGE UNIVERSITY PRESS

Review

Biogenic pyrite and metastable iron sulfides: Emerging formation pathways and geological and societal relevance

Muammar Mansor[1], Arnaud Duverger[2], Virgil Pasquier[3], Aurore Gorlas[4], François Guyot[2,5], Jasmine S. Berg[3], Johanna Marin-Carbonne[3], Julie Cosmidis[6] and Aude Picard[7]

[1]Geomicrobiology, Department of Geosciences, University of Tuebingen, Tübingen, Germany; [2]Sorbonne Université, Muséum National d'Histoire Naturelle, UMR CNRS 7590, Institut de Minéralogie, de Physique des Matériaux et de Cosmochimie (IMPMC), Paris, France; [3]Faculty of Geosciences and Environment, Université de Lausanne, Switzerland; [4]Institute for Integrative Biology of the Cell (I2BC), Université Paris-Saclay, CEA, CNRS, 91198 Gif-sur-Yvette, France; [5]Institut Universitaire de France (IUF), Paris, France; [6]Department of Earth Sciences, University of Oxford, South Parks Road, Oxford OX1 3AN, UK and [7]School of Life Sciences, University of Nevada, Las Vegas, NV, United States

Abstract

Iron sulfide (Fe-S) minerals such as mackinawite (FeS), greigite (Fe_3S_4) and pyrite (FeS_2) are widespread on Earth, where their formation and dissolution are strongly linked to the biogeochemical cycles of iron, sulfur, carbon, oxygen, nutrients and trace metals. Recent studies have shed light on how microorganisms mediate their formation, with breakthroughs linked to biogenic pyrite. In this review, we highlight the formation pathways of Fe-S minerals, starting with the increasingly recognized roles of Fe(III) and intermediate sulfur species (*e.g.* S^0 and polysulfides) during the initial steps. The mechanisms by which microorganisms affect Fe-S mineral formation are compiled and discussed for low (25–35°C) and high (≥ 80°C) temperatures, with specific examples from experimental studies. The morphology and precipitation rates obtained from experiments are compared to natural environments, and their similarities and differences are critically discussed. We then review the current state of the art for Fe-S minerals in the context of the origin of life and as environmental proxies and biosignatures in the geological record using their texture and chemical and isotopic compositions. We end by highlighting the importance of Fe-S minerals for current societal issues, such as the sequestration of organic carbon, the formation of acid drainages, metal recovery and nitrate removal, and their potential use as technological bio-materials in the future.

Keywords: biogenic pyrite; mackinawite; greigite; societal impacts; environmental proxies

(Received 05 August 2024; revised 09 October 2024; manuscript accepted: 04 November 2024)

Introduction

Sedimentary iron sulfide (Fe-S) minerals constitute the most abundant type of sulfide minerals at the surface of the Earth (Fig. 1). Most sulfide in Fe-S minerals originates from a biological process: microbial sulfate reduction (MSR) (Rickard *et al.*, 2017). The most stable of Fe-S minerals, pyrite (FeS_2), is the focus of this review. We also consider the metastable phases, such as mackinawite (FeS) and greigite (Fe_3S_4), as their importance is being increasingly revealed. Fe-S mineral formation was likely widespread on early Earth due to the early onset of MSR, the availability of Fe, mostly in its reduced form, and the absence of oxygen in the atmosphere (Rickard *et al.*, 2017). Although anoxic environments have retreated to subsurface environments after the rise of oxygen in the atmosphere, the formation of Fe-S minerals in sediments is significant for the global geochemical cycles of sulfur, iron, carbon and other nutrients and trace metals. The burial of Fe-S minerals, together with organic carbon, controls the oxygenation of the atmosphere on geological timescales (Berner, 1989; Berner and Raiswell, 1983; Rickard, 2012a).

In modern low-temperature, anoxic environments, interactions involving microorganisms and Fe-S minerals are common. While Fe-S mineral formation pathways have been extensively studied in abiotic conditions (Rickard, 2012b; Rickard 2012c), the impact of microorganisms on the properties of Fe-S minerals is still relatively poorly characterized, and the emphasis is often on controlled intracellular precipitation of Fe-sulfides in magnetotactic bacteria (MTB) (Pósfai and Dunin-Borkowski, 2006; Picard *et al.*, 2016; Park and Faivre, 2022). However, advances in analytical methods have allowed a better understanding of the interplays between biogeochemical cycles; for example, with the description of cryptic cycles (*e.g.* Canfield *et al.*, 2010; Holmkvist *et al.*, 2011). Additionally, well-constrained experimental studies in recent years have allowed significant progress in deciphering biological from abiotic controls on the formation of Fe-S minerals, notably on mackinawite, greigite and pyrite formation.

Corresponding authors: Muammar Mansor and Aude Picard; Emails: muammar.mansor@uni-tuebingen.de; audeamelie.picard@unlv.edu

Cite this article: Mansor M., Duverger A., Pasquier V., Gorlas A., Guyot F., Berg J.S., Marin-Carbonne J., Cosmidis J., & Picard A. (2025). Biogenic pyrite and metastable iron sulfides: Emerging formation pathways and geological and societal relevance. *Geo-Bio Interfaces* **2**, e6, 1–31. https://doi.org/10.1180/gbi.2024.9

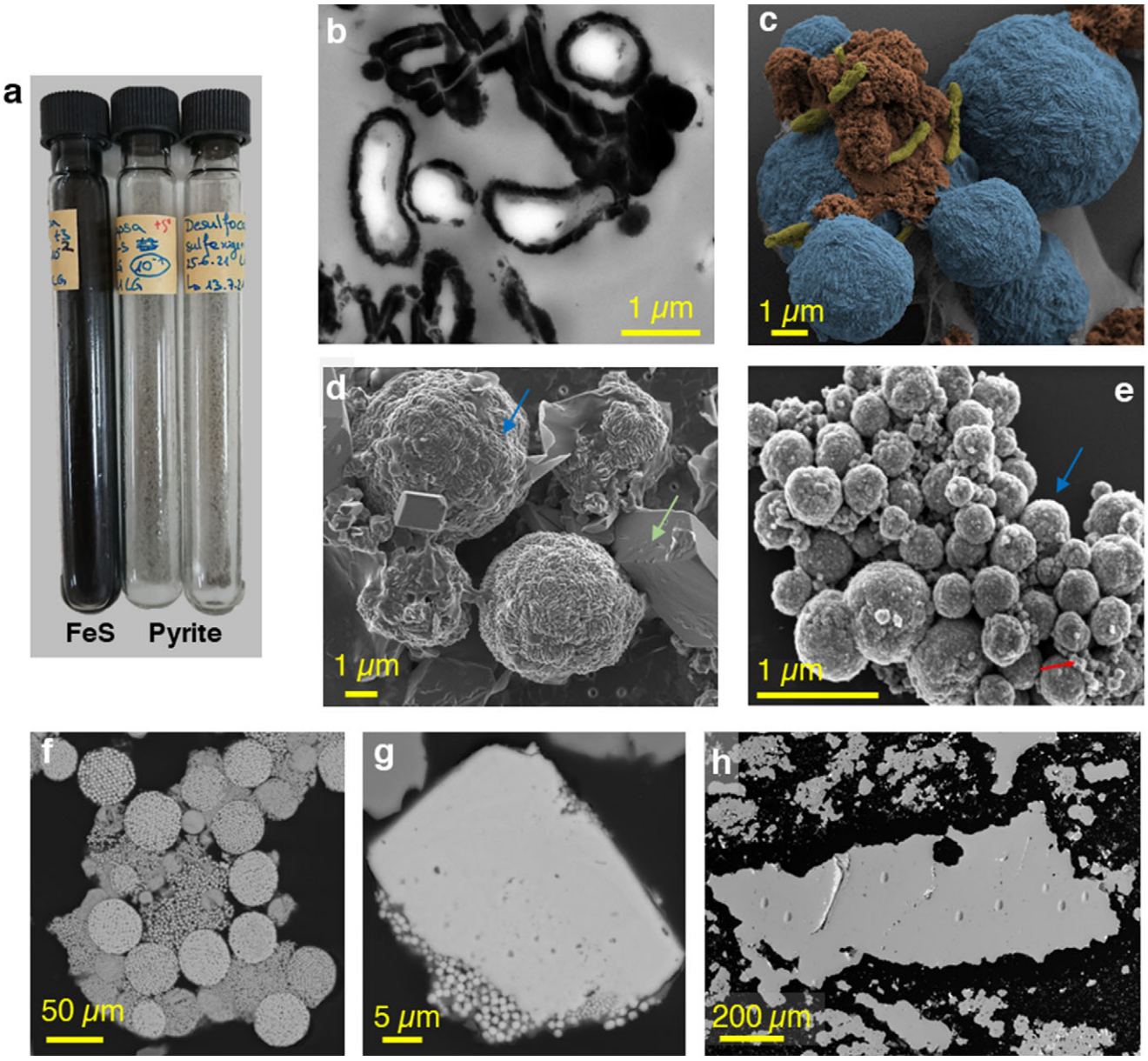

Figure 1. Images of iron sulfide minerals produced experimentally or naturally, representative of common sedimentary sulfides on Earth: (a) Characteristic colours of biogenic Fe sulfides formed in microbial cultures. Mackinawite (FeS) and greigite (Fe_3S_4) tend to form fine black nanoparticles. Initially-formed pyrite can also be black but transforms over time to dense shiny grey particles with increasing crystallinity and size; (b) sulfate-reducing bacteria encrusted in mackinawite, imaged using transmission electron microscopy; (c) false-colour image of pyrite spherules (blue) associated with cells of *Desulfocapsa sulfexigens* (yellow) and residual Fe(III) (oxyhydr)oxides or other Fe sulfides (orange); (d) pyrite spherules (blue arrow) formed together with euhedral vivianite (green arrow) in sulfur/sulfate-reducing enrichment cultures from Lake Pavin; (e) a cluster of pyrite spherules (blue arrow) together with greigite nanocrystals (red arrow) produced by the hyperthermophilic archaeon *Thermococcus prieurii* isolated from hydrothermal deep-sea vents; (f) diversity of the size and shape of pyrite framboids associated with smaller nanocrystals found in the modern Gulf of Lion (PRGL 1-4 borehole); (g) nanocrystals of pyrite in the process of recrystallizing to form a larger euhedral crystal in shelf sediments of the Gulf of Lion (PRGL 1-4 borehole); and (h) recrystallization with time and burial eventually leads to larger-sized euhedral pyrite commonly observed in the geological record, such as in the Mendon sedimentary Formation (3.2 Ga, South Africa). Pittings on the grain originate from in situ spot analysis such as secondary ion mass spectrometry. Images c-h were obtained using scanning electron microscopy.

This review first inventories the sources of Fe and S available for Fe-S mineral formation in natural environments, before delving into the most recent knowledge on how microorganisms affect Fe-S mineral formation, and how Fe-S minerals might have played a role in the origin of life. It is intended to update the recent review by Picard *et al.* (2016) and focuses on extracellular Fe-S mineral formation as a biologically induced mineralization process (Pósfai and Dunin-Borkowski, 2006). For a comprehensive overview of the chemistry of Fe-S minerals, the reader is referred to the book by Rickard (2012a,b,c) and the references contained therein. Furthermore, an excellent layman's introduction to the history of pyrite is available in Rickard (2015). In this review, we focus on linking new knowledge from experimental studies to natural environments, with an emphasis on pyrite, which helps reconstruct ancient environments and could also record the involvement of microbial life in early biogeochemical cycles. Finally, we discuss the societal impacts of Fe-S minerals, such as the importance of Fe-S minerals for the sequestration of organic carbon in anoxic

https://doi.org/10.1180/gbi.2024.9 Published online by Cambridge University Press

environments, the reactivity and stability of Fe-S minerals in (sub)oxic environments and the formation of acid drainages and the potential production of biogenic Fe-S minerals for future industrial applications.

Sources of Fe and S for the formation of iron sulfides

Sources of iron

Iron (Fe) and sulfur (S) are the 4th and 16th most abundant elements in the Earth's crust, respectively. Iron is cycled between its 2+ and 3 + redox states by various abiotic and biotic processes (Kappler *et al.*, 2021). Fe-S mineral formation requires Fe(II), which can come from multiple sources. Direct sources of Fe^{2+} originate from reduced water bodies such as groundwaters, porewaters and hydrothermal vents, as well as from the dissolution of Fe(II)-containing minerals such as siderite ($FeCO_3$), vivianite ($Fe_3(PO_4)_2{\cdot}8H_2O$) and mackinawite (FeS). The reaction between dissolved Fe^{2+} and sulfide (S(-II); the sum of H_2S and HS^-) in microbial cultures typically results in the precipitation of mackinawite without further transformation to pyrite (Picard *et al.*, 2016). Therefore, recent studies on biogenic pyrite formation have shifted focus onto indirect sources of Fe(II) coming from microbial or abiotic reduction of Fe(III)-bearing minerals such as Fe(III) (oxyhydr)oxides, silicates and phosphates, which also produce intermediate sulfur species in the system.

Iron(III) (oxyhydr)oxides such as ferrihydrite ($Fe(OH)_3$), lepidocrocite (γ-FeOOH), goethite (α-FeOOH) and hematite (Fe_2O_3) are common constituents of soils and sediments worldwide (Table 1). In marine sediments and soils that have 3–4 wt.% Fe on average, 20–50% of the Fe exists as Fe(III) (oxyhydr)oxides that are soluble in oxalate, dithionite and/or HCl (Canfield, 1997; Raiswell and Canfield, 1998; Johnson *et al.*, 2020; Pasquier *et al.*, 2022). These minerals exist in various sizes, shapes and crystallinities, which affect their surface areas and reactivity towards sulfide (Poulton *et al.*, 2004b). This in turn affects the supply rate of Fe(II) and the amount of residual reactive surfaces that enable interfacial reactions for pyrite formation (Peiffer *et al.*, 2015; Wan *et al.*, 2017; Hockmann *et al.*, 2020). For example, while ferrihydrite is highly reactive towards sulfide, its surfaces may be dissolved or coated too quickly by FeS or other minerals for pyritization to occur. By contrast, a less reactive mineral such as hematite may react too slowly with sulfide for pyritization to occur at an appreciable rate.

Clays are the most abundant mineral host of Fe in nature, making up around 40–50% of total Fe in marine sediments (Raiswell and Canfield, 1998). Iron-bearing clays are thought to be poorly reactive towards sulfide, with slow pyritization possible but occurring in the timescale of hundreds to thousands of years (Raiswell and Canfield, 1996). This view is, however, slowly changing. Layered clay minerals such as illite, smectite and kaolinite contain Fe(III) in either structural, basal or edge sites with different reactivities (Fan *et al.*, 2023). Some of these Fe(III) are reducible by sulfide produced by sulfate-reducing microorganisms (SRM) within a timescale of days (Li *et al.*, 2004; Liu *et al.*, 2012), making them potentially relevant for rapid pyrite formation (Pasquier *et al.*, 2022). The Fe-S minerals produced from these experiments are poorly characterized. Empirical observations have always noted close associations between diagenetic pyrite (including framboids) and clays (Canfield *et al.*, 1992; Marin-Carbonne *et al.*, 2022; Sanz-Montero *et al.*, 2009; Wang *et al.*, 2020). It is possible that pore spaces with low diffusivity

Table 1. Iron-bearing minerals and their reactivity towards sulfide.

Mineral	Description	Specific surface area (m^2/g)	Half-life in the presence of 1 mM sulfide at pH 7.5
Ferrihydrite $Fe(OH)_3$	First product of Fe^{2+} oxidation, difficult to detect by XRD due to poor crystallinity, occurs as < 5 nm spheroids but easily forms larger aggregates. Colour: dark brown	>150	5 min–12 hr
Lepidocrocite γ-FeOOH	Forms via Fe^{2+} oxidation or Fe(II)-catalysed recrystallization of ferrihydrite, nanosized to larger-sized, laths-shaped. Colour: orange-yellow	15	< 3 days
Goethite α-FeOOH	Forms via ageing of ferrihydrite at alkaline pH or via Fe(II)-catalysed recrystallization of ferrihydrite or lepidocrocite, nanosized to larger-sized, spheroidal to acicular-shaped. Colour: yellow	9–170	12–63 days
Hematite α-Fe_2O_3	Sourced from weathering of parent rock or slow ageing of other Fe(III) (oxyhydr) oxides at ambient temperature. Ageing/ dehydration is accelerated at higher temperatures or higher salinity. Colour: red	2–90	31–182 days
Magnetite Fe_3O_4	Products of extracellular Fe(II)-catalysed recrystallization of ferrihydrite, leading to ~10 nm sized spheroidal magnetite, especially in the presence of Fe(III) reducing microorganisms. Intracellular formation by magnetotactic bacteria leads to <35–120 nm bullet/ tooth/prismatic/ octahedral-shaped particles. Size and shape vary depending on	4–70	72 days (synthetic magnetite) to 105 years (sedimentary magnetite)

(*Continued*)

https://doi.org/10.1180/gbi.2024.9 Published online by Cambridge University Press

Table 1. (*Continued*)

Mineral	Description	Specific surface area (m^2/g)	Half-life in the presence of 1 mM sulfide at pH 7.5
	environmental parameters and microbial species. Colour: black		
Fe-clays	Most abundant solid-phase host of Fe, but thought to be less reactive than other minerals. Layered sheet structure. Colour: brown	65–100 (Illite)	230 years ('reactive' silicates) to 84,000 years (sheet silicates) to days in experiments with SRM
Vivianite $Fe_3(PO_4)_2 \cdot 8H_2O$	Forms micron-sized radiating blades structure in Fe(III) reduction zones when Fe^{2+} and bound P are released from Fe(III) (oxyhydr) oxides. Colour: colourless to white blue	6–40	Slow? Stable under sulfidic conditions in microbial experiments
Ferric phosphate $FePO_4.xH_2O$	Found in ferruginous lakes and estuarine sediments, nanosized precipitates when Fe^{3+} and phosphate are mixed. Colour: white to brown	1–60	Days in experiments with SRM

Information compiled from:
Fe(III) (oxyhydr)oxides: Raiswell and Canfield (1998); Schwertmann and Cornell (2000); Poulton *et al.* (2004b); Sklute *et al.* (2018); Caraballo *et al.* (2022); Jiang *et al.* (2022).
Fe-clays: Langmuir (1997); Raiswell and Canfield (1998); Fan *et al.* (2023).
Magnetite: Amor *et al.* (2020); Kappler *et al.* (2023).
Vivianite & ferric phosphates: Huffman *et al.* (1960); Eynard *et al.* (1992); Hyacinthe and Van Cappellen (2004); Kandori *et al.* (2006); Cosmidis *et al.* (2014); Rothe *et al.* (2016); Schütze *et al.* (2020); Metz *et al.* (2023).

within clays could lead to microenvironments with high supersaturation that encourage pyrite formation.

Besides (oxyhydr)oxides and clays, Fe phosphates are also potential Fe sources for Fe sulfide formation. Recent studies have shown that biogenic pyrite could precipitate via sulfidation of ferric phosphates (Berg *et al.*, 2020; Duverger *et al.*, 2020). Ferric phosphates are key minerals involved in phosphorus cycling, especially in ferruginous lakes and estuarine sediments (Hyacinthe and Van Cappellen, 2004; Cosmidis *et al.*, 2014). Another phosphate mineral, the Fe(II)-containing vivianite, is also commonly formed when dissolved Fe^{2+} and phosphate are released into the solution. Such conditions are found in Fe(III) reducing zones of water columns and sediments or in microbial cultures (Rothe *et al.*, 2016; Bronner *et al.*, 2023). Vivianite could be sulfidized to pyrite as the mineral is buried in deeper sulfate reduction zones. Interestingly, vivianite can persist under sulfidic conditions for months in microbial cultures as observed empirically (Picard *et al.*, 2018; Nabeh *et al.*, 2022; Bronner *et al.*, 2023). Hence, it is unclear if vivianite is an important Fe source for pyrite formation. Nonetheless, the trends in the last few years show that the research field is shifting towards investigating alternative sources of Fe, with different interfacial chemistry, templating effects and microenvironments that promote a multitude of pathways for pyrite formation.

It is important to keep in mind that minerals with the same chemical formula and crystal structure may also exhibit different reactivities depending on their formation pathways, association with organics, trace metal contents and sizes. Natural minerals will probably have associated organics, especially when they are formed by widespread Fe-metabolizing microorganisms (Kappler *et al.*, 2021). Organics and trace metals (*e.g.* Ni) have been shown to retard the extent of sulfidation or pyritization (ThomasArrigo *et al.*, 2020; Duverger *et al.*, 2021; Wang *et al.*, 2023; Wu *et al.*, 2023). Particle sizes also greatly affect pyritization rates. For example, micron-sized magnetite (mixed-valent Fe_3O_4) grains exhibit low reactivity towards sulfide with estimated half-lives in the order of 100 years (Canfield and Berner, 1987). By contrast, freshly precipitated nano-magnetite that are more similar to biogenic magnetite are rapidly sulfidized within days, with pyrite formation accelerated in the presence of elemental sulfur (S^0) and polysulfides (Poulton *et al.*, 2004b; Runge *et al.*, 2023), while being retarded in the presence of organics (Runge *et al.*, 2024).

Sources of sulfur

Mackinawite and greigite are Fe-S minerals in which both sulfur atoms have -2 redox states, while pyrite is an Fe polysulfide in which the sulfur atom has a -1 redox state. The availability of reduced sulfur species is tied to complex sulfur cycling driven by microbial and abiotic processes. Below, we discuss the sources of sulfide, polysulfides and S^0 as the main sulfur-bearing species involved in sedimentary Fe-S mineral formation.

Sulfide (S(-II)) is produced in porewater as the main product of microbial sulfate reduction (MSR), the dominant mode of organic matter oxidation in marine sediments (Jørgensen *et al.*, 2019), where it is fuelled by sulfate ions present at relatively high concentrations in seawater (~28 mM) and diffusing downwards into the sediment. Sulfide speciates into two major species: H_2S and bisulfide (HS^-). The pKa of H_2S is about 7, meaning that at normal seawater pH (around 8), it represents less than 10% of the total dissolved S(-II) pool. The majority of the pool will then be in the form of HS^-. The link between MSR and pyrite formation is potentially weaker in low-sulfate lake sediments, where S(-II) may be derived from the breakdown of biomass containing reduced organic sulfur (Wei *et al.*, 2023). The breakdown of reduced organic sulfur, as well as the reduction of organic sulfite, is also thought to have been a prevalent source of reduced sulfur for pyrite formation in low-sulfate Archean oceans (Fakhraee and Katsev, 2019). Microbial disproportionation or reduction of elemental sulfur (S^0) and thiosulfate may also constitute a source of S(-II) for pyrite formation, as suggested by both microbial culture experiments (Canfield *et al.*, 1998) and observations from natural marine sediments (Zopfi *et al.*, 2008).

Polysulfides are soluble ionic species consisting of relatively short chains of sulfur atoms terminated by negative charges (n in S_n^{2-} is typically smaller than 9, with n = 5, 6, and 4 being the more abundant forms under certain experimental conditions; Kamyshny *et al.*, 2004). At high concentrations, they exhibit a distinct yellow-green colouration with absorbances in the 250–350 nm region (*e.g.* Domingos *et al.*, 2023). At pH values representative of seawater and

https://doi.org/10.1180/gbi.2024.9 Published online by Cambridge University Press

marine pore waters, polysulfides form spontaneously through the chemical reaction of S^0 with S(-II), as depicted in the equation below:

$$HS^{-} + (n-1)\,S^0 = H^+ + S_n{}^{2-} \quad (1)$$

Polysulfides can also form through the oxidation of hydrogen sulfide by O_2, Fe(III) and manganese (oxyhydr)oxides, with kinetic reaction rates in the following order: $MnO_2 > O_2 > Fe(OH)_3 > S^0$, corresponding to characteristic reaction times ranging from a few minutes to about a year at conditions relevant for sulfidic marine sediments (Chen and Morris, 1972; Poulton *et al.*, 2004a; Avetisyan *et al.*, 2019, 2021). They can furthermore be formed biologically, as a by-product of both phototrophic and chemotrophic S-oxidative microbial metabolisms (Findlay, 2016). The environmental prevalence and relative abundance of polysulfide species in the environment have remained relatively elusive until the development of robust analytical methods based on derivatization almost twenty years ago (Kamyshny *et al.*, 2006, 2009), and even today reliably measuring polysulfide concentrations in sediments is a difficult endeavour. However, it has been established that under many conditions, polysulfides can be expected to occur in concentrations approaching calculated equilibrium with elemental sulfur based on reaction (1) (Kamyshny and Ferdelman, 2010). For this reason, we focus our discussion on factors controlling the abundance of sedimentary S^0 in the paragraph below.

In low-temperature environments, S^0 is formed by oxidation of more reduced sulfur species. This oxidation process can occur abiotically in the presence of oxygen or oxidized Fe or Mn phases (*e.g.* Rickard and Luther, 2007) or it can be mediated by S-oxidizing bacteria and archaea (Dahl *et al.*, 2008). Since measured rates of prokaryotic S-oxidation are several orders of magnitudes faster than rates of chemical sulfide oxidation to S^0 by molecular oxygen (Luther *et al.*, 2011), it is often assumed that S^0 formed in low-temperature environments is mostly formed as a result of microbial activity. A diversity of phototrophs and chemotrophs are able to biomineralize S^0 in the form of intra- or extra-cellular S^0 globules (Dahl and Prange, 2006; Cron *et al.*, 2019; Marnocha *et al.*, 2019) or extracellular S^0 filaments (Wirsen *et al.*, 2002; Sievert *et al.*, 2007). Sulfur rarely accumulates in sedimentary environments, due to its chemical and biological instability. Chemically, S^0 is only stable in a very narrow range of Eh-pH conditions, and not at all above neutral pH values (Rickard and Luther, 2007). It has actually been found to be thermodynamically unstable in a range of natural sulfidic waters (Helz, 2014). Biologically, S^0 is used as a source of energy for a diverse range of S-oxidizers, S-reducers and microorganisms that perform S^0 disproportionation (Dahl, 2020a). Some microbes, such as the thermoacidophile *Acidianus*, are particularly efficient at recycling S^0 as they can grow from all three reactions (Amenabar and Boyd, 2018). Abundances of S^0 in sediments typically range from 11 µmol/kg to 60 mmol/kg (see compilations in Ye and Jing (2022), their Table S-1 and Zopfi *et al.* (2004).

Not all forms of S^0 are created equal, as a number of factors can influence the chemical and biological reactivity of S^0 in the environment. Obviously, S^0 biominerals stored intracellularly (Dahl, 2020b) are unavailable for extracellular chemical reactions and consumption by other microorganisms. Some microbes that produce S^0 biominerals as an extracellular energy storage resource have also evolved strategies to increase their environmental stability and/or avoid piracy by other S^0-consuming cells (Cosmidis and Benzerara, 2022). As an example, some S-oxidizers encapsulate their extracellular S^0 globules in an organic membrane, allowing S^0 to be formed and persist in the extracellular medium in a thermodynamically unstable state (Cron *et al.*, 2019, 2021; Marnocha *et al.*, 2019). Sulfur minerals produced chemically by oxidation of sulfide in the presence of organics (a process called S^0 organo-mineralization) can also exist outside of their thermodynamic stability domain (Lau *et al.*, 2017; Cosmidis *et al.*, 2019). The size of S^0 particles affects their chemical reactivity (Steudel, 2003) and bioavailability (Franz *et al.*, 2007), with smaller particles being overall more unstable. In sediments, S^0 is thought to exist mainly as colloidal sols, which are more reactive than crystalline S^0 (Zopfi *et al.*, 2004). Due to its reactivity, colloidal or nanoparticulate S^0 is likely to be the main source of polysulfides in sulfidic sediments (Kleinjan *et al.*, 2005; Mol *et al.*, 2022), but abundances of S^0 particles in the micron or sub-micron size range are rarely reported (Findlay *et al.*, 2014). Such considerations on S^0 reactivity should be taken into account in experimental studies investigating the role of this mineral in Fe-S mineral formation.

Table 2. Example of proposed reactions for pyrite formation.

Name	Reaction	Reference(s)
Direct reaction	$Fe^{2+}_{(aq)} + S^{2-}_{2(aq)} \rightarrow FeS_{2(s)}$	-
Polysulfide pathway	$FeS_{(aq)} + S^{2-}_{x(aq)} \rightarrow FeS_{2(s)} + S^{2-}_{x-1(aq)}$	Rickard (1975)
H_2S pathway	$FeS_{(aq)} + H_2S_{(aq)} \rightarrow FeS_{2(s)} + H_{2(g)}$	Drobner *et al.* (1990); Rickard and Luther (1997)
Sulfur addition	$FeS_{(s)} + S^0_{(s)} \rightarrow FeS_{2(s)}$	Berner (1970)
Iron loss	$2FeS_{(s)} + 2H^+_{(aq)} \rightarrow FeS_{2(s)} + Fe^{2+}_{(aq)} + H_{2(g)}$	Wilkin and Barnes (1996); Benning *et al.* (2000)
Ferric-hydroxide-surface (FHS) pathway	$>Fe^{III}OH + HS^- \leftrightarrow Fe^{III}S^- + H_2O$ $>FeI^{II}S^- \leftrightarrow >Fe^{II}S\bullet$ $>Fe^{II}S\bullet + H_2O \leftrightarrow >Fe^{II}OH_2{}^+ + S\bullet^-$ $>Fe^{II}OH_2{}^+ + 2S\bullet^- \rightarrow H_2O + >Fe^{II}S_2{}^-$ $>Fe^{II}S_2{}^- \rightarrow FeS_2$	Peiffer *et al.* (2015); Wan *et al.* (2017)

Biogenic iron sulfide mineral formation at low temperature

Mackinawite and greigite formation at low temperature

Mackinawite (FeS) and greigite (Fe_3S_4) are described as metastable Fe-S minerals with respect to pyrite (cubic FeS_2). For that reason, they are generally assumed to be present in modern sedimentary environments but absent from ancient rocks and sediments (Rickard, 2012b). Recent modelling studies have nonetheless found that greigite could be much more stable than originally expected (Subramani *et al.*, 2020; Shumway *et al.*, 2022; Son *et al.*, 2022). In natural environments, metastable Fe-S minerals are assumed to be the main constituent of acid-volatile sulfides (AVS), which are the solid and aqueous phases that produce sulfide after treatment of samples with HCl. The contribution of mackinawite and greigite to the AVS fraction is likely to vary depending on the environment considered and it is possible that the AVS fraction does not capture all of the mackinawite and greigite content of an environment, as these two minerals might not completely dissolve in HCl (Rickard and Morse, 2005). While direct identification of mackinawite and greigite is most easily done using X-ray diffraction (XRD) (Berner,

https://doi.org/10.1180/gbi.2024.9 Published online by Cambridge University Press

1962; Evans Jr *et al.*, 1964; Skinner *et al.*, 1964; Lennie, 1995), combined studies including AVS analysis and XRD in sedimentary environments are not common. Biogenic precipitates of mackinawite and greigite are certainly present in anoxic sediments, and understanding their physical properties is of crucial importance because they could react differently from abiotic precipitates to analytical procedures, such as leaching procedures for AVS quantification.

Abiotic mackinawite has a tetragonal layer structure with cell parameters a=b=3.6735 Å and c=5.0329 Å (Lennie, 1995). Greigite has a cubic unit cell, with a=9.876 Å (Skinner *et al.*, 1964). Mackinawite is stoichiometric FeS and precipitates rapidly from the reaction between aqueous Fe^{2+} and dissolved sulfide (H_2S/HS^-) (Rickard, 1995, 2024; Rickard *et al.*, 2006). The chemical formula for the greigite formula is averaged to Fe_3S_4, although its exact composition has not been determined (Rickard, 2012b). Greigite forms through the solid-state transformation of mackinawite, which is driven by the oxidation of Fe atoms and their rearrangement (Rickard, 2012b, Lennie *et al.*, 1997). As greigite does not precipitate directly from the solution, its characterization is difficult because residual mackinawite is always present (Rickard, 2012b). Owing to its magnetic properties, greigite can be detected in the sedimentary record but could be difficult to differentiate from magnetite (Fe_3O_4) (Roberts *et al.*, 2011). In experimental studies and microbial cultures, a strong neodymium magnet can be used to check for its presence.

In low-temperature environments, the main source of sulfide for mackinawite and greigite formation is microbial sulfate reduction (MSR) (Rickard *et al.*, 2017). As discussed in the 'Sources of sulfur' section above, other microbial processes can provide sulfide for metastable Fe-S mineral formation, but their significance varies depending on the environment (*e.g.* Jørgensen *et al.*, 2019; Wu *et al.*, 2021). Mesophilic sulfate-reducing bacteria (SRB) have been used in most experimental studies to decipher the role of microorganisms in the formation of extracellular Fe-S minerals at low temperatures, *e.g.* through biologically induced mineralization (Pósfai and Dunin-Borkowski, 2006; Picard *et al.*, 2016; Park and Faivre, 2022). The few sulfate-reducing archaea (SRA) available in cultures are (hyper)thermophilic and have not been used for Fe-S mineral formation investigations. Experimental studies consist of precipitating biogenic Fe-S minerals by adding a source of Fe to cultures of SRB and (ideally) comparing them to abiotic Fe-S minerals precipitated by adding sulfide to the culture medium containing the same source of Fe. The following strains have been used in a range of temperatures between room temperature and 35°C: *Desulfovibrio capillatus* (Ikogou *et al.*, 2017), *Desulfovibrio desulfuricans* (Rickard, 1969b; Neal *et al.*, 2001; Li *et al.*, 2006; Stanley and Southam, 2018; Duverger *et al.*, 2020), *Desulfovibrio hydrothermalis* (Picard *et al.*, 2018; Nabeh *et al.*, 2022), *Desulfovibrio magneticus* (Nabeh *et al.*, 2022), *Desulfovibrio vulgaris* (Zhou *et al.*, 2014; Mansor *et al.*, 2019), *Desulfovibrio* spp. (Li *et al.*, 2004), *Desulfosporosinus orientis* (Stanley and Southam, 2018), *Desulfotomaculum* sp. (Fortin *et al.*, 1994). Additionally, uncharacterized enrichments of SRB from various environments have also been used in experimental studies (Herbert *et al.*, 1998; Donald and Southam, 1999; Gramp *et al.*, 2010). The redox state of the initial source of Fe in cultures of SRB appears to determine the mineralogy of the final Fe-S mineral products (Rickard, 1969b; Duverger *et al.*, 2020). In experimental studies using Fe^{2+} as a unique source of Fe, mackinawite precipitates first and transforms into greigite over time (Picard *et al.*, 2018). In experimental studies using Fe(III), the reduction of the latter by sulfide produces Fe(II) and intermediate sulfur species, which appear necessary for the formation of pyrite (see the section 'Biogenic pyrite formation at low temperatures' below).

Owing to the semi-conducting properties of Fe-S minerals, the role of mackinawite in improving the efficiency of extracellular electron transfer in microbial cultures has been investigated (Nakamura *et al.*, 2010; Jiang *et al.*, 2014; Kondo *et al.*, 2015; Zhu *et al.*, 2022). These studies have explored the production of biogenic Fe-S minerals by Fe(III)-reducing bacteria, *e.g. Shewanella* or *Geobacter*, which also have the ability to reduce intermediate sulfur species. In those experimental systems, microbial reduction of thiosulfate or elemental sulfur produces sulfide, while microbial and/or chemical reduction of Fe(III) by sulfide is the source of Fe(II) that promotes the precipitation of Fe-S minerals. Although many studies of interest also considered biogenic mackinawite in the context of bioremediation studies (*e.g.* Sharma *et al.*, 2024; Yang *et al.*, 2017), we restrict this section to studies that have attempted to characterize and quantify the differences between abiotic and biogenic mackinawite and greigite experimentally.

Microbial influence on the physical characteristics of mackinawite

The presence of microorganisms in experimental systems does not prevent the formation of mackinawite. However, the availability of cell surfaces as templates for mineral nucleation and growth can impact its physical properties, such as the size of crystallite domains, crystallinity and propensity to aggregate, and can lead to cell encrustation (Picard *et al.*, 2016, 2018, 2021; Mansor *et al.*, 2019; Nabeh *et al.*, 2022). Templating occurs when Fe^{2+} first interacts with negatively charged bacterial cell surfaces before precipitating with sulfide (Beveridge, 1989); *i.e.* when SRBs are grown in a culture medium that contains millimolar concentrations of Fe^{2+} (Picard *et al.*, 2018). Physical and chemical characteristics are important when considering reactivity and transformation of solid phases in natural environments.

X-ray diffractograms of 'templated' minerals display fine peaks with high intensity, while those of 'non-templated' minerals display broad peaks with low intensity (Picard *et al.*, 2018; Mansor *et al.*, 2019; Duverger *et al.*, 2020, 2021, Nabeh *et al.*, 2022). For a quantitative approach, XRD data can be fitted to estimate the average size of the crystalline domains using the Scherrer equation (Wolthers *et al.*, 2003; Unruh and Forbes, 2019). Abiotic mackinawite precipitated in water is nanocrystalline and has an average particle size of 7.4 nm (a/b axis) x 2.9 nm (c axis) (Wolthers *et al.*, 2003; Ohfuji and Rickard, 2006). While there is variability among the few studies that reported crystallite size data, biogenic mackinawite grows along both the a/b axis and the c axis more than the abiotic controls (Zhou *et al.*, 2014; Picard *et al.*, 2018; Mansor *et al.*, 2019). Specifically, crystallite domains of biogenic mackinawite precipitated with SRB grown with Fe^{2+}, and of mackinawite precipitated with dead SRB incubated with Fe^{2+} then with sulfide, are on average significantly larger than those of abiotic mackinawite precipitated in water and the SRB medium (with or without simple or complex organic molecules), and those of biogenic mackinawite precipitated in SRB cultures to which Fe^{2+} has been added after growth and sulfide production (Picard *et al.*, 2018, 2021). When SRBs are grown with Fe(III)-citrate, biogenic mackinawite displays smaller crystallite domains than when Fe^{2+} is directly available (Ikogou *et al.*, 2017). In all conditions in which crystallite domains are small, templating cannot occur for the two following reasons: (1) salts and organic molecules in the medium do not provide

https://doi.org/10.1180/gbi.2024.9 Published online by Cambridge University Press

scaffolds for mineral nucleation and growth and (2) Fe^{2+} does not have the opportunity to bind to cell surfaces if sulfide is already present in the environment. A number of other studies have investigated the formation of biogenic Fe-S sulfide minerals using Fe(III) minerals as starting Fe source (*e.g.* Fe(III) (oxyhydr)oxides, Fe(III)-containing clays, Fe(III) phosphate minerals); however, they did not provide information about the size of crystallite domains (Duverger *et al.*, 2020).

High-resolution studies of biogenic mackinawite indicated that it becomes crystalline very rapidly. Selected-area electron diffraction (SAED) patterns showed a shift from a polycrystalline material after one week to a single-crystal pattern after one month in mackinawite produced in cultures of *Desulfovibrio desulfuricans* grown with Fe^{2+}. As early as one week of incubation, and in longer experiments, the 5 Å d-spacing of mackinawite can be clearly observed using high-resolution transmission electron microscopy (HR-TEM) (Duverger *et al.*, 2020). It is usually assumed in abiotic studies that mackinawite is transient and short-lived in anoxic sedimentary environments. The crystallinity of biogenic mackinawite will probably play an important role in its stability and further transformations and should be considered.

Aggregation of biogenic mackinawite particles in cultures of SRB grown with Fe^{2+} is visible when observing cultures by eye. Minerals observed in unshaken cultures of SRB grown with Fe(II) form sticky clumps, while abiotic mackinawite sediments homogeneously at the bottom of serum vials. When biogenic minerals are resuspended in solutions, they also appear less opaque than abiotic minerals (Picard *et al.*, 2018). Observations using scanning and/or transmission electron microscopy (SEM and/or TEM) reveal that biogenic mackinawite has a flaky texture and can reach mm-range sizes, much larger than aggregates of abiotic mackinawite (Herbert *et al.*, 1998; Gramp *et al.*, 2010; Picard *et al.*, 2018; Duverger *et al.*, 2020). Biogenic particles precipitated in cultures of SRB grown with Fe^{2+} form larger aggregates than abiotic particles precipitated in the culture medium, as determined using dynamic light scattering (Picard *et al.*, 2018).

Cell encrustation by Fe-S minerals has been reported in cultures of SRB grown with Fe^{2+}. This observation is consistent with the ability of cells to serve as templates, *e.g.* when Fe^{2+} is available to bind to the cell surface before interacting with sulfide. Cells from cultures of SRB grown with and without Fe(II) have a similar smooth aspect when imaged with SEM (Picard *et al.*, 2018). To detect the presence of Fe-S crusts at the surface of cells, it is best to prepare thin sections of resin-embedded pellets that contain cells and minerals and to image them using TEM (Shuster *et al.*, 2019; Picard *et al.*, 2018). Fe-S minerals have been directly observed at the surface of both gram-negative and gram-positive SRB using TEM imaging of thin sections prepared after short incubations (Fortin *et al.*, 1994; Donald and Southam, 1999; Picard *et al.*, 2018; Stanley and Southam, 2018). Although no direct mineral characterization of the crusts has been performed in these studies using SAED, encrusted cells were imaged after short periods of time (one week or less), when mackinawite is the only mineral phase detected by powder X-ray diffraction (XRD) (Picard *et al.*, 2018). It is unknown if cell encrustation in Fe-S minerals is a common situation for microbial cells in natural environments. There have been only two reports of microorganisms encrusted with Fe-S minerals in mine tailing sediments, where SRB are ubiquitous (Ferris *et al.*, 1987; Fortin and Beveridge, 1997). The impact of Fe-S mineral encrustation on microbial metabolic activity is also unknown. The assimilation of carbon substrates by bacteria encrusted in Fe(III) oxyhydroxides appears to be inhibited (Miot *et al.*, 2015). Duverger *et al.* (2020) suggested that sulfate reduction in cultures of *Desulfovibrio desulfuricans* grown with Fe^{2+} is hindered by cell encrustation in Fe-S minerals. It is possible that the high concentration of soluble Fe^{2+} (20 mM) used in their study, rather than encrustation, inhibited metabolic activity. Indeed, other studies that described cell crusts around cells used lower concentrations of Fe^{2+} (*e.g.* 3.5–4.0 mM) and did not report inhibition of sulfate reduction (Fortin *et al.*, 1994; Picard *et al.*, 2018). Although Fe(II) is required by SRB for growth, high concentrations of soluble Fe^{2+} might trigger stress or other metabolic responses. SRB released seven unidentified organic molecules in response to 4 mM Fe^{2+} in the growth medium (Picard *et al.*, 2019). It is possible that (1) these extracellular compounds are inhibitory at higher concentrations, and/or that (2) high concentrations of Fe^{2+} are directly inhibitory for SRB. As Fe-S minerals are semi-conducting materials, some studies have evaluated the potential role that biogenic Fe-S minerals could play in enhancing extracellular electron transfer (EET) between microorganisms and solid phases. Direct contact between SRB and Fe-S minerals might be beneficial, and electrochemical studies indicated an increase in electron transfer from cells to electrodes in the presence of biogenic Fe-S minerals (Deng *et al.*, 2020). This observation has also been reported in studies in which *Shewanella* strains produced Fe-S minerals when grown with thiosulfate and a source of Fe (Nakamura *et al.*, 2010; Jiang *et al.*, 2014; Kondo *et al.*, 2015). The facilitated electron transfer through biogenic Fe-S minerals could be of use in energy-depleted environments. As discussed later in this review, Fe-S minerals can store significant amounts of organic carbon that could be potentially accessed as energy sources by SRB and other microorganisms (Picard *et al.*, 2019; Nabeh *et al.*, 2022).

Microbial influence on the transformation of mackinawite to greigite under anoxic conditions

In abiotic experiments, greigite formation from mackinawite requires an oxidant, which can be traces of oxygen at the surface of mackinawite (Benning *et al.*, 2000), aldehydes (with the intention of sterilizing the experimental system) (Rickard *et al.*, 2001), or polysulfides (Benning *et al.*, 2000). High temperature accelerates the abiotic transformation of mackinawite to greigite (Lennie, 1995). A recent modelling study indicated that greigite formation is favourable in anoxic, alkaline and low-temperature environments where Fe is enriched and sulfide limited (Turney *et al.*, 2023). There is experimental evidence that SRM could be driving and/or accelerating the transformation of mackinawite to greigite under strictly anoxic conditions. As noted above, greigite can form in the absence of microorganisms. However, in experimental studies under strict anoxic conditions, greigite forms in cultures of SRM grown with Fe^{2+} at their optimal pH and temperature after several months of incubation, while it does not form in abiotic experiments (Rickard, 1969b; Picard *et al.*, 2018, 2021; Mansor *et al.*, 2019; Nabeh *et al.*, 2022). In old cultures, greigite is stable and does not transform further, and mackinawite is still detectable after several years of incubation, suggesting that the full transformation of mackinawite to greigite in these experimental conditions is slow (Picard *et al.*, 2018; Nabeh *et al.*, 2022; Picard, unpublished). In the study by Mansor et al. (2019), greigite could be detected by SAED in the TEM after six months of incubation but not by XRD, suggesting that transformation yield can vary with experimental conditions and microbial strains. In abiotic studies that maintain strict anoxic conditions, mackinawite remains stable and does not transform into greigite (Benning *et al.*, 2000; Picard *et al.*, 2018, 2021).

https://doi.org/10.1180/gbi.2024.9 Published online by Cambridge University Press

Biogenic greigite produced in cultures of SRB displays an average crystalline domain size of 19.2 nm, which is in the size range of biogenic mackinawite precipitated in cultures of SRB grown with Fe^{2+}, supporting the hypothesis of solid-state transformation from biogenic mackinawite (Picard *et al.*, 2018). The 'small' mackinawite produced in cultures to which Fe^{2+} has been added after sulfide production does not transform to greigite, nor does abiotic mackinawite precipitated with organic molecules or mixtures of complex organics (Picard *et al.*, 2018, 2021). Interestingly, the 'large' mackinawite that is produced at the surface of dead cells also does not transform into greigite (Picard *et al.*, 2018). This indicates that under strict anoxic conditions, crystalline mackinawite and metabolically active cells are required to form greigite. The oxidant necessary to oxidize Fe(II) in mackinawite could originate from H^+ produced by residual activity of SRB in old cultures (Mansor *et al.*, 2019). However, it is unknown why the transformation only takes place after several months, when greigite precipitation is actually favourable in anoxic and alkaline conditions at low temperatures (Turney *et al.*, 2023). The experiments cited above have been performed in anoxic conditions, around neutral pH and at temperatures between RT and 35°C (Rickard, 1969b; Zhou *et al.*, 2014; Picard *et al.*, 2018, 2021; Mansor *et al.*, 2019).

There are still many unknowns into what controls greigite formation in low-temperature environments. Changes in one or several parameters in culture media can promote or suppress the formation of greigite. For example, varying the amount of sulfide produced in cultures of *Desulfovibrio hydrothermalis*, and of *Desulfovibrio magneticus* RS-1 grown with Fe(II) resulted in different patterns of greigite production (Nabeh *et al.*, 2022). A recent report of the formation of greigite in cultures of *Geobacter sulfurreducens* grown with Fe(III) and S(0) suggests that other conditions than the ones described above might exist to promote greigite formation in the presence of microorganisms (Bronner *et al.*, 2023). The encrustation of cells by greigite has not been reported. As noted in the previous section, encrustation has been reported in relatively short-term cultures when mackinawite is the only phase detected by XRD. It is thus unknown how the interactions between SRM and Fe-S minerals evolve and if the transformation of mackinawite to greigite affects the localization of minerals on microbial cells.

While its significance in terms of amounts precipitated is unknown, biogenic greigite produced intracellularly by magnetotactic bacteria (MTB) through biologically controlled mineralization (as opposed to biologically induced mineralization described above) has attracted attention for their potential to participate in the magnetic properties of sediments and sedimentary rocks and to produce biosignatures (Amor *et al.*, 2020). Two morphological types of intracellular greigite producers have been described: magnetotactic multicellular prokaryotes (MMPs) and large rod-shaped bacteria. Intracellular greigite producers are found in reducing and sulfidic environments and use sulfate as an electron acceptor (Farina *et al.*, 1990; Mann *et al.*, 1990; Lefèvre *et al.*, 2011; Descamps *et al.*, 2017). Intracellular greigite formation is favoured at low Fe and high sulfide concentrations (Descamps *et al.*, 2017). Similar to extracellular greigite, intracellular crystals in MTB form from the solid-state transformation of mackinawite (Pósfai *et al.*, 1998). Mackinawite can be detected at the end of magnetosome chains during short periods of time before transforming to greigite in a matter of days to weeks, suggesting that the intracellular formation of greigite is faster than that of extracellular greigite (Pósfai *et al.*, 1998).

Biogenic pyrite formation at low temperatures

Pyrite is the most widespread iron sulfide on the Earth's surface and is often ascribed a biological origin, as microbial sulfate reduction (MSR) is the main pathway to produce sulfide precursors from the particularly stable molecule sulfate. Chemically speaking, pyrite is one of two iron disulfide (FeS_2) polymorphs, along with marcasite. Pyrite's ubiquitous presence in the geological record is due to its incredible thermodynamic stability in comparison to other reduced sulfur minerals (Schoonen, 2004). It is thus tempting to assume that its formation results from the simple precipitation of its constituent cation (Fe^{2+}) and anion (S_2^{2-}), as is the case for most non-silicate authigenic sedimentary minerals (*e.g.* halides, sulfates, carbonates, phosphates). It was therefore assumed that pyrite is relatively easy to obtain in laboratory experiments. Indeed, a long list of recipes for pyrite formation can be found in the literature, as compiled in Rickard (2012).

However, the conditions used to precipitate pyrite in the laboratory are often far removed from those found in natural sediments, particularly those supporting microbial life. Indeed, many experiments have been carried out at so-called 'low temperatures' of <100°C, which are lower than hydrothermal temperatures but not so low in a biological sense. In fact, temperatures above 45°C and 80°C are in the ecological niche ranges of thermophiles and hyperthermophiles, respectively, which are not responsible for most MSR globally. Similarly, experiments carried out at pH levels far from neutral raise questions about the parallels that can be drawn with the natural environment. All these abiotic syntheses have been crucial to understanding the mechanisms of pyrite formation and the different environmental factors at play. However, they do not allow us to correctly decipher the role played by microorganisms in pyrite formation.

Pyrite formation in the presence of microbes has more recently been reported in environmental studies of sediments (Quevedo *et al.*, 2021; Tribovillard *et al.*, 2022), thermal springs (Tsyrenova *et al.*, 2018) and deep geological repositories (Boylan *et al.*, 2019), as well as in numerous recent experimental studies such as in metal corrosion (Etim *et al.*, 2018; Jia *et al.*, 2018, 2019; Rasheed *et al.*, 2019), arsenic bioremediation in contaminated soils (Pi *et al.*, 2017; Saunders *et al.*, 2018; Lee *et al.*, 2019), various microbial enrichment cultures (Gao *et al.*, 2019, 2021; Berg *et al.*, 2020; Allen *et al.*, 2021; Ikkert *et al.*, 2021; Karnachuk *et al.*, 2021; Wei *et al.*, 2023; Yang *et al.*, 2023) and (co-)cultures (Thiel *et al.*, 2019; Zhou *et al.*, 2019; Duverger *et al.*, 2020; Sun *et al.*, 2023; Ke *et al.*, 2024). It should be pointed out that the role of microorganisms in the formation of biogenic pyrite was not the main objective of some of these studies and, therefore, although anoxic conditions were applied during the microbial culture, they were not maintained throughout the experiments, particularly during the analysis, which may result in the transformation of metastable iron sulfide phases into more stable pyrite that may not have been present initially. Moreover, the identification of pyrite in some of these studies is not infallible: SEM images rely solely on morphology, semi-quantitative SEM-EDS analyses may be subject to large errors due to surface effects, chemical extractions are not very selective to pyrite (*e.g.* chromium-reducible sulfur can also contain zero-valent sulfur species if not initially separated with methanol and HNO_3 can also target iron silicates) and there are still poorly indexed X-ray diffractograms in the literature that over-interpret the presence of pyrite, as they are made on multi-phase systems (containing elemental sulfur or vivianite, for example) that generate numerous peaks, many of

https://doi.org/10.1180/gbi.2024.9 Published online by Cambridge University Press

which coincide with those of pyrite. Despite the fact that it is widely accepted that microorganisms play a key role in the production of pyrite, it is interesting to note that most attempts to produce pyrite in the presence of microorganisms have failed (Picard *et al.*, 2016, 2018; Ikogou *et al.*, 2017; Zhou *et al.*, 2017; Stanley and Southam, 2018; Mansor *et al.*, 2019; Zhang *et al.*, 2021; Nabeh *et al.*, 2022) with only a few known exceptions (Rickard, 1969b; Ivarson and Hallberg, 1976; Donald and Southam, 1999; Thiel *et al.*, 2019; Zhou *et al.*, 2019; Berg *et al.*, 2020; Duverger *et al.*, 2020).

For a quarter of a century, there has been a consensus on two reaction pathways for pyrite formation: the polysulfide pathway (Rickard, 1969a, 1975) and the H_2S pathway (Rickard, 1997; Rickard and Luther, 1997). Others have fallen into disuse because they can be interpreted as variants of the two main pathways (Table 2). Recently a third reaction pathway has been proposed under the name ferric-hydroxide-surface pathway (FHS; Wan *et al.*, 2017).

The role of polysulfides in pyrite formation has long been known. Apart from the synthesis of pyrite by metallurgical processes requiring very high temperatures, two almost concurrent works attesting to the formation of pyrite from polysulfides at relatively low temperatures go as far back as the mid-19th century. During an expedition to Iceland following the 1845–1846 Hekla eruption, the formation of pyrite was observed in fumarole systems (Bunsen, 1847). Based on the contemporaneous chemical knowledge about alkaline polysulfide dissolution of ferrous sulfide, which then reprecipitates, it was postulated that hot hydrogen sulfide vapours emitted by fumaroles transform the iron minerals in weathered basalt into pyrite through the transient formation of iron sulfide and polysulfides. Several years later, in pioneering hydrothermal synthesis experiments, several metal sulfide minerals including pyrite were successfully formed from a mixture of iron salts and 'persulfide' (obsolete word for polysulfide S_n^{2-}) in a sealed tube heated to 165–180°C (Senarmont, 1851). Later investigations on hydrothermal synthesis of iron sulfide showed that pyrite could be formed by heating various mixtures of H_2S and iron salts, elemental sulfur and iron sulfide or dissolved polysulfide and ferrous salts, reproducing acidic to alkaline environments (Allen *et al.*, 1912). The authors generalized these three different methods by "the action of sulphur on ferrous sulphide", laying the foundations for a common pathway to pyrite formation regardless of the reagents used. The idea that elemental sulfur is directly involved in the formation of sedimentary pyrite subsequently gained ground, not least because of its common presence in the sediments (GW Harmsen, 1954; Kaplan *et al.*, 1963; Berner, 1970; Sweeney and Kaplan, 1973).

Because the solid-state reaction between elemental sulfur and iron sulfide at low temperatures is mechanically impossible, it is now generally accepted that pyrite formation resulting from the addition of a sulfur compound to iron monosulfide occurs via the dissolved polysulfide reagent. This reaction is known as the polysulfide pathway (Rickard, 1975; Luther, 1991). The reaction of HS^- with elemental sulfur (Reaction 1, Table 2) is a ubiquitous source of dissolved polysulfide which helps explain how pyrite can easily be formed anywhere from modern sediments to early experiments with elemental sulfur and iron sulfide. Isotopic measurements have revealed that pyrite formed by the polysulfide pathway inherits the polysulfide isotopic signature, meaning that the sulfur atom from the initial FeS is replaced by two sulfur atoms of the polysulfide via a cyclic reaction (Butler *et al.*, 2004).

The polysulfide pathway is probably of relevance in transitional redox environments with limited molecular oxygen content (Rickard, 1997). In addition to oxygen, other oxidants could promote this pathway in the environment. For instance, H_2S released by sulfate-reducing microorganisms (SRM) can be oxidized to polysulfide during abiotic ferric iron reduction (Wei and Osseo-Asare, 1997; Morin *et al.*, 2017; Baya *et al.*, 2022). It is interesting to note that under strictly anoxic conditions, the few studies reporting pyrite formation in microbial cultures of SRM have mostly been carried out in the presence of ferric iron: goethite (FeO(OH), Rickard, 1969a), jarosite ($KFe_3(SO_4)_2(OH)_6$, Ivarson and Hallberg, 1976) or ferric phosphate ($FePO_4.2H_2O$, Berg *et al.*, 2020; Duverger *et al.*, 2020). In these various works, amorphous black precipitates were initially observed and pyrite was only detected after longer incubation times. It would therefore seem that the H_2S produced by microbial sulfate reduction (MSR) reacted with the ferric iron minerals, producing not only ferrous iron and subsequently iron sulfide but also intermediate sulfur compounds paving the way for pyrite formation via the polysulfide pathway. A similar mechanism is probably at play in sulfur-disproportionating bacterial cultures that grow only with the addition of Fe(III) (oxyhydr)oxides as a hydrogen sulfide scavenger (Thamdrup *et al.*, 1993; Canfield *et al.*, 1998; Finster *et al.*, 1998). Polysulfides can also be directly produced by microorganisms and eventually released into the environment via polyvalent metabolisms such as incomplete sulfide oxidation (Berg *et al.*, 2014; Findlay, 2016). The rate law for pyrite formation via the polysulfide pathway was derived by Rickard (1975), with a correction later published due to incorrect unit conversion in the original publication (Wan *et al.*, 2017).

The thermodynamic feasibility of pyrite formation via the H_2S pathway, even at low-temperature, biological conditions, was known long before being experimentally demonstrated (Berner, 1970; Rickard, 1997; Rickard and Luther, 1997). The first observations of pyrite formation coupled with dihydrogen production came from hydrothermal experiments (Wikjord *et al.*, 1976, 1980; Taylor *et al.*, 1979). In highly reducing environments where stronger oxidants are absent, H_2S can oxidize FeS to pyrite (Rickard, 1997; Rickard and Luther, 1997). This direct reaction leads to the production of H_2, which can then reduce carbon dioxide to organic molecules in the presence of a mineral or enzyme catalyst. In fact, the formation of pyrite via the H_2S pathway helped fuel the iron-sulfur world hypothesis for the origin of life (Wächtershäuser, 1988, 1992; Drobner *et al.*, 1990). Although another mechanism, known as the iron-loss pathway, was proposed to explain the production of dihydrogen by the oxidation of two FeS molecules to pyrite and dissolved Fe^{2+} (Schoonen and Barnes, 1991; Wilkin and Barnes, 1996), it is now considered to be derived from the H_2S pathway (Butler *et al.*, 2004). There is evidence from the sulfur isotopic composition of pyrite formed via the H_2S route that it is a product of the equimolar mixing of the FeS and H_2S pools (Butler *et al.*, 2004).

Although HS^- is simply the deprotonated form of H_2S, differences in electron orbital energy levels make HS^- an incompatible electron acceptor in the H_2S pathway. For this reason, the H_2S pathway was initially suggested to be dominant in neutral to acidic environments, while the polysulfide pathway is dominant under alkaline conditions (Rickard and Luther, 1997; Thiel *et al.*, 2019). The favourability of the reaction is also influenced by the microbial scavenging of H_2. For example, hydrogenotrophic methanogens growing together with sulfate-reducing bacteria probably maintain this reaction in pyrite-precipitating enrichment cultures (Thiel *et al.*, 2019). The H_2S pathway is assumed to be more widespread

https://doi.org/10.1180/gbi.2024.9 Published online by Cambridge University Press

in strictly anoxic subsurface sediments (Rickard, 1997) and could have been the dominant pyrite formation mechanism in the ferruginous Archean Ocean before the Great Oxygenation Event (Lyons *et al.*, 2014).

Nonetheless, studies have shown that mackinawite and H_2S can remain incredibly stable over months in strict anoxic conditions even during hydrothermal processing (Benning *et al.*, 2000; Cahill *et al.*, 2000; Swanner *et al.*, 2019), in contrast to the fast rates of the H_2S pathway initially reported in Rickard (1997). These studies demonstrated that slightly oxidized iron sulfide precursors actually drove pyrite formation. Anaerobic cultivation techniques and sensing technologies used to measure oxygen have evolved a long way since early experiments (Wikjord *et al.*, 1976; Taylor *et al.*, 1979; Drobner *et al.*, 1990; Rickard, 1997; Rickard and Luther, 1997), so one cannot exclude the possible influence of very low oxygen concentrations in previous studies. In these cases, the surface oxidation of iron sulfide precursors may have been sufficient to drive pyrite formation under not strictly anoxic conditions, perhaps via a combination of different pathways.

Since FeS formation can be directly linked to the sulfidation of Fe(III) (hydr)oxides, it eventually became clear that surface-mediated reactions could play a role in pyrite formation. Nevertheless, it required a combination of bulk chemical and modern micro- to nano-scale imaging methods to finally elucidate the steps following the electron transfer reaction between sulfide and Fe(III) (hydr)oxides. In experiments mixing dissolved sulfide and lepidocrocite, TEM, XRD and Mössbauer were used to observe a very rapid (<2 h) surface reaction with the formation of a mackinawite rim on lepidocrocite, which eventually dissolved at the expense of pyrite precipitation delocalized from the lepidocrocite surface (Hellige *et al.*, 2012). Further investigations with iron minerals of different crystallinity (ferrihydrite < lepidocrocite < goethite) revealed that sulfidation proceeds at different rates and that the formation of FeS (hours) and pyrite (weeks) is decoupled in time (Peiffer *et al.*, 2015). This led to the proposal of a third pathway for pyrite formation catalysed by Fe(III) minerals. The so-called ferric hydroxide surface pathway (FHS) begins with the formation of surface-bound, non-sulfur-associated Fe(II) (>$Fe(II)OH_2^+$) formed through surface complexation reactions (Table 2). These iron-hydroxy groups react with sulfide radicals to form surface-bound $Fe(II)S_2^-$ species and induce pyrite nucleation in conditions below supersaturation by creating a new equilibrium with the aqueous phase. The FHS pathway is predicted to be prominent in aquatic systems with abundant Fe(III) minerals, *i.e.* with terrestrial influence, (Wan *et al.*, 2017) because the reaction only proceeds if the precursor species >$Fe^{II}S_2^-$ incompletely covers the ferric hydroxide surface. Other compounds, like organic matter, have been found to mask ferric hydroxide reactive sites, slowing the formation of pyrite via the FHS pathway from 120 days (Wan *et al.*, 2017) to 12 months (ThomasArrigo *et al.*, 2020). Interestingly, the addition of dissolved (complexed) Fe^{3+} has commonly produced pyrite in abiotic experiments (Wei and Osseo-Asare, 1997; Morin *et al.*, 2017; Baya *et al.*, 2022) but only metastable iron sulfide phases in microbial experiments (Bertel *et al.*, 2012; Ikogou *et al.*, 2017). The few successes in obtaining biogenic pyrite in laboratory experiments have used solid Fe(III) minerals (Rickard, 1969b; Ivarson and Hallberg, 1976; Berg *et al.*, 2020; Duverger *et al.*, 2020). Together, these results suggest that further studies on sulfidization pathways on common iron mineral phases should include organic matter and microorganisms in order to better represent environmental conditions.

Biogenic iron sulfide mineral formation at high temperatures

The black smokers as Fe- and S-rich systems

The most extreme hyperthermophilic microorganisms have been isolated from hydrothermal vents (Huber *et al.*, 1991; Blöchl *et al.*, 1997; Takai *et al.*, 2001), which represent the most biologically active sites in the deep ocean found along mid-ocean ridges and discovered in 1977 (Corliss *et al.*, 1979; Hannington *et al.*, 1995). These environments are characterized by unique physical and chemical properties such as high hydrostatic pressures, high temperatures and often highly dissolved metal contents. Among those, black smokers are iron- and sulfur-rich anaerobic systems (Holden *et al.*, 2012) that form chimneys up to 45 metres tall (Hannington *et al.*, 1995). Cold seawater infiltrates down through the oceanic crust, is heated in contact with the magma chamber, becomes less dense, and then rises to the seafloor, dissolving metals and sulfides from the surrounding basaltic rocks (Humphris and Mccollom, 1998; Fouquet *et al.*, 2010). Sulfur species are abundant and present in several redox states in hydrothermal environments (from –2 to +6), both in inorganic and organic forms. Inorganic sulfur appears in various forms such as metal sulfides (chalcopyrite $CuFeS_2$, pyrite FeS_2, sphalerite ZnS) (Tivey and Delaney, 1986; Peng and Zhou, 2005), as well as nanoparticles of elemental sulfur (S^0), hydrogen sulfide (H_2S), hydrosulfide (HS^-), hydrogen polysulfides (HS_n^-) and polysulfides (S_n^{2-}) (Schwarzenbach and Fischer, 1960; Rickard and Luther, 2007; Gartman *et al.*, 2011). These are predominantly found in plumes and in the reducing parts of hydrothermal chimneys (Findlay *et al.*, 2014; Findlay, 2016). The presence of both oxidized and reduced sulfur compounds in the hydrothermal ecosystem supports the development of metabolically diverse microorganisms (Orcutt *et al.*, 2011; Dick, 2019). Sulfides and hydrogen sulfide can also result from MSR and/or reduction of elemental sulfur. Consequently, the sulfide content of black smokers originates from a mixture of abiotically produced sulfide through high-temperature chemical reactions and biotically produced sulfide *via* microbial activities, complicating the interpretation of sulfur-based biosignatures in such ecosystems.

Iron is found at very high concentrations, up to 25 mM (Holden and Adams, 2003; Tivey, 2007; Toner *et al.*, 2016). In the anaerobic, reducing and high-temperature hydrothermal fluid, iron is mainly present as the soluble ferrous form Fe^{2+}, while in the surrounding oxygenated seawater, iron is rapidly oxidized into the ferric form Fe(III) and precipitates as iron (oxyhydr)oxide minerals (Rickard and Luther, 2007; Scholten *et al.*, 2019). In the fluid (>250°C), Fe^{2+} reacts with sulfide to form inorganic massive iron sulfide deposits, beginning with FeS mackinawite/ pyrrhotite, which is thermodynamically unstable, and then rapidly evolving into FeS_2 pyrite (Rickard and Luther, 2007), the major sulfide component of the interior of black smokers (Fouquet *et al.*, 1997). Whereas Fe_3S_4 greigite is considered an intermediate phase in the process of pyrite formation (Hunger and Benning, 2007), no occurrence of greigite has been reported in hydrothermal chimneys. Pyritization is thus the main process in black smokers but the mechanism of pyrite formation is still being debated, especially for pyrite forming at relatively low temperatures (<150°C) in the external parts of chimneys, which may involve the living compartment (Juniper and Martineu, 1995; McCollom, 2007).

To elucidate the process of microbial synthesis of pyrite, several experiments have aimed to mimic environmental conditions in laboratory experiments using mesophilic microorganisms to produce pyrite (see section 'Biogenic pyrite formation at low temperature'). But pyrite formation in direct connection to the activity of

https://doi.org/10.1180/gbi.2024.9 Published online by Cambridge University Press

hyperthermophilic microorganisms has rarely been reported in the literature (Stetter *et al.*, 1983; Gorlas *et al.*, 2018, 2022; Truong *et al.*, 2023).

Pyrite formation by hyperthermophiles

More than two decades ago, Stetter and colleagues published the first observation of pyrite formation resulting from a biogenic process at a high temperature (Stetter *et al.*, 1983). Pyrite was formed during the growth of the sulfur-reducing archaeon *Pyrodictium occultum* in a medium containing a final concentration of 10 μM $FeSO_4$, in a fermenter at 95°C. This biogenic pyrite formation could be explained by an interaction between the metabolic end-product H_2S, formed from sulfur reduction, with dissolved Fe^{2+} according to the H_2S pathway (Table 2).

Unfortunately, there have been no further studies to confirm or refute this following these initial observations. Recent experiments were specifically designed to investigate the formation of Fe-S minerals by hyperthermophilic Archaea belonging to the *Thermococcales* order (Gorlas *et al.*, 2018), which are predominant inhabitants of the hottest parts of hydrothermal environments (Takai *et al.*, 2001). Under laboratory conditions, the sulfur-reducers *Thermococcales* are able to generate significant amounts of pyrite within a few hours and could be an important contributor to pyrite formation in their ecosystem (Gorlas *et al.*, 2022). Cells grown in a modified rich medium supplemented with S^0 (1 g/L or 31 mM) were incubated with a solution of ferrous sulfate (5 mM of $FeSO_4$), under strict anoxia at 85°C (Gorlas *et al.*, 2018, 2022). The amount of pyrite production increases as the mineralization duration lengthens (Truong *et al.*, 2023). Pyrite nanocrystals are consistently found to have a close association with the cells and with sulfur vesicles produced by *Thermococcales* during their growth (Gorlas *et al.*, 2022). This leads to the production of pyrite spherules with ultra-smooth surfaces having diameters ranging between 200 nm to 1 μm (with a marked abundance maximum around 1 μm) made up of an assemblage of very numerous domains ranging between 5 and 15 nm (Truong *et al.*, 2023). This assembly of small domains explains the ultra-smooth appearance of pyrite spherules. Interestingly, the presence of pyrite was detected only when *Thermococcales* were cultivated in a growth medium initially containing zero-valent sulfur S^0 (Gorlas *et al.*, 2022). In these growth conditions, *Thermococcales* cells internalized high sulfur concentrations leading to the production of numerous sulfur vesicles probably derived from polysulfides. This process has been interpreted as a polysulfide detoxification mechanism (Gorlas *et al.*, 2015). Gorlas *et al.* (2022) proposed that in the presence of abundant Fe^{2+}, those sulfur vesicles allowing reactive sulfur to be exposed at cell surfaces could act as precursors for pyrite formation. Conversely, under growth conditions in which *Thermococcales* do not produce such sulfur vesicles but sulfide instead, no formation of pyrite occurs, suggesting that pyrite is produced through *Thermococcales* preferentially via the polysulfide pathway rather than the H_2S pathway (Gorlas *et al.*, 2022).

The initial occurrence of the FeS nano-mackinawite, observed in short-term experiments (*i.e.* after 5 hours of mineralization) (Truong *et al.*, 2023), could be attributed to the interaction between Fe^{2+} and the H_2S produced during *Thermococcales* growth. Thus Truong *et al.* (2023) proposed that the formation of pyrite particles induced by the presence of *Thermococcales* and their sulfur vesicles occurs due to a redox comproportionation of S^0 (from elemental sulfur) and sulfide (S-II) (from FeS) to yield S (-I) in pyrite particles. This suggests a high degree of metabolic adaptability by *Thermococcales*. This capability allows *Thermococcales* to adjust their metabolic activities in response to variations in sulfur and iron availability, which may fluctuate in hydrothermal vent environments.

Greigite formation by Thermococcales

Thermococcales have also been recognized for producing cuboidal extracellular nanocrystals of Fe_3S_4 greigite within a few days, with sizes ranging from 40 to 60 nm, regardless of the presence or absence of sulfur vesicles (Gorlas *et al.*, 2018, 2022; Truong *et al.*, 2023). Greigite formation occurs in close proximity to cells and vesicles that yield pyrite spherules. While conventional models of greigite formation from FeS typically involve an excess of sulfur or an iron loss pathway (Wilkin and Barnes, 1996), Gorlas *et al.* (2018) proposed that those greigites related to the biological activity of *Thermococcales* were formed by sulfurization of amorphous Fe(III)-bearing phosphates loaded onto cellular debris. Production of greigite was also observed during the growth of the hyperthermophile methanogen *Methanocaldoccus jannaschii* at 80°C when hematite was added to the growth medium (Igarashi *et al.*, 2016). Following the reduction of sulfur by the methanogen, hematite was reduced to form amorphous FeS, subsequently reacting with residual Fe(III) into greigite-like nanoflakes. The presence of Fe(III), either because it is added or because it is intrinsically produced, therefore seems to be a sufficient condition to form greigites in these strictly anoxic environments. In the case of *Thermococcales*, the mechanism by which Fe(III) is generated has yet to be elucidated (Kish *et al.*, 2016). Finally, it is likely that over long periods of time, some of the greigites formed by these processes subsequently evolve into pyrite, but it is clear that in the case of *Thermococcales*, greigite formation is not just an intermediate towards pyrite but constitutes a pathway on its own.

The efficiency with which *Thermococcales* produce pyrite and greigite in laboratory settings suggests that they are able to replicate this biomineralization process in their native environment. Consequently, the hyperthermophiles *Thermococcales* may play a significant role in the formation of 'low temperature' pyrite in their ecosystem. Furthermore, this biologically induced mineralization mechanism of Fe-S minerals by *Thermococcales* could be a key component of their survival strategy to thrive in highly mineralized, high-temperature environments (Gorlas *et al.*, 2022).

Integrating various pyrite formation pathways: Connecting experiments to the environment

Recent experiments have shed light on how microorganisms contribute to pyrite formation beyond the simple role of SRM as providers of sulfide. In this section, we synthesize the relevance of these experiments to natural environments.

As discussed in previous sections, there is a consensus that biogenic pyrite can form via three distinct pathways. In nature, while each of these pathways may be more important under certain conditions, it is likely that all three will operate at the same time. This is in fact what is observed in recent cultivation work (see previous two sections), in which microorganisms (sometimes as a community) affect both the Fe and S cycles, generating intermediates that promote pyrite formation. Therefore, it is important to consider the interactions and processes associated with all the pathways rather than viewing them separately (Fig. 2).

https://doi.org/10.1180/gbi.2024.9 Published online by Cambridge University Press

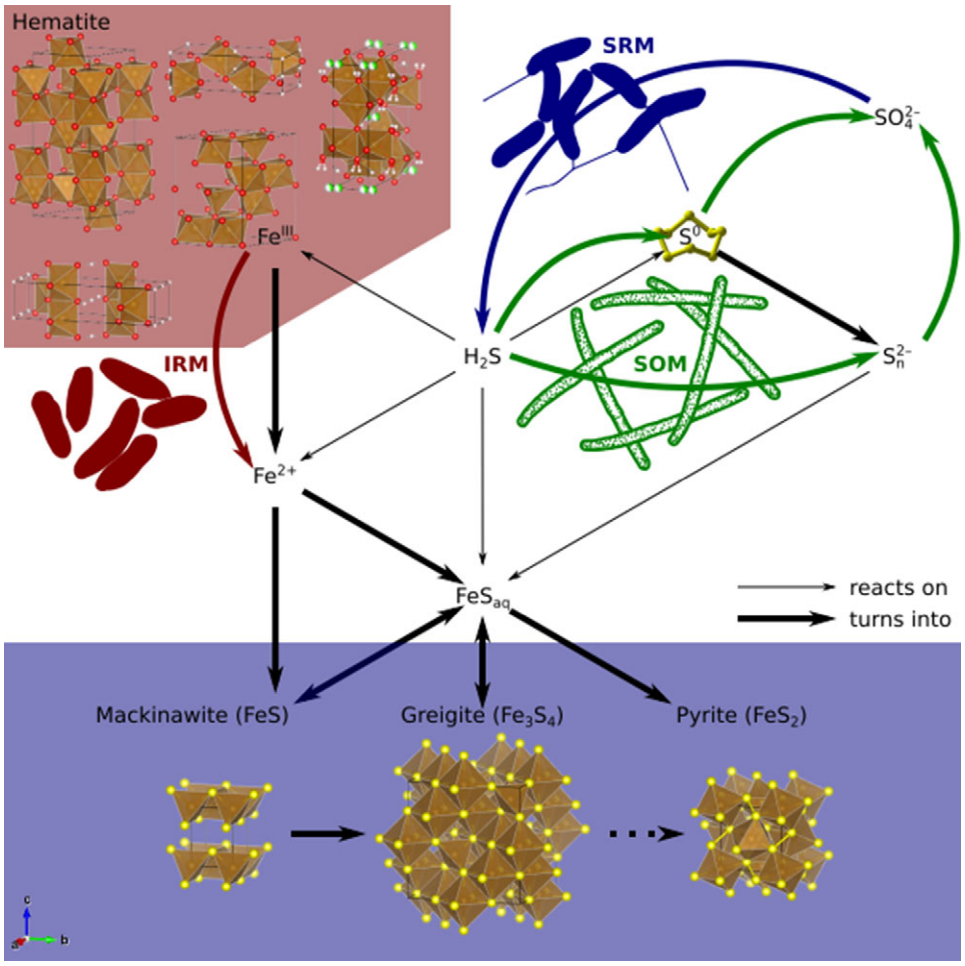

Figure 2. Summary of interactions between Fe and S cycles driven by abiotic and microbial processes to generate Fe sulfide minerals. In this figure, the H_2S, polysulfide and FHS pathways are considered together rather than separately. SRM (blue): sulfate-reducing microorganisms, SOM (green): sulfur/sulfide oxidizing microorganisms, IRM (red): iron-reducing microorganisms.

Biogenic pyrite formed in experiments have adopted either a micrometric spherulitic (Berg *et al.*, 2020; Duverger *et al.*, 2020; Truong *et al.*, 2023) or euhedral morphology (Thiel *et al.*, 2019; Allen *et al.*, 2021), with no reported formation of framboids. It has long been suggested that the unique framboidal morphology is a strong indicator of biological activity, but evidence for that is lacking (Runge *et al.*, 2024). The research focus is now shifting to trying to understand the origin and abundance of pyrite spherules. Reports of framboids and euhedral pyrite are common in nature, perhaps due to their easily recognizable morphology even in complex sediments. By contrast, micrometric pyrite spherules have only recently been reported (Truong *et al.*, 2024) but could be more common once greater scrutiny is applied.

Lastly, as the morphology of pyrite is controlled by precipitation rate (among other factors; see Raiswell, 1982; Butler and Rickard, 2000; Runge *et al.*, 2023, 2024), it is important that the formation rates of biogenic pyrite in experiments match those observed in nature. To this end, we have expanded the pyrite precipitation rate dataset from Mansor and Fantle (2019) to include older data from salt marshes (based on ^{35}S incorporation into pyrite; Howarth and Giblin, 1983; Howarth and Merkel, 1984) and recent data from microbial (Berg *et al.*, 2020; Gorlas *et al.*, 2022; Truong *et al.*, 2023) and abiotic experiments (Hockmann *et al.*, 2020; ThomasArrigo *et al.*, 2020; Baya *et al.*, 2021; Domingos *et al.*, 2023; Runge *et al.*, 2023, 2024). As can be seen in Fig. 3, most microbial pyrite (0.0009–0.35 mM/day) is precipitated at the same rates as in salt marshes (0.0009–0.35 mM/day) and the upper estimates of marine sediments (10^{-5} to 0.09 mM/day). The only exception is the extremely fast pyrite formation by S^0 disproportionaters (0.2–4.3 mM/day; Canfield *et al.*, 1998). This comparison generates confidence that lab studies are indeed relevant to nature. Rates in natural hydrothermal systems were unfortunately not readily available from the literature for comparison.

It is interesting to note that pyrite precipitates faster in salt marshes than in marine sediments, perhaps due to its more dynamic oxic-anoxic cycles that generate redox-active intermediates (*e.g.* S^0 or polysulfides). It is also interesting to note that rates derived for pyrite precipitation within plant cells (Rickard *et al.*, 2007) and the theoretical estimates for framboids (Guilbaud *et al.*, 2011; Rickard, 2019; based on the burst nucleation model) are around 800–17,000 mM/day, which are orders of magnitude higher than most of the dataset. Whether these anomalously fast rates are valid or not remains to be determined. One explanation could be that these rates reflect precipitation in microenvironments with locally enhanced supersaturation, while the rest of the dataset primarily reflects bulk rates averaged over at least centimetre scales. In sediments, the site of pyrite formation is known to be heterogenous and to be enhanced around organic matter, clays or shell remains (*e.g.* Marin-Carbonne *et al.*, 2022). Hence, the elevated rates could in theory be also achievable in cultivation experiments and at the same time remain relevant to nature.

https://doi.org/10.1180/gbi.2024.9 Published online by Cambridge University Press

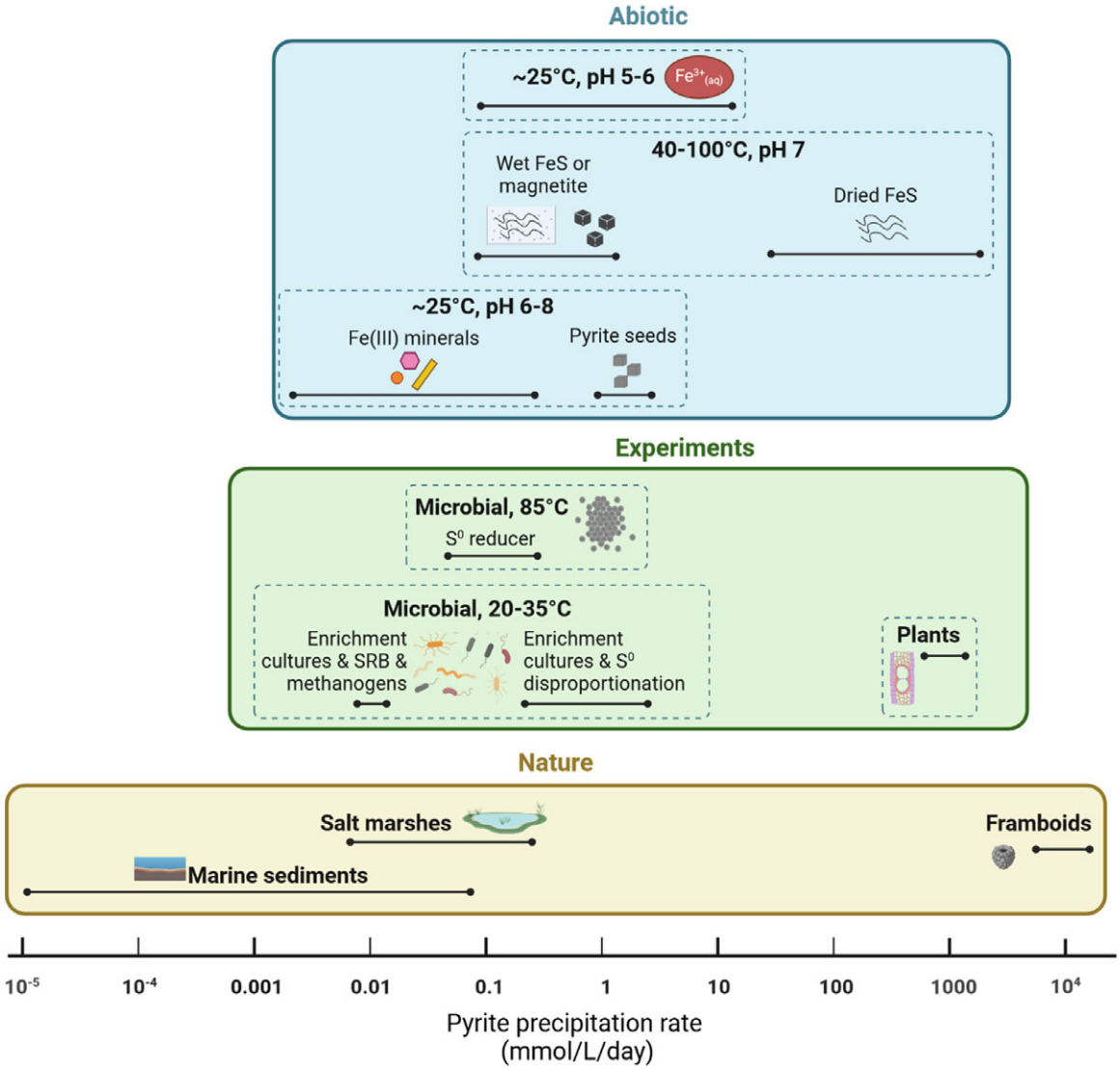

Figure 3. Compiled pyrite precipitation rates in the environment and in biological and abiotic experiments. The figure was updated from Mansor and Fantle (2019) with additional data from: salt marshes – Howarth and Giblin (1983); Howarth and Merkel (1984); framboids – Rickard (2019); microbial 24–35°C – Thiel *et al.* (2019); Berg *et al.* (2020); microbial 85°C – Gorlas *et al.* (2022; Truong *et al.* (2023); abiotic at 25°C with Fe(III) minerals – Hockmann *et al.* (2020); ThomasArrigo *et al.* (2020); abiotic at 40–100°C with wet FeS or magnetite - Domingos *et al.* (2023); Runge *et al.* (2023, 2024) and abiotic at pH 5–6 at 25°C – Baya *et al.* (2021).

Fe-S minerals and the origin of life

Fe-S minerals probably played a pivotal role in the genesis of life by actively participating in the generation of prebiotic molecules (Picard *et al.*, 2021) and/or by preserving ancient traces of life (Wacey *et al.*, 2011; Baumgartner *et al.*, 2019, 2020). Ferredoxin, one of the oldest biological catalysts, contains Fe-S clusters, which suggests an ancient origin. Examples of Fe-S clusters are widespread in biogeochemistry, where they serve as active centres in essential proteins, including NADH dehydrogenase, coenzyme Q – cytochrome C reductase, hydrogenases and nitrogenase (Beinert, 2000; Johnson *et al.*, 2005; Huang *et al.*, 2024).

Wächterhauser introduced the 'iron sulfur world' prebiotic model in 1988, proposing that iron sulfides in hydrothermal conditions could facilitate the formation of prebiotic molecules such as amino acids. This theory suggests that mineral surfaces provide the catalytic properties necessary for the formation of simple organic molecules from inorganic compounds. In high temperature, high-pressure conditions, H_2 and CO_2 can interact with metal sulfides leading to the synthesis of amino acids, peptides (Bonfio *et al.*, 2017) and eventually nucleotides, the building blocks of life (Table 3). Pyrite precipitation provides the energy required for CO_2 reduction, leading to the creation of reduced sulfur organic molecules (Huber and Wächterhäuser, 1997). Negatively charged organic molecules can then bind to the positively charged pyrite surface, catalysing their transformation into more complex molecules and enhancing molecular diversity. Experimental successes include the production of thiolated formic acid and CH_3COSH, a precursor for the citrate cycle acetyl coenzyme A (Huber and Wächterhäuser, 1997). Thermodynamic calculations have also supported the formation of amino acids in hydrothermal conditions (Amend and Shock, 1998 and references therein). Notably, experiments on other sulfides, such as chalcopyrite or sphalerite, have not yielded amino acids, emphasizing the unique role of Fe-S minerals (and sometimes nickel sulfides) in these prebiotic processes (Schreiner *et al.*, 2011).

https://doi.org/10.1180/gbi.2024.9 Published online by Cambridge University Press

Table 3. Production of reduced organic molecules from CO_2 reactions with metal.

H source	Fe source	Molecules produced	References
H_2	Metal	Formate, acetate	He *et al.* (2010)
H_2	Metal	Formate, acetate, methanol pyruvate	Varma *et al.* (2018)
H_2S	Greigite	Formate, acetate, methanol, pyruvate	áde Leeuw (2015)
H_2S	Pyrite, awaruite, CoS, MoS, CuS	Formate	He *et al.* (2019)
H_2	Greigite, magnetite, awaruite	Formate, acetate, methanol pyruvate	Muchowska *et al.* (2019); Preiner *et al.* (2020)
H_2	Co oxide and silica particles	Formate, acetate, methane, ethane	Belthle *et al.* (2022)
H_2	Awaruite, metal	Formate, acetate, pyruvate	Beyazay *et al.* (2023)
H_2	Fe-Ni particles	Formate, acetate, pyruvate	Belthle and Tüysüz (2023)

An alternative theory suggests that mackinawite or greigite can serve as catalytic centres, with FeS bubbles acting as proto-cell membranes, instead of lipids, that promote the formation of organic molecules (Russell *et al.*, 2010). In this model, FeS bubbles can precipitate when alkaline fluids are injected into acidic Fe^{2+}-rich solutions, mimicking conditions in hydrothermal regions of the Hadean Ocean. The geochemical pH gradient then provides energy through the FeS membrane (Fig. 4). Nucleic acids can bind to mackinawite nanoparticles, as demonstrated by Hatton and Rickard (2008). This hypothesis suggests that the compartmentalization of membranous FeS precipitates is crucial for maintaining a chemical gradient needed for carbon fixation metabolism (Fig. 4).

Moreover, iron sulfide surfaces can also support an autocatalytic chemolithotrophic metabolism driven by the exergonic formation of pyrite, leading to a chemoautotrophic origin of primordial metabolisms (Wächtershäuser, 1988; Cody, 2004). The hypothesis of protometabolism catalysed by ancient iron sulfur active centres has been successfully tested (Bonfio *et al.*, 2017). Recent studies have highlighted that greigite can catalyse the fixation of CO_2 under hydrothermal alkaline conditions, thus potentially preceding the enzyme route for the acetyl-CoA pathway (Preiner *et al.*, 2020). Similarities between the spatial organization of enzymes and Fe-S minerals have been recognized, suggesting an abiotic origin of these catalysts (Russell *et al.*, 2014). Other experimental studies have indicated that Fe-S minerals (Fig. 4) possess the capability to support a proto-metabolic process (Lazcano and Miller, 1999; Cody, 2004; Goldford *et al.*, 2019).

An ancient origin for Fe and S microbial metabolisms is supported by phylogenetic studies and other geochemical indicators (Lepot, 2020; Lyons *et al.*, 2024). Indeed, microorganisms that are closely related to the last common ancestor are mainly anaerobic and sulfur-reducing hyperthermophiles. Isotopic studies on ancient pyrite sediments have constrained the antiquity of microbial sulfate reduction at 3.5 Ga (Shen and Buick, 2004), with further evidence at 2.7 Ga (Archer and Vance, 2006; Marin-Carbonne *et al.*, 2018). Experimental studies have also shown that both archaea and bacteria closely related to the last common ancestor can reduce Fe (III) (Vargas *et al.*, 1998; Lovley *et al.*, 2022), suggesting an early origin of dissimilatory iron reduction. Geochemical studies on ancient pyrite have thus identified isotopic fingerprints of this metabolism in the geological record, from 3.2 Ga (Marin-Carbonne *et al.*, 2020), to the late Archean (Archer and Vance, 2006; Craddock and Dauphas, 2011; Czaja *et al.*, 2016). These findings highlight the important role that microbial metabolism played in shaping the early Earth's

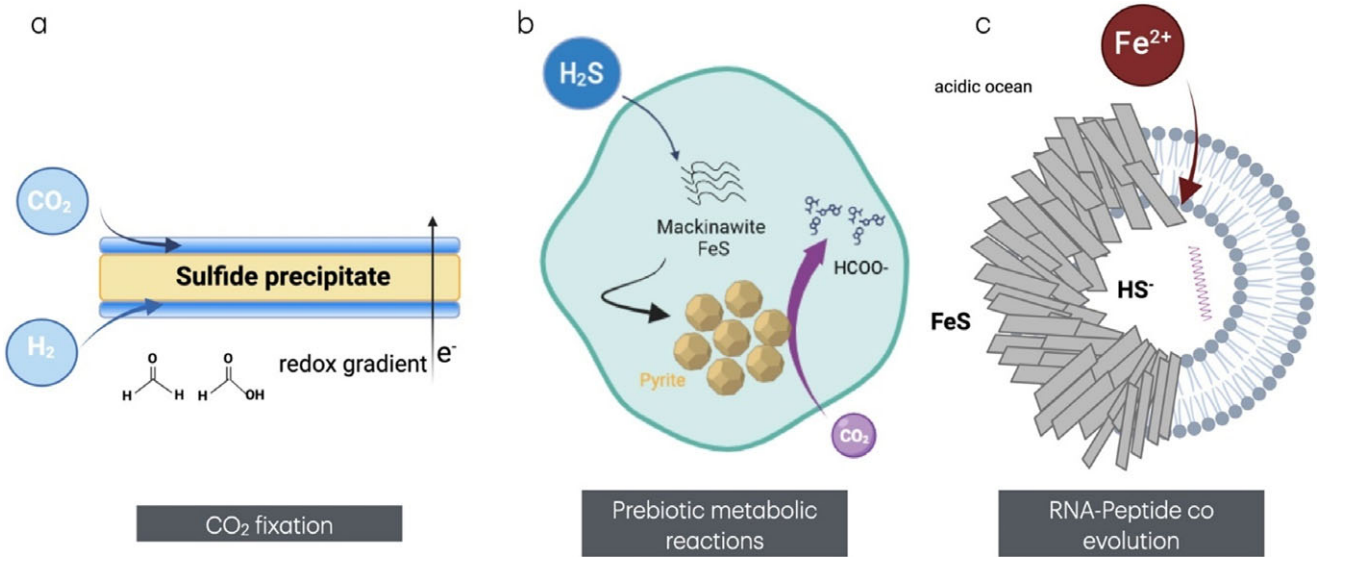

Figure 4. Various examples of reactions relevant to the origin of life that involve Fe-S minerals, (a) CO_2 fixation schematic modified from De Graaf *et al.* (2023), based on prior experiments (Herschy *et al.*, 2014; Sojo *et al.*, 2016; Hudson *et al.*, 2020), (b) prebiotic metabolic reaction in a protocell modified from Alpermann *et al.* (2011) and (c) RNA-peptide co-evolution around hydrothermal vents. Bubbles from vents could form a membrane associated with iron sulfides. RNA bound to the minerals could act as a template for peptide formation (Russell and Hall, 1997).

https://doi.org/10.1180/gbi.2024.9 Published online by Cambridge University Press

environment and lay the groundwork for the identification of biosignatures in the sedimentary record.

Sedimentary pyrite as environmental proxies and biosignatures

Background

In contrast to metastable iron sulfides, pyrite is prevalent in sedimentary rocks, with its presence dating back to approximately 3.8 billion years ago (Ga) (Smith *et al.*, 2005). The ubiquity of pyrite in sedimentary rocks, as shown in Fig. 1, has led to the use of pyrite abundance, isotopic characteristics, and trace metal concentrations to reconstruct past environmental conditions, aiding in the understanding of historical atmospheric oxygen levels, as well as global sulfur and iron geochemical cycles over Earth's geological history. For instance, the recognition of detrital pyrite grains apparently eroded by flowing water serves as a robust indicator of low oxygen (O_2) levels before approximately 2.4 Ga (Johnson *et al.*, 2014). This timing aligns with the loss of sulfur mass-independent fractionation (S-MIF, see box), which is commonly attributed to the shift from an anoxic atmosphere ($pO_2 < 10^{-15}$ PAL) to an oxic atmosphere (Farquhar *et al.*, 2000).

Furthermore, the primary mechanism for the long-term storage of reduced sulfur species on geological timescales is the formation and subsequent burial of pyrite. This process, in conjunction with the burial of organic carbon, contributes significantly to maintaining the oxidized surface conditions of Earth (Canfield and Farquhar, 2009). Consequently, methods have been developed to gauge past oxidation states and water chemistry by examining the iron (-sulfur) mineralogy in sediment and sedimentary rocks (Raiswell and Canfield, 2012; Raiswell *et al.*, 2018). These methods are grounded in the differential reactivity of iron phases towards sulfide, and thus, rely on pyrite precipitation. The presently utilized framework (Poulton and Canfield, 2005), known as the 'Fe speciation' proxy, involves quantifying the ratio of highly reactive iron to total iron (Fe_{HR}/Fe_T) and the ratio of pyrite to highly reactive iron (Fe_{PYR}/Fe_{HR}). The application of Fe speciation data, whether derived from stratigraphic variations or collected across various locations over time or space, has significantly contributed to our understanding of the evolution of ocean redox conditions (Poulton, 2021 and references therein). It has revealed that during the Archean and Phanerozoic eras, oceans were predominantly ferruginous (characterized by anoxic conditions and high Fe^{2+} levels) and oxygenated, respectively. In the Proterozoic era, rising oxygen levels facilitated the development of euxinic conditions at mid-depth, particularly in restricted basins while the deep ocean maintained predominantly ferruginous conditions (Poulton *et al.*, 2004a; Planavsky *et al.*, 2011; Ostrander *et al.*, 2019). It is important to note that recent concerns have been raised regarding the effectiveness of the extraction protocol in retrieving the targeted mineral phases (Hepburn *et al.*, 2020; Slotznick *et al.*, 2020) and the influence of early diagenesis (Eroglu *et al.*, 2021; Hutchings and Turchyn, 2021; Pasquier *et al.*, 2022). These concerns question the capacity of the 'Fe speciation' approach to accurately constrain the chemistry and oxidation state of water columns, both in the present and in the past (Pasquier *et al.*, 2022).

Box: Isotope notation

Most chemical reactions, including those involved in the formation of pyrite, distribute isotopes proportionally to their mass. Here, we illustrate this concept using the four stable sulfur isotopes (^{32}S, ^{33}S, ^{34}S and ^{36}S) as an example. A similar analysis can be conducted with the iron isotopic system (Dauphas *et al.*, 2017).

In Mass-Dependent Fractionation (MDF), it is anticipated that the enrichment or depletion in ^{34}S is roughly twice and half of that in ^{33}S and ^{36}S, respectively. The theoretical slopes of the ^{33}S-^{34}S and ^{36}S-^{34}S MDF, denoted as $^{33}\lambda$ and $^{36}\lambda$, are 0.515 and 1.89, respectively (Young *et al.*, 2002; Farquhar *et al.*, 2003). However, various physical and (bio)chemical processes exhibit mass dependencies that subtly deviate from these values (Farquhar *et al.*, 2003; Ono *et al.*, 2006; Johnston *et al.*, 2007). When these slight variations appear in the isotopic composition of pyrite (and other materials), they are commonly represented as $\Delta^{3x}S$, where the superscript 3x denotes one of the rare isotopes of sulfur, ^{33}S, or ^{36}S. In its linear definition, $\Delta^{3x}S = \delta^{3x}S - {}^{3x}\lambda \times \delta^{34}S$, where $\delta^{3x}S=[(^{3x}S/^{32}S)_{sample} / (^{3x}S/^{32}S)_{standard}-1]*1000$. The values of $\delta^{3x}S$ are reported in permil (‰) with respect to the sulfur isotope international standard Vienna Canyon Diablo Troilite (VCDT). The observation that different processes exhibit distinct mass dependencies (*e.g.* Young *et al.*, 2002; Johnston *et al.*, 2007; Zerkle *et al.*, 2009; Johnston, 2011; Wing and Halevy, 2014; Eldridge and Farquhar, 2018) suggests that studying MDF may offer a more comprehensive understanding of how biological processes and/or local sedimentological conditions influence sulfur cycling in marine sediments.

A notable characteristic of early Earth sulfur-bearing material is the preservation of ^{33}S-^{32}S and ^{36}S-^{32}S ratios that significantly deviate from MDF, known as Mass-Independent Fractionation (MIF, or S-MIF; (Farquhar *et al.*, 2000). Based on experimental SO_2 photolysis and an atmospheric chemistry model, the conservation of substantial and variable S-MIF signals in Archean and early Paleoproterozoic sedimentary rocks necessitates an extremely low partial pressure of O_2 (Farquhar *et al.*, 2001; Catling and Zahnle, 2020). Therefore, the S-MIF signal is considered one of the strongest pieces of evidence for an anoxic atmosphere before ≈2.4 Ga. Although the atmospheric production of S-MIF is well established, the exact underlying mechanism and the identity of its carriers to the surface remain unclear and subject to intense debate (Halevy *et al.*, 2010; Halevy, 2013; Endo *et al.*, 2019; Reed *et al.*, 2022; Oduro *et al.*, 2023).

Texture and composition

Pyrite grains display a large range of sizes, spanning from centimetres to nanometres, and a variety of textures, *e.g.* euhedral/anhedral, nodule and framboidal are among the most common (see Fig. 1). Framboids, in particular, are characterized as spherical to subspherical clusters comprised of numerous microcrystals of pyrite, predominantly found in sedimentary environments (Wang and Morse, 1996; Wilkin and Barnes, 1997; Rickard, 2019). Irrespective of its shape, during its crystallization, pyrite has the capability to integrate various trace elements (TE), with chalcophile and siderophile elements being the most frequently encountered. These TE can be integrated into pyrite through two distinct mechanisms: either by substituting for Fe or S within the pyrite structure, or by existing as inclusions of distinct mineral phases or amorphous masses enclosed within the pyrite matrix (Gregory, 2020 and references therein). Of particular interest in enhancing our understanding of past environmental conditions is the observation that the TE content in pyrite is directly linked to the TE content of the water from which it precipitates (Gregory *et al.*, 2014). Consequently, TE within pyrite has been utilized to decipher the formation of ore deposits (Kusebauch *et al.*, 2019) and to unravel the evolution of ocean and atmospheric chemistry (*e.g.* Large *et al.*, 2014; Gregory *et al.*, 2017). Nevertheless, recent investigations have revealed that pyrite's TE concentration varies with depth within the sediment, ultimately reaching a plateau in composition (Gregory *et al.*, 2022a). This suggests that the relationship between the water column and pyrite's TE concentration is more intricate than previously assumed. Hence, TE contents in pyrite not only reflect the composition of the water column but also the composition of pore water, maybe allowing for tracking the release of trace elements from organic matter and/or iron (oxyhydr)oxides during

https://doi.org/10.1180/gbi.2024.9 Published online by Cambridge University Press

diagenesis, particularly when examined at a finer spatial resolution (Tribovillard *et al.*, 2006; Gregory *et al.*, 2022b; Atienza *et al.*, 2023). Biogenic pyrite experiments in the presence of TE have not been performed and it is unclear how biological activities can affect the incorporation of TE into pyrite. A recent study has also highlighted the importance of pyrite growth via particle attachment under certain conditions, which might impact the morphology and distribution of trace metals and isotopes within pyrite (Domingos *et al.*, 2023).

Sulfur isotopes

Sedimentary pyrite retains a distinct isotopic signature that reflects a combination of microbial metabolic processes and physical transport and mineralization. A broad taxonomic spectrum of microbes can change the oxidation state of sulfur to gain the energy required for cellular function and growth. Three main metabolic pathways are particularly important for the sulfur isotopic composition of pyrite: microbial sulfate reduction (MSR), sulfur disproportionation, and sulfide oxidation (Fike *et al.*, 2015; Jørgensen *et al.*, 2019). From each of them arises a metabolic-specific microbial fractionation of sulfur isotopes which discriminates heavy isotopes, reported afterwards as $^{34}\varepsilon$-$^{33}\lambda$ (see isotope notation box).

Over the past several decades, laboratory experiments using pure cultures of SRM have yielded variable apparent isotopic fractionation, from 65‰ to ≈5‰ (Detmers *et al.*, 2001; Johnston *et al.*, 2005b; Hoek *et al.*, 2006; Johnston *et al.*, 2007; Sim *et al.*, 2011a; Sim *et al.*, 2011b; Sim *et al.*, 2012; Leavitt *et al.*, 2013; Deusner *et al.*, 2014; Pellerin *et al.*, 2015; Bradley *et al.*, 2016; Smith *et al.*, 2020). However, it was not until we understood the enzymatic processes that drive MSR that the debate over the extent of microbial fractionation could be settled (Goldhaber and Kaplan, 1980; Ohmoto *et al.*, 1990; Rudnicki *et al.*, 2001; Wortmann *et al.*, 2001; Brunner *et al.*, 2005). Recent work shows that the microbial reduction of sulfate to sulfide is catalysed by a reaction network of four enzymatic steps, all of which are reversible (Johnston *et al.*, 2005b; Johnston *et al.*, 2007; Sim *et al.*, 2011a; Sim *et al.*, 2011b; Sim *et al.*, 2012; Leavitt *et al.*, 2013, 2024; Bradley *et al.*, 2016; Smith *et al.*, 2020). The emerging picture from laboratory cultures, bio-isotopic models, and modern environments is that a large $^{34}\varepsilon_{DSR}$ predominates in natural environments, ranging from 66 to 78‰ (Wing and Halevy, 2014; Halevy *et al.*, 2023). This substantial fractionation, which closely resembles the thermodynamic equilibrium between sulfate and sulfide (*i.e.* ≈70‰ at 20°C; Eldridge *et al.*, 2016), is attributed to the inherently low cell-specific sulfate reduction rates (csSRR) in marine sediments. In other words, all steps of the enzymatic pathway are fully reversible (*i.e.* equilibrium between reactant and product; Wing and Halevy, 2014). The observed inverse relationship between the $^{34}\varepsilon_{DSR}$ and the csSRR is responsible for the overall deviation from thermodynamic equilibrium observed in laboratory experiments (*i.e.* lower apparent fractionation). This relationship between $^{34}\varepsilon_{DSR}$ and csSRR can be extended to ^{33}S and, consequently, one can expect sulfide produced from MSR to be characterized by large, near-equilibrium $^{34}\varepsilon_{DSR}$ and $^{33}\lambda_{DSR}$ values. Culture experiments with green sulfur bacteria that oxidize sulfide showed smaller microbial S-isotope fractionations and small but nonzero $^{33}\lambda$ deviations from equilibrium (Zerkle *et al.*, 2009), whereas larger microbial S-isotope fractionations and $^{33}\lambda$ deviations from equilibrium were observed in pure cultures of sulfur disproportionators (Johnston *et al.*, 2005a; Fig. 5).

Once generated, a portion of this ^{34}S-depleted sulfide can react with dissolved ferrous iron (Fe^{2+}) or iron-bearing minerals (Fe(III)) to form FeS. The formation of FeS and its subsequent transformation into pyrite involves a relatively small isotopic fractionation, typically not exceeding a few ‰ (>5‰; Fry *et al.*, 1986; Böttcher *et al.*, 1998). Consequently, pyrite captures the isotopic composition of the products of microbial sulfur metabolisms (H_2S, HS^-), including small deviations from MDF, and thus may serve as a good recorder of past microbial activity. Interestingly, bulk pyrite S-isotope data do not meet the experimental expectations above. Several non-unique explanations that involve mixing between different sulfur pools or combinations of metabolic effects have been invoked to explain the apparent mismatch, clearly demonstrating that our current methodology is not suitable for uniquely distinguishing the various microbial pathways involved in pyrite formation (see Johnston, 2011 for a recent review).

The uncertainty in the interpretation of bulk $\delta^{34}S_{PYR}$ data can be resolved by studying the isotopic composition of individual pyrite grains, which collectively contribute to the bulk signal (Fike *et al.*, 2015; Marin-Carbonne *et al.*, 2022; Bryant *et al.*, 2023). As illustrated in Fike *et al.* (2015), when MSR occurs in a transport-limited system, the concentration of residual sulfate in porewater decreases, as do $\delta^{34}S_{SO4}$ and $\Delta^{33}S_{SO4}$, due to Rayleigh distillation. This results in a parallel increase in the instantaneous $\delta^{34}S_{H2S}$-$\Delta^{33}S_{H2S}$ that can be preserved in the accumulated pyrite pool. The magnitude of this enrichment depends on the fraction of sulfate consumed, the connectivity of the porewater sulfate pool with the overlying seawater column, and the fractionation associated with the redox transformation itself. Most of these factors depend on the local sedimentation regime, including the sedimentation rate, the iron and organic carbon loading and reactivity (Pasquier *et al.*, 2017; Liu *et al.*, 2021; Pasquier *et al.*, 2021a; Pasquier *et al.*, 2021b; Houghton *et al.*, 2022; Bryant *et al.*, 2023; Halevy *et al.*, 2023). As pyrite grains grow within the sediment, they continuously sample the evolving isotopic composition of microbially-produced sulfide throughout the sample's burial history, and when pyrite grains grow quickly, over short durations as for framboid morphology, it is expected that a time series of increasing $\delta^{34}S_{PYR}$ values will be recorded within the population of pyrite grains in each sample. In such instances, the minimum $\delta^{34}S_{PYR}$ can be used to assess the microbial fractionation specific to the depositional environment (Marin-Carbonne *et al.*, 2022; Bryant *et al.*, 2023) whereas the overall distribution of δ^{34}S is more likely to reflect the diagenetic evolution over the history of the sediment burial (Halevy *et al.*, 2023).

Assuming that MSR was established approximately 3.5 billion years ago (Shen and Buick, 2004; Mateos *et al.*, 2023), the sulfur isotopic compositions of pyrite (denoted as $\delta^{34}S_{PYR}$) are commonly utilized in both contemporary and ancient contexts to gain insights into the processes and fluxes within the global sulfur cycle. Within the framework of a global steady-state S cycle, the lowest δ^{34}S values reflect the maximum microbial fractionation whereas the departure from those low microbial values toward higher values indicates the evolution of MSR during the burial history of the sediment, irrespectively of the local and/or global oxygenation (Fig. 5). This pattern is typically interpreted as indicative of rising oxygen levels over time. This increase in oxygen may have resulted in more elevated oceanic sulfate levels and/or a reduction of the pyrite burial flux in response to more efficient organic matter oxidation (*i.e.* more aerobic respiration; Habicht *et al.*, 2002; Wu *et al.*, 2010; Leavitt *et al.*, 2013).

To delve further into this, Archean sedimentary rocks exhibit relatively low apparent fractionation between sulfate and pyrite

https://doi.org/10.1180/gbi.2024.9 Published online by Cambridge University Press

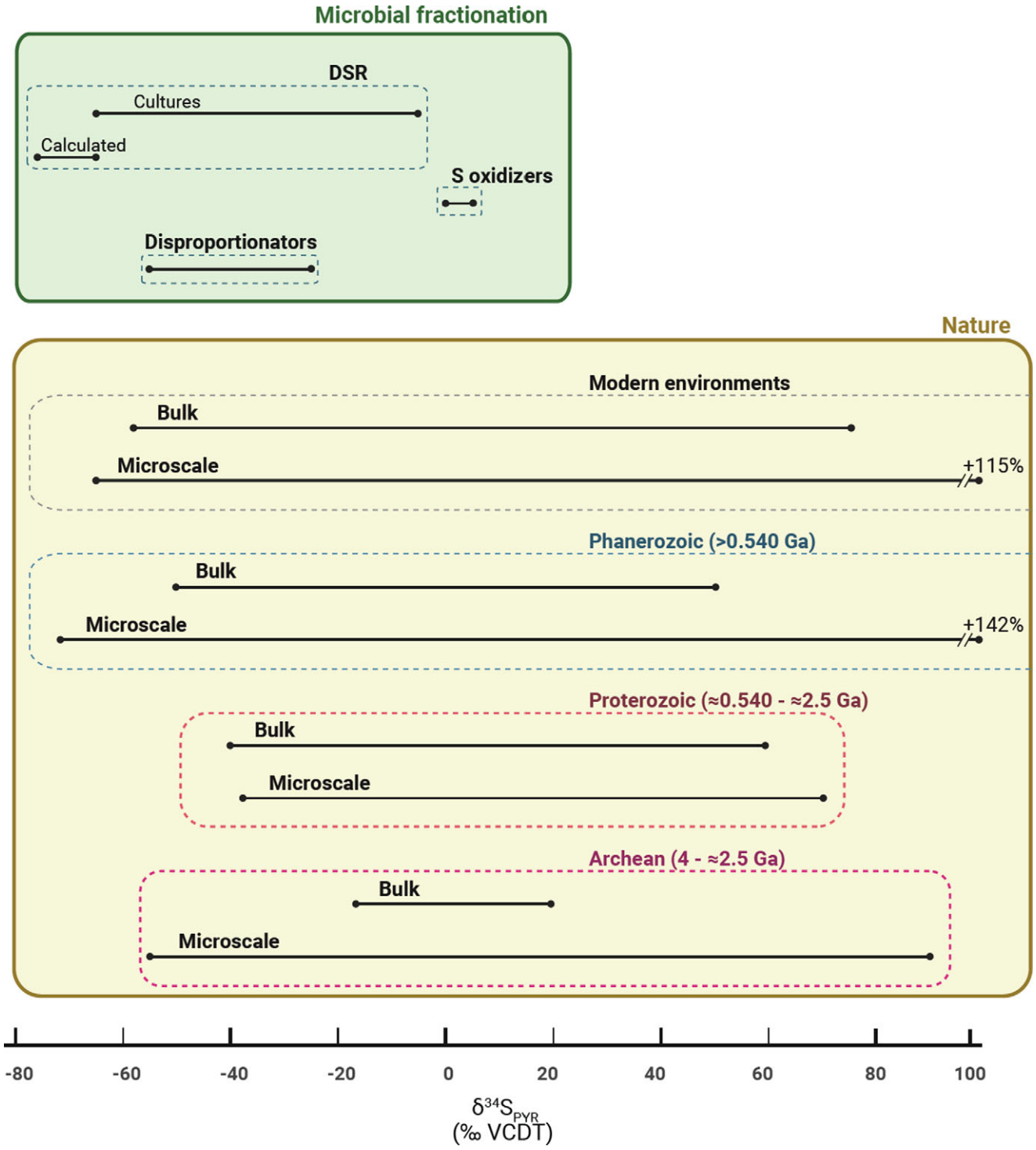

Figure 5. Comparison of S-isotope measurements in culture experiments to assess isotopic microbial fractionation, with the S-isotopic composition of pyrite preserved in natural samples over the geological record (measured by bulk and microscale techniques). Data are from: MSR (Detmers *et al.*, 2001; Johnston *et al.*, 2005b; Hoek *et al.*, 2006; Johnston *et al.*, 2007; Sim *et al.*, 2011a; 2011b; Sim *et al.*, 2012; Leavitt *et al.*, 2013, 2024; Deusner *et al.*, 2014; Pellerin *et al.*, 2015; Bradley *et al.*, 2016; Smith *et al.*, 2020); S-oxidizers (Zerkle *et al.*, 2009); disproportionators (Johnston *et al.*, 2005a); bulk and microscale pyrite (Halevy *et al.*, 2023). Modelled DSR refers to bio-isotopic model outputs analysed under a wide range of environmental parameters (*i.e.* temperature, sulfate, organic matter and Fe availabilities) expected to reflect modern marine conditions.

(Δ_{PYR}) values, which are often interpreted as a consequence of the limited sulfate reservoir in the ancient oceans (Habicht *et al.*, 2002), with sulfate estimates ranging from hundreds to tens of micromoles per litre (μM) (Crowe *et al.*, 2014). While the rates and isotopic implications of organic sulfur breakdown remain uncertain, both modelling and observations suggest that organic sulfur probably played a role in extremely low-sulfate systems (Fakhraee and Katsev, 2019). This has potential implications for understanding the pathways and isotopic compositions involved in early Earth pyrite formation. The transition from the Archean to the Early

https://doi.org/10.1180/gbi.2024.9 Published online by Cambridge University Press

Proterozoic era is marked by the gradual oxidation of the Earth's surface environment. This led to an increase in seawater sulfate content, resulting in the disappearance of sulfur mass-independent fractionation (S-MIF) signals (see Box) and an overall rise in Δ_{PYR} values (Fig. 5). Throughout much of the Proterozoic era, $\delta^{34}S_{PYR}$ values exhibit significant variability, which is commonly attributed to fluctuations in the pyrite burial rate and shifts in ocean redox conditions, such as changes in the extent of ocean anoxia (Emmings *et al.*, 2022). After the oxygenation of the ocean atmosphere, the range of $\delta^{34}S_{PYR}$ values remained relatively constant at around -50‰ (Fig. 5), and the observed decreases during the Paleozoic era are probably associated with marine sulfate isotopic secular evolution (Fig. 5; *e.g.* Owens *et al.*, 2013; Gomes *et al.*, 2016; Raven *et al.*, 2018). An essential aspect of the Phanerozoic era is the emergence of episodic intervals of ocean anoxia, known as Oceanic Anoxic Events (OAEs), driven by large-scale disturbances in the carbon cycle. High-resolution analysis of pyrite and seawater sulfate sulfur isotopic compositions and their utilization in isotopic box models have unveiled brief intervals of severe anoxia which led to significant drawdown of the seawater sulfate during those brief episodes of Earth's history (100s kyr to My, Song *et al.*, 2014; Bauer *et al.*, 2022).

More recently, an alternative reading of the first-order pattern preserved in the S-isotope geologic record has emerged due to a growing body of evidence highlighting the importance of local sedimentary processes in shaping the preserved isotopic composition of pyrite (Fike *et al.*, 2015; Halevy *et al.*, 2023). These findings are based on the study of stratigraphic $\delta^{34}S_{PYR}$ variations within 100 kyr Pleistocene glacial-interglacial cycles, which have been linked to sedimentary parameters such as sedimentation rates and the availability and reactivity of iron and/or organic carbon, rather than changes in microbial fractionation (Bryant *et al.*, 2023). These findings challenge the conventional view that sedimentary archives merely passively record the global sulfur cycle, especially given the long residence time of sulfate in the ocean (13 Myr, Kah *et al.*, 2004). The emerging understanding suggests that, in addition to the expansion of the marine sulfate reservoir, sedimentary parameters through their influence on the accessibility of sulfate within the sediment play a crucial role in shaping the wide spectrum of Δ_{PYR} preserved in sedimentary rock records, rather than large-scale temporal shifts in the global sulfur cycle.

Iron isotopes

The formation of pyrite necessitates the presence of Fe(II), which in natural environments mostly originates from either dissimilatory iron reduction (DIR) or from abiotic sulfidization of Fe(III) (oxyhydr)oxides. When Fe(III) reducers are grown in pure cultures, they produce Fe^{2+} that exhibits a ^{56}Fe-depletion of approximately 2.9±0.9‰ compared to the initial Fe(III) substrates (Crosby *et al.*, 2005, 2007). This microbial fractionation remains consistent across different Fe(III) substrates and bacterial strains, and it closely matches the thermodynamic equilibrium fractionation between Fe(III) and Fe(II) (Welch *et al.*, 2003) (Fig. 6). In contrast, laboratory experiments involving the abiotic sulfidization of Fe(III) (oxyhydr)oxides release Fe^{2+} with a ^{56}Fe-depletion of approximately 0.8±0.3‰ relative to the Fe(III) minerals (McAnena *et al.*, 2024). Interestingly, this abiotic fractionation appears to be independent of the dissolution rate of the Fe(III) (oxyhydr)oxides, which itself seems to be influenced by the mineralogy of Fe(III) or the S(-II):Fe(III) ratio.

Furthermore, apart from the isotopic fractionation associated with the reduction step, the conversion of Fe^{2+} to FeS species also leads to a noticeable isotopic fractionation. Laboratory experiments have shown that this fractionation can vary between –0.8±0.2‰ (Butler *et al.*, 2005) and an apparent equilibrium FeS-Fe^{2+} isotope fractionation of +0.4±0.2‰ (Wu *et al.*, 2012). Near-equilibrium between Fe^{2+} to FeS in natural environments is consistent with the observed isotopic exchange between FeS and aqueous sulfide (Butler *et al.*, 2004). Under laboratory conditions, the formation of pyrite from FeS results in pyrite that is ^{56}Fe-depleted by 0.5 to 2.2‰ compared to the FeS pool (Guilbaud *et al.*, 2011; Mansor and Fantle, 2019). The overall Fe isotope fractionation between pyrite and Fe^{2+} (or Fe(III) (oxyhydr)oxides) depends on the relative importance of these reactions and the rate-dependent expression of kinetic and equilibrium isotope effects associated with these processes.

A limited number of studies (n=9) collectively provide valuable insights into δ^{56}Fe values associated with pyrite found in modern marine sedimentary environments, thereby enhancing our understanding of the influences of water column redox processes (*e.g.* Busigny *et al.*, 2014; Rolison *et al.*, 2018), offering a contemporary perspective on the benthic iron shuttle (Severmann *et al.*, 2008; Scholz *et al.*, 2014), and examining how early diagenesis can impact $\delta^{56}Fe_{PYR}$ in marine sediments (as observed in Fehr *et al.*, 2008, 2010; Lin *et al.*, 2017, 2018). However, it should be noted that the majority of bulk $\delta^{56}Fe_{PYR}$ data fail to align with the combined expectations derived from experimental and theoretical considerations mentioned earlier. One can expect that with recent advancements in *in situ* $\delta^{56}Fe_{PYR}$ analyses, they can be used to remove some of the uncertainty in interpreting bulk $\delta^{56}Fe_{PYR}$ data, particularly when conducted across a range of well-defined modern depositional settings.

By taking into account some of the effects mentioned above, researchers have employed the iron isotopic composition of pyrite, denoted as $\delta^{56}Fe_{PYR}$, to explore how the biogeochemical iron (Fe) cycle in Earth's oceans and the processes underlying pyrite formation may have evolved over geological history. In contrast to S-isotopes, the $\delta^{56}Fe_{PYR}$ record is fragmented, with a primary focus on significant shifts in Earth's redox history, particularly associated with two major events of atmospheric oxygenation – the Great Oxidation Event (GOE) and the Neoproterozoic Oxidation Event (NOE). Consequently, it remains challenging to construct a comprehensive long-term narrative of the Fe cycle's evolution.

Various environmental factors, whether in conjunction with the co-evolution of microbial life or not, have been suggested as potential explanations for the bulk negative isotopic variations that occurred prior to the GOE around 2.4 billion years ago. For instance, Rouxel *et al.*, (2005) leveraged $\delta^{56}Fe_{PYR}$ values to glean insights into the oxygenation status of ancient oceans. Lighter $\delta^{56}Fe_{PYR}$ values were associated with partial oxidation of a vast Fe^{2+} oceanic reservoir indicative of more reducing conditions, while heavier values were indicative of more oxidizing conditions leading up to the GOE. Furthermore, the transition towards more positive $\delta^{56}Fe_{PYR}$ values has been suggested to attest to the onset of pyrite weathering (Heard *et al.*, 2020). This would have significantly increased the availability of sulfate in the ocean, thereby affecting the interplay between kinetic and equilibrium processes during pyrite precipitation (Mansor and Fantle, 2019; Heard *et al.*, 2020). Alternatively, the prevalence of low $\delta^{56}Fe_{PYR}$ values during the Neoarchean era (2.8–2.5 billion years ago) has been used to underscore the early emergence of DIR and the inference of a microbially driven Fe cycle (Johnson *et al.*, 2008). These low values

https://doi.org/10.1180/gbi.2024.9 Published online by Cambridge University Press

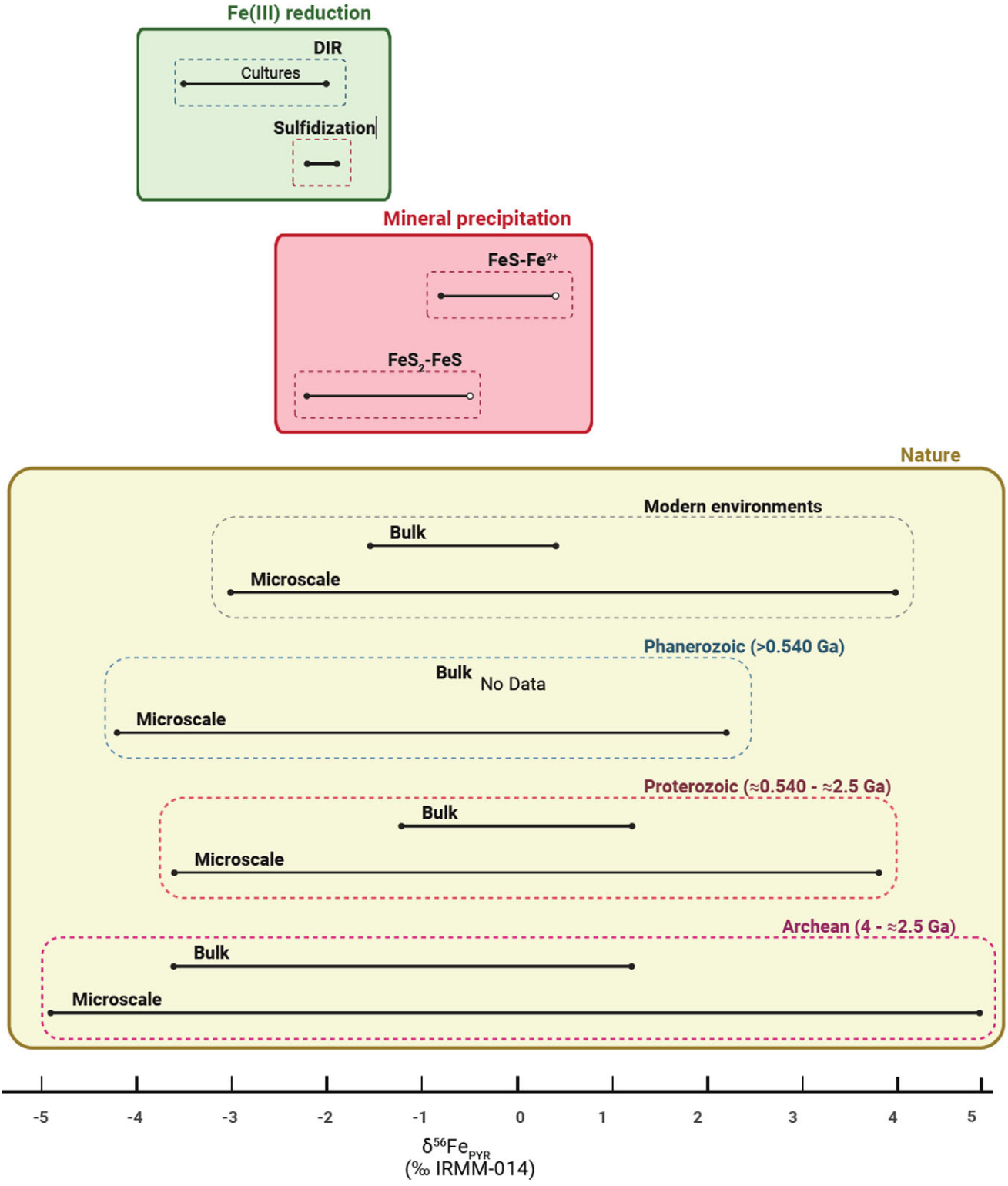

Figure 6. Compilation of Fe-isotopes measurements during the reduction of Fe(III) minerals, from abiotic processes involved during mineral precipitation and from pyrite preserved in modern environments over the geological record (measured by bulk and microscale techniques). Data are from: dissimilatory iron reduction DIR (Crosby *et al.*, 2005, 2007); sulfidization (McAnena *et al.*, 2024); bulk and microscale pyrite (Dupeyron *et al.*, 2023).

have also been interpreted as reflecting strong kinetic effects during the abiotic formation of pyrite from FeS precursors (Guilbaud *et al.*, 2011). It's important to highlight that a recent collection of microscale $\delta^{56}Fe_{PYR}$ values across the GOE presents distinctive patterns when compared with results obtained through conventional bulk analyses (Dupeyron *et al.*, 2023). The discrepancy in the evolution of $\delta^{56}Fe_{PYR}$ between bulk and *in situ* measurements may be linked to a sampling bias, because the majority of traditional bulk investigations have been performed on millimetre-scale pyrite grains, often extracted from black shale matrices.

https://doi.org/10.1180/gbi.2024.9 Published online by Cambridge University Press

Societal impacts of Fe sulfides in modern and future environments

Sequestration of organic carbon by Fe-S minerals

Associations between Fe-S minerals and organic carbon have been hardly investigated, even though they might provide a mechanism for the long-term preservation of organic matter in rocks and sediments. Anoxic zones in the global ocean are expanding as a result of warming climate (Keeling *et al.*, 2010; Levin and Bris, 2015; Keil, 2017; Breitburg *et al.*, 2018; Ruvalcaba Baroni *et al.*, 2020). Therefore, understanding interactions between Fe-S minerals and organic carbon might be of importance to predict how the biogeochemical cycles of Fe, S and C might evolve in marine environments. The importance of Fe(III) (oxyhydr)oxides for the preservation of organic carbon has been well explored and recognized because of their abundance in oxygenated surface environments (Lalonde *et al.*, 2012; Longman *et al.*, 2022; Moore *et al.*, 2023). Recent experimental work highlighted the role of microbial cell surfaces in the growth and nucleation of Fe-S minerals, therefore suggesting that some type of association must form between microbial organic carbon and Fe-S minerals (Picard *et al.*, 2018). It has been suggested that Fe-S minerals might play an important role in the preservation of organic carbon in anoxic marine sediments (Barber *et al.*, 2017).

In laboratory experiments, Fe-S minerals can bind organic matter from various sources: live and dead microbial cells (Herbert *et al.*, 1998; Picard *et al.*, 2019, 2021; Nabeh *et al.*, 2022; Truong *et al.*, 2023), simple organic molecules (i.e. sugars, amino acids) and complex organic mixtures used in microbiological media (i.e. tryptone and yeast extract) (Picard *et al.*, 2021; Nabeh *et al.*, 2022), water-soluble extracts from aged compost soil, microalgae biomass and corn leaf (Tétrault and Gélinas, 2022). The capacity of mackinawite to sequester organic carbon is at least comparable to that of ferrihydrite (Wang *et al.*, 2019; Ma *et al.*, 2022). Light elements (*e.g.* C, O) can be detected in Fe-S minerals by energy dispersive X-ray spectroscopy (EDS) in the scanning electron microscope (SEM) (Picard *et al.*, 2019). To characterize the speciation and redox state of light elements, the use of spectroscopic methods, such as X-ray photoelectron spectroscopy (XPS) and near-edge X-ray absorption fine structure (NEXAFS) spectroscopy, is required. These methods identified C and N in biogenic Fe-S minerals originating from organic molecules, and O originating from organic functional groups rather than from oxidation of Fe-S minerals (Herbert *et al.*, 1998; Picard *et al.*, 2019, 2021). The use of scanning transmission X-ray microscopy (STXM), coupled with NEXAFS spectroscopy, determined that organic carbon is homogenously distributed on biogenic Fe-S mineral aggregates precipitated with SRB, on biogenic pyrite and Fe-S minerals produced in cultures of sulfur-reducing archaea, and on abiotic minerals precipitated with simple and complex organic mixtures (Picard *et al.*, 2019, 2021; Truong *et al.*, 2023). Some organic carbon also occurs as 'hot spots' in mineral aggregates precipitated with SRB (whether Fe^{2+} was in the growth medium or added after growth), interpreted as the preservation of intact cells and contents (Picard *et al.*, 2019, 2021).

In long-term laboratory experiments, Fe-S minerals could sequester significant amounts of organic carbon and nitrogen, as quantified by elemental analysis of solid phases (Nabeh *et al.*, 2022). The sequestered amounts decreased as a function of time but stabilized rapidly within a few months (Nabeh *et al.*, 2022). Semi-quantitative analysis from STXM/NEXAFS data also (Picard *et al.*, 2021). The highest stabilized levels of C and N were 13.5 w/w% and 3.3 w/w%, respectively. In a marine medium, the organic carbon removal capacity of Fe-S minerals was higher when microbial biomass was present (42–51% organic carbon removed from medium) than when organic mixtures that did not contain cells (*e.g.* amino acid mixtures, tryptone, yeast extract) were used (1.2–5.2% organic carbon removed from medium). In freshwater medium, the removal capacity of microbial biomass was even higher than in marine medium (67–137%; values above 100% linked to uncertainties in elemental analysis of biomass) (Nabeh *et al.*, 2022).

The nature of associations between Fe-S minerals and organic carbon has yet to be thoroughly investigated. Quantification of organic carbon in the studies reported above was done after several washes with anoxic ultrapure water, therefore removing loosely bound and water-soluble organics. Spectroscopic studies indicated that glucose and mannose bind less to Fe-S minerals than protein-rich organic mixtures (Picard *et al.*, 2021). Synthetic mackinawite studied with Fourier transform infrared spectroscopy (FTIR) revealed that it mostly associates with polysaccharides when adsorbed to extracts from natural organic matter (corn leaf, marine algae and soil) (Tetrault and Gelinas 2022). The only study on natural pyrite (n = 5 framboids) determined fairly high organic carbon contents of 2.8–6.5 wt.% (Tribovillard *et al.*, 2022). Overall, the studies indicated a high association between Fe-S minerals and organic carbon, which needs to be investigated further in the context of climate and long-term organic carbon preservation (Fig. 7).

Pyrite oxidation in the context of acidic drainages, metal recovery and nitrate removal

Pyrite oxidation in nature has been a subject of intense interest due to its key role in generating acid mine drainages (AMD) (Fig. 7). Decades of ore and metal mining have left pyrite-containing deposits exposed to the air and susceptible to oxidation mediated by aerobic Fe(II) and sulfur-oxidizing microorganisms, generating Fe^{3+} and sulfuric acid. Further oxidation of pyrite by Fe^{3+} generates a feedback loop that amplifies the oxidative reaction, resulting in AMD with low pH (< 5) and elevated toxic metals (*e.g.* Fe, Ni, Co, Cu, Zn) that negatively affect ecosystems worldwide (Baker and Banfield, 2003).

Despite its negative associations, research on acidic drainages presents some exciting opportunities to understand life in extreme environments. It is being increasingly recognized that some acidic drainages are natural and are better termed acid rock drainages (ARD) to distinguish them from anthropogenically-generated AMD. The most famous example is perhaps the Río Tinto, a 92 km long river that drains the Iberian Pyrite Belt in southwest Spain. Biogeochemical conditions in such acidic environments are similar to those that could have been found on ancient Mars as well as on early Earth (Amils and Fernández-Remolar, 2021). In particular, it was proposed that widespread ARDs occurred on the early Earth ~2.4 billion years ago, due to the GOE that accelerated terrestrial pyrite weathering (Konhauser *et al.*, 2011). Thus, modern AMD and ARD act as analogues to provide valuable insights into ancient life and biogeochemical cycles that may have operated in the past and other habitable worlds.

Further downstream, the toxicity of acidic drainages is mitigated by several processes including hydrological dilution, pH buffering by bedrock (*e.g.* limestone) and sulfate reduction by SRM.

https://doi.org/10.1180/gbi.2024.9 Published online by Cambridge University Press

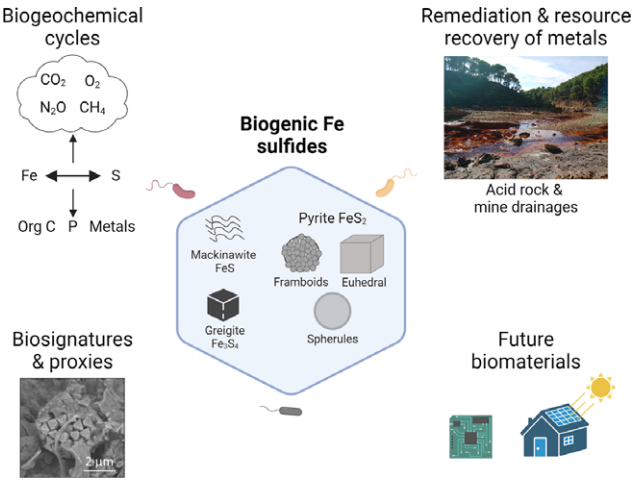

Figure 7. Summary of the relevance of biogenic Fe-S minerals in various research fields and current societal issues.

Enhancing the activity of microbial sulfate reduction is of particular interest in bioremediation and resource recovery, as sulfate reduction increases pH and generates sulfide that reacts readily with metals, immobilizing them as various metal sulfides (*e.g.* FeS, CuS, ZnS, NiS). The precious metals can then be recovered and used for other applications (Fig. 7). Selective metal recovery has been demonstrated in some cases using precise pH control in bioreactors, although the efficiency highly depends on the specific composition of the feed solution (reviewed in Johnson and Sánchez-Andrea, 2019).

Besides aerobic pyrite oxidation, the environmental relevance of pyrite oxidation under anoxic conditions is being increasingly recognized. In fact, most of the pyrite oxidation that contributes to the aforementioned Río Tinto system is now thought to come primarily from subsurface pyrite oxidation coupled with nitrate reduction by anaerobic microorganisms (Amils *et al.*, 2023). This process is also one of the major controls for the fate of agriculturally-sourced nitrate, a pollutant of ground- and drinking water in various parts of the world. It has been shown that pyrite of different sizes and shapes are associated with different degrees of pyrite oxidation and nitrate removal, and whether the final product is dissolved ammonium, harmless N_2 gas or the greenhouse gas N_2O (Bosch *et al.*, 2011; Yan *et al.*, 2019; Mansor and Xu, 2020; Pang and Wang, 2020; Jakus *et al.*, 2021; Kappler *et al.*, 2021). Subsurface pyrite oxidation is also an important factor to consider in engineering, as this process can lead to ground collapse and significant loss of economic and public life (Czerewko and Cripps, 2023).

While this section is focused primarily on pyrite oxidation, it is important to recognize that redox heterogeneity is expected in space and time (Peiffer *et al.*, 2021). For example, sediment cores in Río Tinto are black within a few centimetres of depth, which can be attributed to sulfate reduction at depth (Sánchez-Andrea *et al.*, 2012) and the formation of new metal sulfides that probably include pyrite. In the subsurface, hydrological fluctuations over time can shift redox conditions from being conducive to pyrite oxidation to being conducive to pyrite formation via the activity of sulfate/sulfur/iron-reducing microorganisms. It is likely that new pyrite is continuously being formed and redissolved in the environment. Thus, investigating biogenic pyrite formation will be key to understanding the reactivity of these dynamic phases.

Biogenic pyrite as future photovoltaics and semiconductors

As the world's population continues to increase, there is a need for environmentally sustainable solutions to meet the future demands in energy. The optimization of energy gain from solar cells and output efficiencies of various electronics are considered high priorities in this regard. Silicon-based materials have traditionally dominated the field of photovoltaics and semiconductors. In recent years, it has been recognized that pyrite has the potential to replace silicon-based materials at a lower cost and with higher efficiency (Fig. 7). Pyrite has a suitable band gap (energy gap between two electron states) around 0.95 eV, which is neither too small (*i.e.* as a conductor) or too large (*i.e.* insulator) for it to function as a semiconductor. It further has a light absorption coefficient that is about two orders of magnitude higher than silicon. The relative abundance and non-toxicity of pyrite components (*e.g.* Fe, S) also make it more attractive compared to other explored materials (Wadia *et al.*, 2009).

For pyrite to be feasible as an energy material of the future, a method to obtain high-quality pyrite in sufficient quantities needs to be developed. Thin films of pyrite have initially been synthesized through various methods such as hydro/solvothermal, hot injection and vapour deposition. Modifications of these procedures can lead to different sizes, shapes and trace metal contents, which allow for tunable band gap energy and electrical current production. These methods often require high temperatures and toxic solvents and tend to produce impurities such as the high-temperature phase marcasite (orthorhombic FeS_2) and pyrrhotite (Fe_7S_8) (Zaka *et al.*, 2022). High-energy milling of pyrite ore can be used to obtain nanoparticles prior to thin film preparation, but there are concerns that this will exacerbate environmental problems associated with acid mine drainages. Furthermore, robust supplies of high-quality pyrite ore cannot be guaranteed as there are huge variations in the semiconductive properties of pyrite even within a deposit (Wang *et al.*, 2021).

Could pyrite in the future be grown as a biomanufactured material? (Cosmidis, 2023). This approach takes its inspiration from nature, which has produced pyrite sustainably at a rate of ~200,000 tons per day for the last millions of years (Rickard, 2015). A mechanistic understanding of biogenic pyrite formation will be essential to allow for tunable bio-synthesis. The gap between laboratory experiments to large-scale production is vast. However, achieving this will be a worthwhile target.

Acknowledgements. MM thanks the German Research Foundation (DFG) for support through project ID 503493769 and the Tuebingen Structural Microscopy Core Facility (funded through the Federal Ministry of Education and Research BMBF, the Baden-Württemberg Ministry of Science and DFG project ID INST 37/1027-1 for financial support for the acquisition of the cryogenic focused ion beam scanning electron microscope). AG thanks the Agence Nationale de la Recherche (ANR) for support through project HYPER-BIOMIN (ANR-20-CE02-0001-01). JMC and VP thank the European Union's Horizon H2020 research and innovation programme ERC (STROMATA, grant agreement 759289; PI Johanna Marin-Carbonne). JC thanks the ERC program (BioFacts, grant agreement 101076666). AP acknowledges the support of the Nevada NASA space grant consortium research infrastructure program This material is based upon the work supported by the NVSGC under Grant# 80NSSC20M0043.

Figures 3, 4, 5, 6 and 7 were created with BioRender.com.

Author contributions. MM & AP– conceived the original idea and outline, created Figures 1, 3 and 7, wrote the Abstract, Introduction and all other sections not listed below, and led the review and editing process; AD & JB – wrote 'Biogenic pyrite formation at low temperatures' section, created Figure 2; VP – wrote 'Sedimentary pyrite as environmental proxies and biosignatures' section,

https://doi.org/10.1180/gbi.2024.9 Published online by Cambridge University Press

created Figures 5 and 6; AG & FG – wrote 'Biogenic iron sulfide mineral formation at high temperature' section; JMC – wrote 'Iron sulfides and the origin of life' section, created Figure 4; JC – wrote 'Sources of sulfur' section; All authors reviewed and edited the paper.

Reference

Áde Leeuw N.H. (2015) Bio-inspired CO_2 conversion by iron sulfide catalysts under sustainable conditions. *Chemical Communications*, **51**, 7501–7504.

Allen E.T., Crenshaw J.L., Johnston J. and Larsen E.S. (1912) The Mineral Sulphides of Iron; with Crystallographic Study by E. S. Larsen. *American Journal of Science*, **s4-33**, 169–236.

Allen K.D., Wegener G., Sublett D.M., Bodnar R.J., Feng X., Wendt J. and White R.H. (2021) Biogenic formation of amorphous carbon by anaerobic methanotrophs and select methanogens. *Science Advances*, **7**, eabg9739.

Alpermann T., Rüdel K., Rüger R., Steiniger F., Nietzsche S., Filiz V., Förster S., Fahr A. and Weigand W. (2011) Polymersomes Containing Iron Sulfide (FeS) as Primordial Cell Model. *Origins of Life and Evolution of Biospheres*, **41**, 103–119.

Amenabar M.J. and Boyd E.S. (2018) Mechanisms of mineral substrate acquisition in a thermoacidophile. *Applied and Environmental Microbiology*, **84**, e003334–18.

Amend J.P. and Shock E.L. (1998) Energetics of amino acid synthesis in hydrothermal ecosystems. *Science*, **281**, 1659–1662.

Amils R. and Fernández-Remolar D. (2021) Río Tinto: An extreme acidic environmental model of astrobiological interest. Pp. 21–44 in: *Extremophiles as Astrobiological Models* (J. Seckbah H. Stan-Lotter, editors). Scrivener Publishing, Beverly, MA.

Amils R., Escudero C., Oggerin M., Puente Sánchez F., Arce Rodríguez A., Fernández Remolar D., Rodríguez N., García Villadangos M., Sanz J.L., Briones C., Sánchez M., Gómez F., Leandro T., Moreno-Paz M., Prieto-Ballesteros O., Molina A., Tornos F., Sánchez-Andrea I., Timmis K., Pieper D.H. and Parro V. (2023) Coupled C, H, N, S and Fe biogeochemical cycles operating in the continental deep subsurface of the Iberian Pyrite Belt. *Environmental Microbiology*, **25**, 219–594.

Amor M., Mathon F.P., Monteil C.L., Busigny V. and Lefevre C.T. (2020) Iron-biomineralizing organelle in magnetotactic bacteria: functioN., synthesis and preservation in ancient rock samples. *Environmental Microbiology*, **22**(9), 3611–3632.

Archer C. and Vance D. (2006) Coupled Fe and S isotope evidence for Archean microbial Fe(III) and sulfate reduction. *Geology*, **34**, 153–156.

Atienza N., Gregory D., Taylor S., Swing M., Perea D., Owens J. and Lyons T. (2023) Refined views of ancient ocean chemistry: Tracking trace element incorporation in pyrite framboids using atom probe tomography. *Geochimica et Cosmochimica Acta*, **357**, 1–12.

Avetisyan K., Buchshtav T. and Kamyshny A. (2019) Kinetics and mechanism of polysulfides formation by a reaction between hydrogen sulfide and orthorhombic cyclooctasulfur. *Geochimica et Cosmochimica Acta*, **247**, 96–105.

Avetisyan K., Zweig I., Luther G.W. and Kamyshny A. (2021) Kinetics and mechanism of polysulfides and elemental sulfur formation by a reaction between hydrogen sulfide and δ-MnO_2. *Geochimica et Cosmochimica Acta*, **313**, 21–37.

Baker B.J. and Banfield J.F. (2003) Microbial communities in acid mine drainage. *FEMS Microbiology Ecology*, **44**, 139–152.

Barber A., Brandes J., Leri A., Lalonde K., Balind K., Wirick S., Wang J. and Gélinas Y (2017) Preservation of organic matter in marine sediments by inner-sphere interactions with reactive iron. *Scientific Reports*, **7**, 1–10.

Bauer K.W., Bottini C., Katsev S., Jellinek M., Francois R., Erba E. and Crowe SA (2022) Ferruginous oceans during OAE1a and collapse of the marine sulfate pool. *Earth and Planetary Science Letters*, **578**, 117324.

Baumgartner R.J., Kranendonk M.J. VaN., Wacey D., Fiorentini M.L., Saunders M., Caruso S., Pages A., Homann M. and Guagliardo P (2019) Nano-porous pyrite and organic matter in 3.5-billion-year-old stromatolites record primordial life. *Geology*, **47**, 1039–1043.

Baumgartner R.J., Caruso S., Fiorentini M.L., Van Kranendonk M.J., Martin L., Jeon H., Pagès A. and Wacey D. (2020) Sulfidization of 3.48 billion-year-old stromatolites of the Dresser Formation, Pilbara Craton: Constraints from in-situ sulfur isotope analysis of pyrite. *Chemical Geology*, **538**, 119488.

Baya C., Le Pape P., Baptiste B., Brest J., Landrot G., Elkaim E., Noël V., Blanchard M., Ona-Nguema G., Juillot F. and Morin G. (2021) Influence of trace level As or Ni on pyrite formation kinetics at low temperature. *Geochimica et Cosmochimica Acta*, **300**, 333–353.

Baya C., Le Pape P., Baptiste B., Menguy N., Delbes L., Morand M., Rouelle M., Aubry E., Ona-Nguema G., Noël V., Juillot F. and Morin G. (2022) A methodological framework to study the behavior and kinetic influence of V, Mn, Co, Ni, Cu, Zn, As, Se and Mo during pyrite formation via the polysulfide pathway at ambient temperature. *Chemical Geology*, **613**, 121139.

Beinert H. (2000) Iron-sulfur proteins: Ancient structures, still full of surprises. *Journal of Biological Inorganic*, **5**, 2–15.

Belthle K.S., Beyazay T., Ochoa-Hernández C., Miyazaki R., Foppa L., Martin W.F. and Tüysüz H. (2022) Effects of Silica Modification (Mg, Al, Ca, Ti, and Zr) on Supported Cobalt Catalysts for H_2-Dependent CO_2 Reduction to Metabolic Intermediates. *Journal of the American Chemical Society*, **144**, 21232–21243.

Belthle K.S. and Tüysüz H. (2023) Linking Catalysis in Biochemical and Geochemical CO_2 Fixation at the Emergence of Life. *ChemCatChem*, **15**, e202201462.

Benning L.G., Wilkin R.T., Barnes H.L. (2000) Reaction pathways in the Fe-S system below 100°C. *Chemical Geology*, **167**, 25–51.

Berg J.S., Schwedt A., Kreutzmann A-C., Kuypers M.M.M. and Milucka J. (2014) Polysulfides as intermediates in the oxidation of sulfide to sulfate by *Beggiatoa* spp. *Applied and Environmental Microbiology*, **80**, 629–636.

Berg J.S., Duverger A., Cordier L., Christel L-R., Guyot F. and Miot J. (2020) Rapid pyritization in the presence of a sulfur / sulfate-reducing bacterial consortium. *Scientific Reports*, **10**, 1–13.

Berner R.A. (1962) Tetragonal iron sulfide. *Science*, **137**, 669–669.

Berner R.A. (1970) Sedimentary pyrite formation. *American Journal of Science*, **268**, 1–23.

Berner R.A. (1989) Biogeochemical cycles of carbon and sulfur and their effect on atmospheric oxygen over phanerozoic time. *Global and Planetary Change*, **1**, 97–122.

Bertel D., Peck J., Quick T.J. and Senko J.M. (2012) Iron Transformations Induced by an Acid-Tolerant *Desulfosporosinus* Species. *Applied and Environmental Microbiology*, **78**, 81–88.

Beveridge T.J. (1989) Role of cellular design in bacterial metal accumulation and mineralization. *Annual Review of Microbiology*, **43**, 147–171.

Beyazay T., Martin W.F. and Tüysüz H. (2023) Direct Synthesis of Formamide from CO_2 and H_2O with Nickel–Iron Nitride Heterostructures under Mild Hydrothermal Conditions. *Journal of the American Chemical Society*, **145**, 19768–19779.

Blöchl E., Rachel R., Burggraf S., Hafenbradl D., Jannasch H.W. and Stetter K.O. (1997) *Pyrolobus fumarii*, gen. and sp. nov., represents a novel group of archaea, extending the upper temperature limit for life to 113°C. *Extremophiles*, **1**, 14–21.

Bonfio C., Valer L., Scintilla S., Shah S., Evans D.J., Jin L., Szostak J.W., Sasselov D.D., Sutherland J.D. and Mansy S.S. (2017) UV-light-driven prebiotic synthesis of iron-sulfur clusters. *Nature Chemistry*, **9**, 1229–1234.

Bosch J., Lee K.Y., Jordan G., Kim K-W. and Meckenstock R.U. (2011) Anaerobic., nitrate-dependent oxidation of pyrite nanoparticles by *Thiobacillus denitrificans*. *Environmental Science and Technology*, **46**, 2095–2101.

Böttcher M., Smock A. and Cypionka H. (1998) Sulfur isotope fractionation during experimental precipitation of iron (II) and manganese (II) sulfide at room temperature. *Chemical Geology*, **146**, 127–134.

Boylan A.A., Perez-Mon C., Guillard L., Burzan N., Loreggian L., Maisch M., Kappler A., Byrne J.M. and Bernier-Latmani R. (2019) H_2-Fuelled Microbial Metabolism in Opalinus Clay. *Applied Clay Science*, **174**, 69–76.

Bradley A.S., Leavitt W.D., Schmidt M., Knoll A.H., Girguis P.R. and Johnston D.T. (2016) Patterns of sulfur isotope fractionation during microbial sulfate reduction. *Geobiology*, **14**, 91–101.

Breitburg D., Levin L.A., Oschlies A., Grégoire M., Chavez F.P., Conley D.J., Garçon V., Gilbert D., Gutiérrez D., Isensee K., Jacinto G.S., Limburg K.E., Montes I., Naqvi S.W.A., Pitcher G.C., Rabalais N.N., Roman M.R., Rose K. A., Seibel B.A., Telszewski M., Yasuhara M. and Zhang J. (2018)

https://doi.org/10.1180/gbi.2024.9 Published online by Cambridge University Press

Declining oxygen in the global ocean and coastal waters. *Science*, **359**(6371), eaam7240.

Bronner R., Thompson K., Dreher C., Runge E., Voggenreiter E., Shuster J., Wan B., Joshi P., Fischer S., Duda JP., Kappler A. and Mansor M. (2023) Co-reduction of Fe(III) and S^0 drives Fe-S biomineral formation and phosphate mobilisation. *Geochemical Perspectives Letters*, **24**, 27–32.

Brunner B., Bernasconi S., Kleikemper J. and Schroth M. (2005) A model for oxygen and sulfur isotope fractionation in sulfate during bacterial sulfate reduction processes. *Geochimica et Cosmochimica Acta*, **69**, 4773–4785.

Bryant R.N., Houghton J.L., Jones C., Pasquier V., Halevy I. and Fike D.A. (2023) Deconvolving microbial and environmental controls on marine sedimentary pyrite sulfur isotope ratios. *Science*, **382**, 912–915.

Bunsen R. (1847) Ueber den innern Zusammenhang der Pseudovulkanischen Erscheinungen Islands. *Justus Liebigs Annalen der Chemie*, **62**, 1–59.

Busigny V., Planavsky N.J., Jézéquel D., Crowe S., Louvat P., Moureau J., Viollier E. and Lyons T.W. (2014) Iron isotopes in an Archean ocean analogue. *Geochimica et Cosmochimica Acta*, **133**, 443–462.

Butler I.B. and Rickard D. (2000) Framboidal pyrite formation via the oxidation of iron (II) monosulfide by hydrogen sulphide. *Geochimica et Cosmochimica Acta*, **64**, 2665–2672.

Butler I.B., Böttcher M.E., Rickard D. and Oldroyd A. (2004) Sulfur isotope partitioning during experimental formation of pyrite via the polysulfide and hydrogen sulfide pathways: Implications for the interpretation of sedimentary and hydrothermal pyrite isotope records. *Earth and Planetary Science Letters*, **228**, 495–509.

Butler I.B., Archer C., Vance D., Oldroyd A. and Rickard D. (2005) Fe isotope fractionation on FeS formation in ambient aqueous solution. *Earth and Planetary Science Letters*, **236**, 430–442.

Berner, R.A. and Raiswell, R. (1983) Burial of organic carbon and pyrite sulfur in sediments over Phanerozoic time: a new theory. *Geochimica et Cosmochimica Acta*, **47**(5), 855–862.

Cahill C.L., Benning L.G., Barnes H.L. and Parise J.B. (2000) In situ time-resolved X-ray diffraction of iron sulfides during hydrothermal pyrite growth. *Chemical Geology*, **167**, 53–63.

Canfield D.E. (1997) The geochemistry of river particulates from the continental USA: Major elements. *Geochimica et Cosmochimica Acta*, **61**, 3349–3365.

Canfield D.E. and Berner R.A. (1987) Dissolution and pyritization of magnetite in anoxic marine sediments. *Geochimica et Cosmochimica Acta*, **51**, 6.

Canfield D.E. and Farquhar J. (2009) Animal evolution, bioturbation, and the sulfate concentration of the oceans. *PNAS*, **106**, 8123–8127.

Canfield D.E., Raiswell R. and Bottrell S. (1992) The reactivity of sedimentary iron minerals toward sulfide. *American Journal of Science*, **292**, 659–683.

Canfield D.E., Thamdrup B. and Fleischer S. (1998) Isotope fractionation and sulfur metabolism by pure and enrichment cultures of elemental sulfur-disproportionating bacteria. *Limnology and Oceanography*, **43**, 253–264.

Canfield D.E., Stewart F.J., Thamdrup B., de Brabandere L., Dalsgaard T., Delong E.F., Revsbech N.P. and Ulloa O. (2010) A cryptic sulfur cycle in oxygen-minimum-zone waters off the Chilean coast. *Science*, **330**, 1375–1378.

Caraballo M.A., Asta M.P., Perez J.P.H. and Hochella M.F. (2022) Past, present and future global influence and technological applications of iron-bearing metastable nanominerals. *Gondwana Research*, **110**, 283–304.

Catling D.C. and Zahnle K.J. (2020) The Archean atmosphere. *Science Advances*, **6**, eaax1420.

Chen K. and Morris J. (1972) Kinetics of oxidation of aqueous sulfide by O_2. *Environmental Science & Technology*, **6**, 529–537.

Cody G.D. (2004) Transition metal sulfides and the origins of metabolism. *Annual Review of Earth and Planetary Sciences*, **32**, 569–599.

Corliss J.B., Dymond J., Gordon L.I., Edmond J.M., von Herzen R.P., Ballard R. D., Green K., Williams D., Bainbridge A., Crane K. and Andel T.H. Van (1979) Submarine thermal springs on the Galápagos Rift. *Science*, **203**, 1073.

Cosmidis J. (2023) Will tomorrow's mineral materials be grown? *Microbial Biotechnology*, **16**, 1713–1722.

Cosmidis J. and Benzerara K. (2022) Why do microbes make minerals? *Comptes Rendus - Geoscience*, **354**, 1–39.

Cosmidis J., Benzerara K., Morin G., Busigny V., Lebeau O., Jézéquel D., Noël V., Dublet G. and Othmane G. (2014) Biomineralization of iron-phosphates in the water column of Lake Pavin (Massif Central., France). *Geochimica et Cosmochimica Acta*, **126**, 78–96.

Cosmidis J., Nims C.W., Diercks D. and Templeton A.S. (2019) Formation and stabilization of elemental sulfur through organomineralization. *Geochimica et Cosmochimica Acta*, **247**, 59–82.

Craddock P.R. and Dauphas N. (2011) Iron and carbon isotope evidence for microbial iron respiration throughout the Archean. *Earth and Planetary Science Letters*, **303**, 121–132.

Cron B., Henri P., Chan CS., Macalady J.L. and Cosmidis J. (2019) Elemental sulfur formation by *Sulfuricurvum kujiense* is mediated by extracellular organic compounds. *Frontiers in Microbiology*, **10**, 499541.

Cron B., Macalady J.L. and Cosmidis J. (2021) Organic stabilization of extracellular elemental sulfur in a *Sulfurovum*-rich biofilm: A new role for extracellular polymeric substances? *Frontiers in Microbiology*, **12**, 720101.

Crosby H.A., Johnson C.M., Roden E.E. and Beard B.L. (2005) Coupled Fe(II)-Fe(III) electron and atom exchange as a mechanism for Fe isotope fractionation during dissimilatory iron oxide reduction. *Environmental Science and Technology*, **39**, 6698–6704.

Crosby H.A., Roden E.E., Johnson C.M. and Beard B.L. (2007) The mechanisms of iron isotope fractionation produced during dissimilatory Fe(III) reduction by *Shewanella putrefaciens* and *Geobacter sulfurreducens*. *Geobiology*, **5**, 169–189.

Crowe S.A., Paris G., Katsev S., Jones C., Kim S-T., Zerkle A.L., Nomosatryo S., Fowle D.A., Adkins J.F., Sessions A.L., Farquhar J. and Canfield D.E. (2014) Sulfate was a trace constituent of Archean seawater. *Science*, **346**, 735–739.

Czaja A.D., Beukes N.J. and Osterhout J.T. (2016) Sulfur-oxidizing bacteria prior to the Great Oxidation Event from the 2.52 Ga Gamohaan Formation of South Africa. *Geology*, **44**, 983–986.

Czerewko M.A. and Cripps J.C. (2023) Implications of sulfur mineralogy and consequences of pyrite oxidation for ground engineering. *Journal of the Geological Society*, **180**(4), jgs2022-101.

Dahl C. (2020a) A biochemical view on the biological sulfur cycle. Pp.55–96 in: *Environmental Technologies to Treat Sulphur Pollution: Principles and Engineering*, (Piet N. L. Lens, editor). IWA Publishing, London.

Dahl C. (2020b) Bacterial Intracellular Sulphur Globules Pp. 19–51 in: *Bacterial Organelles and Organelle-like Inclusions. Microbiology Monographs*, (D. Jendrossek, editor). Springer, Cham, Switzerland.

Dahl C. and Prange A. (2006) Bacterial sulfur globules: Occurrence, structure and metabolism. Pp. 21–51 in: *Inclusions in Prokaryotes*, (J.M. Shively, editor). Springer, Berlin.

Dahl C., Schulte A., Stockdreher Y., Hong C., Grimm F., Sander J., Kim R., Kim S.H. and Shin D.H. (2008) Structural and molecular genetic insight into a widespread sulfur oxidation pathway. *Journal of Molecular Biology*, **384**, 1287–1300.

Dauphas N., John S. and Rouxel O. (2017) Iron isotope systematics. *Reviews in Mineralogy and Geochemistry*, **82**, 415–510.

Deng X., Dohmae N., Kaksonen A.H. and Okamoto A. (2020) Biogenic iron sulfide nanoparticles to enable extracellular electron uptake in sulfate-reducing bacteria. *Angewandte Chemie*, **132**, 6051–6055.

Descamps E.C.T., Monteil C.L., Menguy N., Ginet N., Pignol D., Bazylinski D.A. and Lefèvre C.T. (2017) *Desulfamplus magnetovallimortis* gen. nov., sp. nov., a magnetotactic bacterium from a brackish desert spring able to biomineralize greigite and magnetitE., that represents a novel lineage in the *Desulfobacteraceae*. *Systematic and Applied Microbiology*, **40**, 280–289.

Detmers J., Brüchert V., Habicht K.S. and Kuever J. (2001) Diversity of sulfur isotope fractionations by sulfate-reducing prokaryotes. *Applied and Environmental Microbiology*, **67**, 888–894.

Deusner C., Holler T., Arnold G., Bernasconi S., Formolo M. and Brunner B. (2014) Sulfur and oxygen isotope fractionation during sulfate reduction coupled to anaerobic oxidation of methane is dependent on methane concentration. *Earth and Planetary Science Letters*, **399**, 61–73.

Dick G.J. (2019) The microbiomes of deep-sea hydrothermal vents: Distributed globally, shaped locally. *Nature Reviews Microbiology*, **17**(5), 271–283.

Domingos J.M., Runge E., Dreher C., Chiu T-H., Shuster J., Fischer S., Kappler A., Duda J-P., Xu J. and Mansor M. (2023) Inferred pyrite growth via the particle attachment pathway in the presence of trace metals. *Geochemical Perspectives Letters*, **26**, 14–19.

https://doi.org/10.1180/gbi.2024.9 Published online by Cambridge University Press

Donald R. and Southam G. (1999) Low temperature anaerobic bacterial diagenesis of ferrous monosulfide to pyrite. *Geochimica et Cosmochimica Acta*, **63**, 2019–2023.

Drobner E., Huber H., Wächtershäuser G., Rose D. and Stetter K.O. (1990) Pyrite formation linked with hydrogen evolution under anaerobic conditions. *Nature*, **346**, 742–744.

Dupeyron J., Decraene M.N., Marin-Carbonne J. and Busigny V. (2023) Formation pathways of Precambrian sedimentary pyrite: Insights from in situ Fe isotopes. *Earth and Planetary Science Letters*, **609**, 118070.

Duverger A., Berg J.S., Busigny V., Guyot F., Bernard S. and Miot J. (2020) Mechanisms of pyrite formation promoted by sulfate-reducing bacteria in pure culture. *Frontiers in Earth Science*, **8**, 1–15.

Duverger A., Bernard S., Viennet J., Miot J. and Busigny V. (2021) Formation of pyrite spherules from mixtures of biogenic FeS and organic compounds during experimental diagenesis. *Geochemistry, Geophysics., Geosystems*, **22**, 1–16.

Eldridge D.L. and Farquhar J. (2018) Rates and multiple sulfur isotope fractionations associated with the oxidation of sulfide by oxygen in aqueous solution. *Geochimica et Cosmochimica Acta*, **237**, 240–260.

Eldridge D., Guo W. and Farquhar J. (2016) Theoretical estimates of equilibrium sulfur isotope effects in aqueous sulfur systems: Highlighting the role of isomers in the sulfite and sulfoxylate systems. *Geochimica et Cosmochimica Acta*, **195**, 171–200.

Emmings J.F., Poulton S.W., Walsh J., Leeming K.A., Ross I. and Peters S.E. (2022) Pyrite mega-analysis reveals modes of anoxia through geological time. *Science Advances*, **8**, 5687.

Endo Y, Danielache S.O. and Ueno Y. (2019) Total pressure dependence of sulfur mass-independent fractionation by SO_2 photolysis. *Geophysical Research Letters*, **46**, 483–491.

Eroglu S., Scholz F., Salvatteci R., Siebert C., Schneider R. and Frank M. (2021) The impact of postdepositional alteration on iron-and molybdenum-based redox proxies. *Geology*, **49**, 1411–1415.

Etim I-I. N., Wei J., Dong J., Xu D., Chen N., Wei X., Su M. and Ke W. (2018) Mitigation of the Corrosion-Causing *Desulfovibrio Desulfuricans* Biofilm Using an Organic Silicon Quaternary Ammonium Salt in Alkaline Media Simulated Concrete Pore Solutions. *Biofouling*, **34**, 1121–1137.

Evans Jr H.T., Milton C., Chao E., Adler I., Mead C., Ingram B. and Berner R.A. (1964) Valleriite and the new iron sulfide., mackinawite. *US Geological Survey Professional Paper*, **475**, 64–69.

Eynard A., del Campillo M.C., Barrón V. and Torrent J (1992) Use of vivianite ($Fe_3(PO_4)_2.8H_2O$) to prevent iron chlorosis in calcareous soils. *Fertilizer Research*, **31**, 61–67.

Fakhraee M. and Katsev S. (2019) Organic sulfur was integral to the Archean sulfur cycle. *Nature Communications*, **10**, 4556.

Fan Q., Wang L., Fu Y, Li Q., Liu Y, Wang Z. and Zhu H. (2023) Iron redox cycling in layered clay minerals and its impact on contaminant dynamics: A review. *Science of the Total Environment*, **855**, 159003.

Farina M., Esquivel D.M.S. and Lins de Barros H.G.P. (1990) Magnetic iron-sulphur crystals from a magnetotactic microorganism. *Nature*, **343**, 256–258.

Farquhar J., Bao H. and Thiemens M. (2000) Atmospheric influence of Earth's earliest sulfur cycle. *Science*, **289**, 756–758.

Farquhar J., Savarino J., Airieau J. and Thiemens M. (2001) Observation of wavelength-sensitive mass-independent sulfur isotope effects during SO_2 photolysis: Implications for the early atmosphere. *Journal of Geophysical Research: Planets*, **106**, 32829–32839.

Farquhar J., Johnston D.T., Wing B.A., Habicht K.S., Canfield D.E., Airieau S. and Thiemens M.H. (2003) Multiple sulphur isotopic interpretations of biosynthetic pathways: implications for biological signatures in the sulphur isotope record. *Geobiology*, **1**, 27–36.

Fehr M.A., Andersson P.S., Hålenius U. and Mörth C.M. (2008) Iron isotope variations in Holocene sediments of the Gotland Deep, Baltic Sea. *Geochimica et Cosmochimica Acta*, **72**, 807–826.

Fehr M.A., Andersson P.S., Hålenius U., Gustafsson O. and Morth C.M. (2010) Iron enrichments and Fe isotopic compositions of surface sediments from the Gotland Deep, Baltic Sea. *Chemical Geology*, **277**, 310–322.

Ferris F.G., Fyfe W.S. and Beveridge T.J. (1987) Bacteria as nucleation sites for authigenic minerals in a metal-contaminated lake sediment. *Chemical Geology*, **63**, 225–232.

Fike D., Bradley A. and Rose C. (2015) Rethinking the ancient sulfur cycle. *Annual Review of Earth and Planetary Sciences*, **43**, 593–622.

Findlay AJ (2016) Microbial impact on polysulfide dynamics in the environment. *FEMS Microbiology Letters.*

Findlay A.J., Gartman A., Macdonald D.J., Hanson T.E., Shaw T.J. and Luther G. W. (2014) Distribution and size fractionation of elemental sulfur in aqueous environments: The Chesapeake Bay and Mid-Atlantic Ridge. *Geochimica et Cosmochimica Acta*, **142**, 334–348.

Finster K., Liesack W. and Thamdrup B. (1998) Elemental sulfur and thiosulfate disproportionation by *Desulfocapsa sulfoexigens* sp. nov., a new anaerobic bacterium isolated from marine surface sediment. *Applied and Environmental Microbiology*, **64**, 119–125.

Fortin D. and Beveridge T.J. (1997) Microbial sulfate reduction within sulfidic mine tailings: Formation of diagenetic Fe sulfides. *Geomicrobiology Journal*, **14**, 1–21.

Fortin D., Southam G. and Beveridge T.J. (1994) Nickel sulfide, iron-nickel sulfide and iron sulfide precipitation by a newly isolated *Desulfotomaculum* species and its relation to nickel resistance. *FEMS Microbiology Ecology*, **14**, 121–132.

Fouquet Y, Schultz A., Herrington R. and Nesbitt R.W. (1997) Where are the large hydrothermal sulphide deposits in the oceans? *Source: Philosophical Transactions: Mathematical, Physical and Engineering Sciences*, **355**, 427–441.

Fouquet Y, Cambon P., Etoubleau J., Charlou J., Ondréas H., Barriga F., Cherkashov G., Semkova T., Poroshina I., Bohn M. and Donval J. (2010) Geodiversity of hydrothermal processes along the Mid-Atlantic Ridge and ultramafic-hosted mineralization: A new type of oceanic Cu-Zn-Co-Au volcanogenic. *Diversity of hydrothermal systems on slow spreading ocean ridges*, **188**, 321–367.

Franz B., Lichtenberg H., Hormes J., Modrow H., Dahl C. and Prange A. (2007) Utilization of solid "elemental" sulfur by the phototrophic purple sulfur bacterium *Allochromatium vinosum*: A sulfur K-edge X-ray absorption spectroscopy study. *Microbiology*, **153**, 1268–1274.

Fry B., Cox J., Gest H. and Hayes J.M. (1986) Discrimination between ^{34}S and ^{32}S during bacterial metabolism of inorganic sulfur-compounds. *Journal of Bacteriology*, **165**, 328–330.

Gao J., Zheng T., Deng Y. and Jiang H. (2021) Microbially Mediated Mobilization of Arsenic from Aquifer Sediments under Bacterial Sulfate Reduction. *Science of The Total Environment*, **768**, 144709.

Gao K., Jiang M., Guo C., Zeng Y, Fan C., Zhang J., Reinfelder J.R., Huang W., Lu G. and Dang Z. (2019) Reductive dissolution of jarosite by a sulfate reducing bacterial community: Secondary mineralization and microflora development. *Science of The Total Environment*, **690**, 1100–1109.

Gartman A., Yücel M., Madison A., Chu D., Ma S., Janzen C., Becker E., Beinart R., Girguis P. and Luther III G. (2011) Sulfide Oxidation across Diffuse Flow Zones of Hydrothermal Vents. *Aquatic Geochemistry*, **17**, 583–601.

Goldford J.E., Hartman H., Marsland R. and Segrè D. (2019) Environmental boundary conditions for the origin of life converge to an organo-sulfur metabolism. *Nature Ecology & Evolution*, **3**, 1715–1724.

Goldhaber M. and Kaplan I. (1980) Mechanisms of sulfur incorporation and isotope fractionation during early diagenesis in sediments of the Gulf of California. *Marine Chemistry*, **9**, 95–143.

Gomes M., Hurtgen M. and Sageman B. (2016) Biogeochemical sulfur cycling during Cretaceous oceanic anoxic events: A comparison of OAE1a and OAE2. *Paleoceanography*, **31**, 233–251.

Gorlas A., Marguet E., Gill S., Geslin C., Guigner J., Guyot F. and Forterre P. (2015) Sulfur vesicles from *Thermococcales*: A possible role in sulfur detoxifying mechanisms. *Biochimie*, **118**, 356–364.

Gorlas A., Jacquemot P., Guigner J.M., Gill S., Forterre P. and Guyot F. (2018) Greigite nanocrystals produced by hyperthermophilic archaea of *Thermococcales* order. *PLoS ONE*, **13**, 1–10.

Gorlas A., Mariotte T., Morey L., Truong C., Bernard S., Guigner J-M., Oberto J., Baudin F., Landrot G., Baya C., Le Pape P., Morin G., Forterre P. and Guyot F. (2022) Precipitation of greigite and pyrite induced by *Thermococcales*: an advantage to live in Fe- and S-rich environments? *Environmental Microbiology*, **24**, 626–642.

Graaf R. D.E., De Decker Y., Sojo V. and Hudson R. (2023) Quantifying Catalysis at the Origin of Life. *Chemistry – A European Journal*, **29**, e202301447.

https://doi.org/10.1180/gbi.2024.9 Published online by Cambridge University Press

Gramp J.P., Bigham J.M., Jones F.S. and Tuovinen O.H. (2010) Formation of Fe-sulfides in cultures of sulfate-reducing bacteria. *Journal of Hazardous Materials*, **175** (1–3), 1062–1067.

Gregory D.D. (2020) *The Pyrite Trace Element Paleo-Ocean Chemistry Proxy*,. Cambridge University Press, UK.

Gregory D., Meffre S. and Large R. (2014) Comparison of metal enrichment in pyrite framboids from a metal-enriched and metal-poor Estuary. *American Mineralogist*, **99**, 633–644.

Gregory D.D., Lyons T.W., Large R.R., Jiang G., Stepanov A.S., Diamond C.W., Figueroa M.C. and Olin P. (2017) Whole rock and discrete pyrite geochemistry as complementary tracers of ancient ocean chemistry: an example from the Neoproterozoic Doushantuo Formation. *Geochimica et Cosmochimica Acta*, **216**, 201–220.

Gregory D.D., Kovarik L., Taylor S.D., Perea D.E., Owens J.D., Atienza N. and Lyons T.W. (2022a) Nanoscale trace-element zoning in pyrite framboids and implications for paleoproxy applications. *Geology*, **50**, 736–740.

Gregory D.D., Lyons T.W., Large R.R. and Stepanov A.S. (2022b) Ground-truthing the pyrite trace element proxy in modern euxinic settings. *American Mineralogist*, **107**, 848–859.

Guilbaud R., Butler I.B. and Ellam R.M. (2011) Abiotic pyrite formation produces a large Fe isotope fractionation. *Science*, **332**, 1548–1551.

Habicht K.S., Gade M., Thamdrup B., Berg P. and Canfield D.E. (2002) Calibration of sulfate levels in the Archean ocean. *Science*, **298**, 2372–2374.

Halevy I. (2013) Production, preservation, and biological processing of mass-independent sulfur isotope fractionation in the Archean surface environment. *PNAS*, **110**, 17644–17649.

Halevy I., Johnston D.T. and Schrag D.P. (2010) Explaining the structure of the Archean mass-independent sulfur isotope record. *Science*, **329**, 204–207.

Halevy I., Fike D.A., Pasquier V., Bryant R.N., Wenk C.B., Turchyn A.V., Johnston D.T. and Claypool G.E. (2023) Sedimentary parameters control the sulfur isotope composition of marine pyrite. *Science*, **382**, 946–952.

Hannington M., Tivey M., Larocque A., Petersen S. and Rona P. (1995) The occurrence of gold in sulfide deposits of the TAG hydrothermal field, Mid-Atlantic Ridge. *The Canadian Mineralogist*, **33**, 1285–1310.

Harmsen G.W.(1954) Observations on the formation and oxidation of pyrite in the soil. *Plant and Soil*, **5**(4), 324–348.

Hatton B. and Rickard D. (2008) Nucleic acids bind to nanoparticulate iron (II) monosulphide in aqueous solutions. *Origins of Life and Evolution of Biospheres*, **38**, 257–270.

He C., Tian G., Liu Z. and Feng S. (2010) A mild hydrothermal route to fix carbon dioxide to simple carboxylic acids. *Organic Letters*, **12**, 649–651.

He R., Hu B., Zhong H., Jin F., Fan J., Hu Y.H. and Jing Z. (2019) Reduction of CO_2 with H_2S in a simulated deep-sea hydrothermal vent system. *Chemical Communications*, **55**, 1056–1059.

Heard A.W., Dauphas N., Guilbaud R., Rouxel O.J., Butler I.B., Nie N.X. and Bekker A. (2020) Triple iron isotope constraints on the role of ocean iron sinks in early atmospheric oxygenation. *Science*, **370**, 446–449.

Hellige K., Pollok K., Larese-Casanova P., Behrends T. and Peiffer S. (2012) Pathways of ferrous iron mineral formation upon sulfidation of lepidocrocite surfaces. *Geochimica et Cosmochimica Acta*, **81**, 69–81.

Helz G.R. (2014) Activity of zero-valent sulfur in sulfidic natural waters. *Geochemical Transactions*, **15**, 1–13.

Hepburn L.E., Butler I.B., Boyce A. and Schröder C. (2020) The use of operationally-defined sequential Fe extraction methods for mineralogical applications: A cautionary tale from Mössbauer spectroscopy. *Chemical Geology*, **543**, 119584.

Herbert R.B., Benner S.G., Pratt A.R. and Blowes D.W. (1998) Surface chemistry and morphology of poorly crystalline iron sulfides precipitated in media containing sulfate-reducing bacteria. *Chemical Geology*, **144**, 87–97.

Herschy B., Whicher A., Camprubi E., Watson C., Dartnell L., Ward J., Evans J. R.G. and Lane N. (2014) An Origin-of-Life Reactor to Simulate Alkaline Hydrothermal Vents. *Journal of Molecular Evolution*, **79**, 213–227.

Hockmann K., Planer-Friedrich B., Johnston S.G., Peiffer S. and Burton E.D. (2020) Antimony mobility in sulfidic systems: Coupling with sulfide-induced iron oxide transformations. *Geochimica et Cosmochimica Acta*, **282**, 276–296.

Hoek J., Reysenbach A., Habicht K. and Canfield D. (2006) Effect of hydrogen limitation and temperature on the fractionation of sulfur isotopes by a deep-sea hydrothermal vent sulfate-reducing bacterium. *Geochimica et Cosmochimica Acta*, **70**, 5831–5841.

Holden J.F. and Adams M.W.W. (2003) Microbe–metal interactions in marine hydrothermal environments. *Current Opinion in Chemical Biology*, **7**, 160–165.

Holden J.F., Breier J., Rogers K., Schulte M. and Toner B. (2012) Biogeochemical processes at hydrothermal vents: Microbes and minerals, bioenergetics, and carbon fluxes. *Oceanography*, **1**, 196–208.

Holmkvist L., Ferdelman T.G. and Jørgensen B.B. (2011) A cryptic sulfur cycle driven by iron in the methane zone of marine sediment (Aarhus Bay, Denmark). *Geochimica et Cosmochimica Acta*, **75**, 3581–3599.

Houghton J., Scarponi D., Capraro L. and Fike D. (2022) Impact of sedimentation, climate and sea level on marine sedimentary pyrite sulfur isotopes: Insights from the Valle di Manche section (Lower-Middle Pleistocene, southern Italy). *Palaeogeography, Palaeoclimatology, Palaeoecology*, **585**, 110730.

Howarth R.W. and Giblin A. (1983) Sulfate reduction in the salt marshes at Sapelo Island, Georgia. *Limnology and Oceanography*, **28**, 70–82.

Howarth R.W. and Merkel S. (1984) Pyrite formation and the measurement of sulfate reduction in salt marsh sediments. *Limnology and Oceanography*, **29**, 598–608.

Huang X.L., Harmer J.R., Schenk G. and Southam G. (2024) Inorganic Fe-O and Fe-S oxidoreductases: paradigms for prebiotic chemistry and the evolution of enzymatic activity in biology. *Frontiers in Chemistry*, **12**, 1349020.

Huber C. and Wächterhäuser G. (1997) Activated acetic acid by carbon fixation on (Fe,Ni)S under primordial conditions. *Science*, **276**, 245–247.

Huber G., Huber R., Jones B.E., Lauerer G., Neuner A., Segerer A., Stetter K.O. and Degens E.T. (1991) Hyperthermophilic archaea and bacteria occurring within Indonesian hydrothermal areas. *System. Appl. Microbiol*, **14**, 397–404.

Hudson R., de Graaf R., Strandoo R.M., Ohno A., Lane N., McGlynn S.E., Yamada Y.M.A., Nakamura R., Barge L.M., Braun D. and Sojo V. (2020) CO_2 reduction driven by a pH gradient. *Proceedings of the National Academy of Sciences*, **117**, 22873–22879.

Huffman E.O., Cate W.E. and Deming M.E. (1960) Rates and mechanisms of dissolution of some ferric phosphates. *Soil Science*, **90**, 8–15.

Humphris S.E. and Mccollom T. (1998) The Cauldron Beneath the Seafloor. *Oceanus*, **41**, 18–21.

Hunger S., Benning L.G. (2007) Greigite: A true intermediate on the polysulfide pathway to pyrite. *Geochemical Transactions*, **8**, 1–20.

Hutchings A. and Turchyn A. (2021) A quantification of the effect of diagenesis on the paleoredox record in mid-Proterozoic sedimentary rocks. *Geology*, **49**, 1143–1147.

Hyacinthe C. and Van Cappellen P. (2004) An authigenic iron phosphate phase in estuarine sediments: Composition, formation and chemical reactivity. *Marine Chemistry*, **91**, 227–251.

Igarashi K., Yamamura Y. and Kuwabara T. (2016) Natural synthesis of bioactive greigite by solid–gas reactions. *Geochimica et Cosmochimica Acta*, **191**, 47–57.

Ikkert O.P., Ivanov M.V., Ukhova A., Zuysman V.S., Glukhova L.B., Avakyan M. R. and Karnachuk O.V. (2021) *Desulfovibrio* Isolate from the Microbiote of Children with Autistic Spectrum Disorders Immobilizes Iron in Poorly Soluble Crystalline Sulfides. *Microbiology*, **90**, 268–271.

Ikogou M., Ona-Nguema G., Juillot F., Le Pape P., Menguy N., Richeux N., Guigner JM., Noël V., Brest J., Baptiste B. and Morin G. (2017) Long-term sequestration of nickel in mackinawite formed by *Desulfovibrio capillatus* upon Fe(III)-citrate reduction in the presence of thiosulfate. *Applied Geochemistry*, **80**, 143–154.

Ivarson K.C. and Hallberg R.O. (1976) Formation of mackinawite by the microbial reduction of jarosite and its application to tidal sediments. *Geoderma*, **16**, 1–7.

Jakus N., Mellage A., Carmen H., Maisch M., Byrne J.M., Mueller C.W., Grathwohl P. and Kappler A. (2021) Anaerobic neutrophilic pyrite oxidation by a chemolithoautotrophic nitrate-reducing iron(II)-oxidizing culture enriched from a fractured aquifer. *Environmental Science & Technology*, **55**, 9876–9884.

Jia R., Tan JL., Jin P., Blackwood DJ., Xu D. and Gu T (2018) Effects of Biogenic H_2S on the Microbiologically Influenced Corrosion of Carbon Steel by Sulfate Reducing *Desulfovibrio Vulgaris* Biofilm. *Corrosion Science*, **130**, 1–11.

https://doi.org/10.1180/gbi.2024.9 Published online by Cambridge University Press

Jia R., Wang D., Jin P., Unsal T., Yang D., Yang J., Xu D. and Gu T. (2019) Effects of ferrous ion concentration on microbiologically influenced corrosion of carbon steel by sulfate reducing bacterium *Desulfovibrio vulgaris*. *Corrosion Science*, **153**, 127–137.

Jiang X., Hu J., Lieber A.M., Jackan C.S., Biffinger J.C., Fitzgerald L.A., Ringeisen B.R. and Lieber C.M. (2014) Nanoparticle facilitated extracellular electron transfer in microbial fuel cells. *Nano Letters*, **14**, 6737–6742.

Jiang Z., Liu Q., Roberts A.P., Dekkers M.J., Barrón V., Torrent J. and Li S. (2022) The magnetic and color reflectance properties of hematite: From Earth to Mars. *Reviews of Geophysics*, **60**, e2020RG000698

Johnson C., Beard B. and Weyer S. (2020) *Iron geochemistry: An isotopic perspective*,. Springer, Cham, Switzerland.

Johnson C.M., Beard B.L. and Roden E.E. (2008) The iron isotope fingerprints of redox and biogeochemical cycling in modern and ancient Earth. *Annual Review of Earth and Planetary Sciences*, **36**, 457–493.

Johnson D.B. and Sánchez-Andrea I. (2019) Dissimilatory reduction of sulfate and zero-valent sulfur at low pH and its significance for bioremediation and metal recovery. *Advances in Microbial Physiology*, **75**, 205–231.

Johnson D.C., Dean D.R., Smith A.D. and Johnson M.K. (2005) Structure, function, and formation of biological iron-sulfur clusters. *Annual Review of Biochemistry*, **74**, 247–281.

Johnson J.E., Gerpheide A., Lamb M.P. and Fischer W.W. (2014) O_2 constraints from Paleoproterozoic detrital pyrite and uraninite. *Geological Society of American Bulletin*, **126**, 813–830.

Johnston D. (2011) Multiple sulfur isotopes and the evolution of Earth's surface sulfur cycle. *Earth-Science Reviews*, **106**, 161–183.

Johnston D., Wing B., Farquhar J., Wing B., Kaufman A., Canfield D. and Habicht K. (2005a) Active microbial sulfur disproportionation in the Mesoproterozoic. *American Journal of Science*, **305**, 645–660.

Johnston D.T., Farquhar J. and Canfield D.E. (2007) Sulfur isotope insights into microbial sulfate reduction: When microbes meet models. *Geochimica et Cosmochimica Acta*, **71**, 3929–3947.

Johnston D.T., Farquhar J., Wing B.A., Kaufman A.J., Canfield D.E. and Habicht K.S. (2005b) Multiple sulfur isotope fractionations in biological systems: A case study with sulfate reducers and sulfur disproportionators. *American Journal of Science*, **305**, 645–660.

Jørgensen B.B., Findlay A.J. and Pellerin A. (2019) The biogeochemical sulfur cycle of marine sediments. *Frontiers in Microbiology*, **10**, 1–27.

Juniper S.K. and Martineu P. (1995) Alvinellids and sulfides at hydrothermal vents of the Eastern Pacific: A review. *American Zoologist*, **35**, 174–185.

Kah L.C., Lyons T.W. and Frank T.D. (2004) Low marine sulphate and protracted oxygenation of the Proterozoic biosphere. *Nature*, **431**, 834–838.

Kamyshny A., Borkenstein C.G. and Ferdelman T.G. (2009) Protocol for quantitative detection of elemental sulfur and polysulfide zero-valent sulfur distribution in natural aquatic samples. *Geostandards and Geoanalytical Research*, **33**, 415–435.

Kamyshny A., Ekeltchik I., Gun J. and Lev O. (2006) Method for the determination of inorganic polysulfide distribution in aquatic systems. *Analytical Chemistry*, **78**, 2631–2639.

Kamyshny A. and Ferdelman T.G. (2010) Dynamics of zero-valent sulfur species including polysulfides at seep sites on intertidal sand flats (Wadden Sea, North Sea). *Marine Chemistry*, **121**, 17–26.

Kamyshny A., Goifman A., Gun J., Rizkov D. and Lev O. (2004) Equilibrium distribution of polysulfide ions in aqueous solutions at 25 °C: A new approach for the study of polysulfides' equilibria. *Environmental science & technology*, **38**, 6633–6644.

Kandori K., Kuwae T. and Ishikawa T. (2006) Control on size and adsorptive properties of spherical ferric phosphate particles. *Journal of Colloid and Interface Science*, **300**, 225–231.

Kaplan I.R., Emery K.O. and Rittenbebg S.C. (1963) The distribution and isotopic abundance of sulphur in recent marine sediments off southern California. *Geochimica et Cosmochimica Acta*, **27**, 297–331.

Kappler A., Bryce C., Mansor M., Lueder U., Byrne J.M. and Swanner E.D. (2021) An evolving view on biogeochemical cycling of iron. *Nature Reviews Microbiology*, **19**(6), 360–374.

Kappler A., Thompson A. and Mansor M. (2023) Impact of biogenic magnetite formation and transformation on biogeochemical cycles. *Elements*, **19**, 222–227.

Karnachuk O.V., Ikkert O.P., Avakyan M.R., Knyazev Y.V., Volochaev M.N., Zyusman V.S., Panov V.L., Kadnikov V.V., Mardanov A.V. and Ravin N.V. (2021) *Desulfovibrio Desulfuricans* AY5 Isolated from a Patient with Autism Spectrum Disorder Binds Iron in Low-Soluble Greigite and Pyrite. *Microorganisms*, **9**, 2558.

Ke C., Deng Y, Zhang S., Ren M., Liu B., He J., Wu R., Dang Z. and Guo C. (2024) Sulfate availability drives the reductive transformation of schwertmannite by co-cultured iron- and sulfate-reducing bacteria. *Science of the Total Environment*, **906**, 167690.

Keeling R.F., Körtzinger A. and Gruber N. (2010) Ocean deoxygenation in a warming world. *Annual Review of Marine Science*, **2**, 199–229.

Keil R. (2017) Anthropogenic forcing of carbonate and organic carbon preservation in marine sediments. *Annual Review of Marine Science*, **9**, 151–172.

Kish A., Miot J., Lombard C., Guigner J-M., Bernard S., Zirah S. and Guyot F. (2016) Preservation of archaeal surface layer structure during mineralization. *Scientific Reports*, **6**, 26152.

Kleinjan W., De Keizer A. and Janssen A.J.H. (2005) Kinetics of the reaction between dissolved sodium sulfide and biologically produced sulfur. *ACS Publications*, **44**, 309–317.

Kondo K., Okamoto A., Hashimoto K. and Nakamura R. (2015) Sulfur-Mediated Electron Shuttling Sustains Microbial Long-Distance Extracellular Electron Transfer with the Aid of Metallic Iron Sulfides. *Langmuir*, **31**, 7427–7434.

Konhauser K.O., Lalonde S.V., Planavsky N.J., Pecoits E., Lyons T.W., Mojzsis S. J., Rouxel O.J., Barley M.E., Rosìere C., Fralick P.W., Kump L.R. and Bekker A. (2011) Aerobic bacterial pyrite oxidation and acid rock drainage during the Great Oxidation Event. *Nature*, **478**, 369–373.

Kusebauch C., Gleeson S.A. and Oelze M. (2019) Coupled partitioning of Au and As into pyrite controls formation of giant Au deposits. *Science Advances*, **5**, eaav5891.

Lalonde K., Mucci A., Ouellet A. and Gélinas Y. (2012) Preservation of organic matter in sediments promoted by iron. *Nature*, **483**, 198–200.

Langmuir D. (1997) *Aqueous Environmental Geochemistry*,. Prentice Hall, New Jersey.

Large R.R., Halpin J.A., Danyushevsky L.V., Maslennikov V.V., Bull S.W., Long J.A., Gregory D.D., Lounejeva E., Lyons T.W., Sack P.J., McGoldrick P.J. and Calver C.R. (2014) Trace element content of sedimentary pyrite as a new proxy for deep-time ocean-atmosphere evolution. *Earth and Planetary Science Letters*, **389**, 209–220.

Lau G.E., Cosmidis J., Grasby S.E., Trivedi C.B., Spear J.R. and Templeton A.S. (2017) Low-temperature formation and stabilization of rare allotropes of cyclooctasulfur (β-S_8 and γ-S_8) in the presence of organic carbon at a sulfur-rich glacial site in the Canadian High Arctic. *Geochimica et Cosmochimica Acta*, **200**, 218–231.

Lazcano A. and Miller S.L. (1999) On the origin of metabolic pathways. *Journal of Molecular Evolution*, **49**, 424–431.

Leavitt W.D., Halevy I., Bradley A.S. and Johnston D.T. (2013) Influence of sulfate reduction rates on the Phanerozoic sulfur isotope record. *PNAS*, **110**, 11244–11249.

Leavitt W.D., Waldbauer J., Venceslau S.S., Sub S.M., Zhang L., Boidi F.J., Plummer S., Diaz J.M., Pereira I.A.C. and Bradley A.S. (2024) Energy flux couples sulfur isotope fractionation to proteomic and metabolite profiles in *Desulfovibrio vulgaris*. *Geobiology*, **22**, e12600.

Lee M-K., Saunders J.A., Wilson T., Levitt E., Ghandehari S., Dhakal P., Redwine J., Marks J., Billor Z.M., Miller B., Han D. and Wang L. (2019) Field-Scale Bioremediation of Arsenic-Contaminated Groundwater Using Sulfate-Reducing Bacteria and Biogenic Pyrite. *Bioremediation Journal*, **23**, 1–21.

Lefèvre C.T., Menguy N., Abreu F., Lins U., Pósfai M., Prozorov T., Pignol D., Frankel R.B. and Bazylinski D.A. (2011) A Cultured Greigite-Producing Magnetotactic Bacterium in a Novel Group of Sulfate-Reducing Bacteria. *Science*, **334**, 1720–1723.

Lennie A.R. (1995) Synthesis and Rietveld crystal structure refinement of mackinawite, tetragonal FeS. *Mineralogical Magazine*, **59**, 677–683.

Lennie, A.R., Redfern, S.A., Champness, P.E., Stoddart, C.P., Schofield, P.F. and Vaughan, D.J. (1997). Transformation of mackinawite to greigite; an insitu X-ray powder diffraction and transmission electron microscope study. *American Mineralogist*, **82**(3-4), 302–309.

https://doi.org/10.1180/gbi.2024.9 Published online by Cambridge University Press

Lepot K. (2020) Signatures of early microbial life from the Archean (4 to 2.5 Ga) eon. *Earth-Science Reviews*, **209**, 103296.

Levin L.A. and Bris N.L. (2015) The deep ocean under climate change. *Science*, **350**, 766–768.

Li Y.L., Vali H., Sears S.K., Yang J., Deng B. and Zhang C.L. (2004) Iron reduction and alteration of nontronite NAu-2 by a sulfate-reducing bacterium. *Geochimica et Cosmochimica Acta*, **68**, 3251–3260.

Li Y-L., Vali H., Yang J., Phelps T.J. and Zhang C.L. (2006) Reduction of iron oxides enhanced by a sulfate-reducing bacterium and biogenic H_2S. *Geomicrobiology Journal*, **23**, 103–117.

Lin Z., Sun X., Lu Y, Strauss H., Xu L., Gong J., Teichert B.M.A., Lu R., Lu H., Sun W. and Peckmann J. (2017) The enrichment of heavy iron isotopes in authigenic pyrite as a possible indicator of sulfate-driven anaerobic oxidation of methane: Insights from the South China Sea. *Chemical Geology*, **449**, 15–29.

Lin Z., Sun X., Lu Y, Strauss H., Xu L., Chen T., Lu H. and Peckmann J. (2018) Iron isotope constraints on diagenetic iron cycling in the Taixinan seepage area, South China Sea. *Journal of Asian Earth Sciences*, **168**, 112–124.

Liu D., Dong H., Bishop M.E., Zhang J., Wang H., Xie S., Wang S., Huang L. and Eberl D.D. (2012) Microbial reduction of structural iron in interstratified illite-smectite minerals by a sulfate-reducing bacterium. *Geobiology*, **10**, 150–162.

Liu J., Antler G., Pellerin A., Izon G., Dohrmann I., Findlay A.J., Røy H., Ono S., Turchyn A.V., Kasten S. and Jørgensen B.B. (2021) Isotopically "heavy" pyrite in marine sediments due to high sedimentation rates and non-steady-state deposition. *Geology*, **49**, 816–821.

Longman J., Faust J.C., Bryce C., Homoky W.B. and März C. (2022) Organic carbon burial with reactive iron across global environments. *Global Biogeochemical Cycles*, **36**, e2022GB007447.

Lovley D.R., Coates J.D., Saffarini D.A. and Lonergan D.J. (2022) Dissimilatory Iron Reduction. Pp. 187–215 in: *Transition Metals in Microbial Metabolism*,. CRC Press, London.

Luther G.W. (1991) Pyrite synthesis via polysulfide compounds. *Geochimica et Cosmochimica Acta*, **55**, 2839–2849.

Luther G.W., Findlay A.J., MacDonald D.J., Owings S.M., Hanson T.E., Beinart R.A. and Girguis P.R. (2011) Thermodynamics and kinetics of sulfide oxidation by oxygen: A look at inorganically controlled reactions and biologically mediated processes in the environment. *Frontiers in Microbiology*, **2**, 1–9.

Lyons T.W., Reinhard C.T. and Planavsky N.J. (2014) The rise of oxygen in Earth's early ocean and atmosphere. *Nature*, **506**, 307–15.

Lyons T.W., Tino C.J., Fournier G.P., Anderson R.E., Leavitt W.D., Konhauser K.O. and Stüeken E.E. (2024) Co-evolution of early Earth environments and microbial life. *Nature Reviews Microbiology*, **22**, 572–586.

Ma W.W., Zhu M.X., Yang G.P., Li T., Li Q.Q., Liu S.H. and Li J.L. (2022) Stability and molecular fractionation of ferrihydrite-bound organic carbon during iron reduction by dissolved sulfide. *Chemical Geology*, **594**, 120774.

Mann S., Sparks N., Frankel R., Bazylinski D. and Jannasch H. (1990) Biomineralization of Ferrimagnetic Greigite (Fe_3S_4) and Iron Pyrite (FeS_2) in a Magnetotactic Bacterium. *Nature*, **343**, 258–261.

Mansor M., Berti D., Hochella Jr M.F., Murayama M. and Xu J. (2019) Phase, morphology, elemental composition and formation mechanisms of biogenic and abiogenic Fe-Cu-sulfide nanoparticles: A comparative study on their occurrences under anoxic conditions. *American Mineralogist*, **104**, 703–717.

Mansor M. and Fantle M.S. (2019) A novel framework for interpreting pyrite-based Fe isotope records of the past. *Geochimica et Cosmochimica Acta*, **253**, 39–62.

Mansor M. and Xu J. (2020) Benefits at the nanoscale: A review of nanoparticle-enabled processes favouring microbial growth and functionality. *Environmental Microbiology*, **22**, 3633–3649.

Marin-Carbonne J., Remusat L., Sforna M.C., Thomazo C., Cartigny P. and Philippot P. (2018) Sulfur isotope's signal of nanopyrites enclosed in 2.7 Ga stromatolitic organic remains reveal microbial sulfate reduction. *Geobiology*, **16**, 121–138.

Marin-Carbonne J., Busigny V., Miot J., Rollion-Bard C., Muller E., Drabon N., Jacob D., Pont S., Robyr M., Bontognali T.R.R., François C., Reynaud S., Zuilen M VaN. and Philippot P. (2020) In Situ Fe and S isotope analyses in pyrite from the 3.2 Ga Mendon Formation (Barberton Greenstone Belt, South Africa): Evidence for early microbial iron reduction. *Geobiology*, **18**, 306–325.

Marin-Carbonne J., Decraene M-N., Havas R., Remusat L., Pasquier V., Alléon J., Zeyen N., Bouton A., Bernard S., Escrig S., Olivier N., Vennin E., Meibom A., Benzerara K. and Thomazo C. (2022) Early precipitated micropyrite in microbialites: A time capsule of microbial sulfur cycling. *Geochemical Perspectives*, **21**, 7–12.

Marnocha C.L., Sabanayagam C.R., Modla S., Powell D.H., Henri P.A., Steele A. S., Hanson T.E., Webb S.M. and Chan C.S. (2019) Insights into the mineralogy and surface chemistry of extracellular biogenic S^0 globules produced by *Chlorobaculum tepidum*. *Frontiers in Microbiology*, **10**, 1–11.

Mateos K., Chappell G., Klos A., LE B., Boden J., Stüeken E. and Anderson R. (2023) The evolution and spread of sulfur cycling enzymes reflect the redox state of the early Earth. *Science Advances*, **9**, eade4847.

McAnena A., Severmann S., Guilbaud R. and Poulton S.W. (2024) Iron isotope fractionation during sulfide-promoted reductive dissolution of iron (oxyhydr)oxide minerals. *Geochimica et Cosmochimica Acta*, **369**, 17–34.

McCollom T.M. (2007) Geochemical constraints on sources of metabolic energy for chemolithoautotrophy in ultramafic-hosted deep-sea hydrothermal systems. *Astrobiology*, **7**, 933–950.

Metz R., Kumar N., Schenkeveld W.D.C. and Kraemer SM (2023) Rates and Mechanism of Vivianite Dissolution under Anoxic Conditions. *Environmental Science and Technology*, **57**, 17266–17277.

Miot J., Remusat L., Duprat E., Gonzalez A., Pont S. and Poinsot M. (2015) Fe biomineralization mirrors individual metabolic activity in a nitrate-dependent Fe(II)-oxidizer. *Frontiers in Microbiology*, **6**, 1–13.

Mol A.R., Pruim S., de Korte M., Meuwissen D.J.M., van der Weijden R.D., Klok J.B.M., Keesman K.J. and Buisman C.J.N. (2022) Removal of small elemental sulfur particles by polysulfide formation in a sulfidic reactor. *Water Research*, **227**, 119296.

Moore O.W., Curti L., Woulds C., Bradley J.A., Babakhani P., Mills B.J.W., Homoky W.B., Xiao K.Q., Bray A.W., Fisher B.J., Kazemian M., Kaulich B., Dale A.W. and Peacock C.L. (2023) Long-term organic carbon preservation enhanced by iron and manganese. *Nature*, **621**, 312–317.

Morin G., Noël V., Menguy N., Brest J., Baptiste B., Tharaud M., Ona-Nguema G., Ikogou M., Viollier E. and Juillot F. (2017) Nickel accelerates pyrite nucleation at ambient temperature. *Geochemical Perspectives Letters*, **5**, 6–11.

Muchowska K.B., Chevallot-Beroux E. and Moran J. (2019) Recreating ancient metabolic pathways before enzymes. *Bioorganic & Medicinal Chemistry*, **27**, 2292–2297.

Nabeh N., Brokaw C. and Picard A. (2022) Quantification of organic carbon sequestered by biogenic iron sulfide minerals in long-term anoxic laboratory incubations. *Frontiers in Microbiology*, **13**, 662219.

Nakamura R., Okamoto A., Tajima N., Newton G.J., Kai F., Takashima T. and Hashimoto K. (2010) Biological Iron-Monosulfide Production for Efficient Electricity Harvesting from a Deep-Sea Metal-Reducing Bacterium. *ChemBioChem*, **11**, 643–645.

Neal A.L., Techkarnjanaruk S., Dohnalkova A., McCready D., Peyton BM. and Geesey GG (2001) Iron sulfides and sulfur species produced at hematite surfaces in the presence of sulfate-reducing bacteria. *Geochimica et Cosmochimica Acta*, **65**, 223–235.

Oduro H., Ono S., Alrasheed F. and Eldridge D. (2023) Organosulfur aerosols likely carried sulfur MIF signatures in the early Earth's atmosphere. *Geochemistry, Geophysics, Geosystems*, **24**, e2022GC010777.

Ohfuji H. and Rickard D (2006) High resolution transmission electron microscopic study of synthetic nanocrystalline mackinawite. *Earth and Planetary Science Letters*, **241**, 227–233.

Ohmoto H., Kaiser C. and Geer K. (1990) Systematics of sulfur isotopes in recent marine sediments and ancient sediment-hosted base metal deposits. *University of Western Australia Extension Publication*, **23**, 70–120.

Ono S., Wing B., Johnston D., Farquhar J. and Rumble D. (2006) Mass-dependent fractionation of quadruple stable sulfur isotope system as a new tracer of sulfur biogeochemical cycles. *Geochimica et Cosmochimica Acta*, **70**, 2238–2252.

Orcutt B.N., Sylvan J.B., Knab N.J. and Edwards K.J. (2011) Microbial Ecology of the Dark Ocean above, at, and below the Seafloor. *Microbiology and Molecular Biology Reviews*, **75**, 361–422.

Ostrander C.M., Nielsen S.G., Owens J.D., Kendall B., Gordon G.W., Romaniello S.J. and Anbar A.D. (2019) Fully oxygenated water columns over continental shelves before the Great Oxidation Event. *Nature Geoscience*, **12**, 186–191.

https://doi.org/10.1180/gbi.2024.9 Published online by Cambridge University Press

Owens J.D., Gill B.C., Jenkyns H.C., Bates S.M., Severmann S., Kuypers M.M.M., Woodfine R.G. and Lyons T.W. (2013) Sulfur isotopes track the global extent and dynamics of euxinia during Cretaceous Oceanic Anoxic Event 2. *PNAS*, **110**, 18407–18412.

Pang Y. and Wang J. (2020) Insight into the mechanism of chemoautotrophic denitrification using pyrite (FeS_2) as electron donor. *Bioresource Technology*, **318**, 124105.

Park Y. and Faivre D. (2022) Diversity of microbial metal sulfide biomineralization. *ChemPlusChem*, **87**, e202100457.

Pasquier V., Bryant R.N., Fike D.A. and Halevy I. (2021a) Strong local, not global, controls on marine pyrite sulfur isotopes. *Science Advances*, **7**, 1–10.

Pasquier V., Fike D.A. and Halevy I. (2021b) Sedimentary pyrite sulfur isotopes track the local dynamics of the Peruvian oxygen minimum zone. *Nature Communications*, **12**, 1–10.

Pasquier V., Fike D.A., Révillon S. and Halevy I. (2022) A global reassessment of the controls on iron speciation in modern sediments and sedimentary rocks: A dominant role for diagenesis. *Geochimica et Cosmochimica Acta*, **335**, 211–230.

Pasquier V., Sansjofre P., Rabineau M., Revillon S., Houghton J. and Fike D.A. (2017) Pyrite sulfur isotopes reveal glacial-interglacial environmental changes. *PNAS*, **114**, 5941–5945.

Peiffer S., Behrends T., Hellige K., Larese-Casanova P., Wan M. and Pollok K. (2015) Pyrite formation and mineral transformation pathways upon sulfidation of ferric hydroxides depend on mineral type and sulfide concentration. *Chemical Geology*, **400**, 44–55.

Peiffer S., Kappler A., Haderlein S.B., Schmidt C., Byrne J.M., Kleindienst S., Vogt C., Richnow H.H., Obst M., Angenent L.T., Bryce C., McCammon C. and Planer-Friedrich B. (2021) A biogeochemical–hydrological framework for the role of redox-active compounds in aquatic systems. *Nature Geoscience*, **14**, 264–272.

Pellerin A., Anderson-Trocmé L., Whyte L.G., Zane G.M., Wall J.D. and Wing B. A. (2015) Sulfur isotope fractionation during the evolutionary adaptation of a sulfate-reducing bacterium. *Applied and Environmental Microbiology*, **81**, 2676–2689.

Peng X. and Zhou H. (2005) Growth history of hydrothermal chimneys at EPR 9-10 N: A structural and mineralogical study. *Science in China Series D: Earth Sciences*, **48**, 1891–1899.

Pi K., Wang Y., Xie X., Ma T., Liu Y., Su C., Zhu Y. and Wang Z. (2017) Remediation of Arsenic-Contaminated Groundwater by in-Situ Stimulating Biogenic Precipitation of Iron Sulfides. *Water Research*, **109**, 337–346.

Picard A., Gartman A. and Girguis P.R. (2016) What do we really know about the role of microorganisms in iron sulfide mineral formation? *Frontiers in Earth Science*, **4**, 1–10.

Picard A., Gartman A., Clarke D.R. and Girguis P.R. (2018) Sulfate-reducing bacteria influence the nucleation and growth of mackinawite and greigite. *Geochimica et Cosmochimica Acta*, **220**, 367–384.

Picard A., Gartman A., Cosmidis J., Obst M., Vidoudez C., Clarke D.R. and Girguis P.R. (2019) Authigenic metastable iron sulfide minerals preserve microbial organic carbon in anoxic environments. *Chemical Geology*, **530**, 119343.

Picard A., Gartman A. and Girguis P.R. (2021) Interactions between iron sulfide minerals and organic carbon: Implications for biosignature preservation and detection. *Astrobiology*, **21**, 587–604.

Planavsky N.J., McGoldrick P., Scott C.T., Li C., Reinhard C.T., Kelly A.E., Chu X., Bekker A., Love G.D. and Lyons T.W. (2011) Widespread iron-rich conditions in the mid-Proterozoic ocean. *Nature*, **477**, 448–451.

Pósfai M., Buseck P.R., Bazylinski D.A. and Franke R.B. (1998) Iron sulfides from magnetotactic bacteria: Structure, composition, and phase transitions. *American Mineralogist*, **83**, 1469–1481.

Pósfai M. and Dunin-Borkowski R.E. (2006) Sulfides in Biosystems. *Reviews in Mineralogy & Geochemistry*, **61**, 679–714.

Poulton S. and Canfield D. (2005) Development of a sequential extraction procedure for iron: Implications for iron partitioning in continentally derived particulates. *Chemical Geology*, **214**, 209–221.

Poulton S., Fralick P. and Canfield D. (2004a) The transition to a sulphidic ocean∼ 1.84 billion years ago. *Nature*, **431**, 173–177.

Poulton S.W., Krom M.D. and Raiswell R. (2004b) A revised scheme for the reactivity of iron (oxyhydr)oxide minerals towards dissolved sulfide. *Geochimica et Cosmochimica Acta*, **68**, 3703–3715.

Poulton S.W. (2021) The Iron Speciation Paleoredox Proxy. Elements in Geochemical Tracers in Earth System Science,. Cambridge University Press, UK.

Preiner M., Igarashi K., Muchowska K.B., Yu M., Varma S.J., Kleinermanns K., Nobu M.K., Kamagata Y., Tüysüz H., Moran J. and Martin W.F. (2020) A hydrogen-dependent geochemical analogue of primordial carbon and energy metabolism. *Nature Ecology & Evolution*, **4**, 534–542.

Quevedo C.P., Jiménez-Millán J., Cifuentes G.R., Gálvez A., Castellanos-Rozo J. and Jiménez-Espinosa R. (2021) The Potential Role of S-and Fe-Cycling Bacteria on the Formation of Fe-Bearing Mineral (Pyrite and Vivianite) in Alluvial Sediments from the Upper Chicamocha River Basin, Colombia. *Minerals*, **11**, 1148.

Raiswell R. (1982) Pyrite texture, isotopic composition and the availability of iron. *American Journal of Science*, **282**, 1244–1263.

Raiswell R. and Canfield D.E. (1996) Rates of reaction between silicate iron and dissolved sulfide in Peru Margin sediments. *Geochimica et Cosmochimica Acta*, **60**, 2777–2787.

Raiswell R. and Canfield D.E. (1998) Sources of iron for pyrite formation in marine sediments. *American Journal of Science*, **298**, 219–245.

Raiswell R. and Canfield D.E. (2012) The iron biogeochemical cycle past and present. *Geochemical Perspectives*, **1**, 1–232.

Raiswell R., Hardisty D.S., Lyons T.W., Canfield D.E., Owens J.D., Planavsky N. J., Poulton S.W. and Reinhard C.T. (2018) The iron paleoredox proxies: A guide to the pitfalls., problems and proper practice. *American Journal of Science*, **318**, 491–526.

Rasheed P.A., Jabbar K.A., Rasool K., Pandey R.P., Sliem M.H., Helal M., Samara A., Abdullah A.M. and Mahmoud K.A. (2019) Controlling the Biocorrosion of Sulfate-Reducing Bacteria (SRB) on Carbon Steel Using ZnO/Chitosan Nanocomposite as an Eco-Friendly Biocide. *Corrosion Science*, **148**, 397–406.

Raven M.R., Fike D.A., Gomes M.L., Webb S.M., Bradley A.S. and McClelland H.L.O. (2018) Organic carbon burial during OAE2 driven by changes in the locus of organic matter sulfurization. *Nature Communications*, **9**, 3409.

Reed N.W., Wing B.A., Tolbert M.A. and Browne E.C. (2022) Trace H_2S promotes organic aerosol production and organosulfur compound formation in Archean analog haze photochemistry experiments. *Geophysical Research Letters*, **49**, e2021GL097032.

Rickard D. (1969a) The microbiological formation of iron sulphides. *Stockholm contributions in geology*, **20**, 49–66.

Rickard D. (1969b) The Chemistry of Iron Sulphide Formation at Low Temperatures. *Stockholm Contributions to Geology*, **20**, 67–95.

Rickard D. (1975) Kinetics and mechanism of pyrite formation at low temperatures. *American Journal of Science*, **275**, 636–652.

Rickard D. (1995) Kinetics of FeS precipitation: Part 1. Competing reaction mechanisms. *Geochimica et Cosmochimica Acta*, **59**, 4367–4379.

Rickard D. (2012a) Chapter 15 - The geochemistry of sulfidic sedimentary rocks. Pp. 685–766 in: *Sulfidic Sediments and Sedimentary Rocks*, (David Rickard, editor) (D. Rickard, editor). Elsevier., Oxford, UK.

Rickard D. (2012b) Chapter 5 - Metastable sedimentary iron sulfides. Pp. 233–285 in: *Sulfidic Sediments and Sedimentary Rocks*,. Elsevier., Oxford, UK.

Rickard D. (2012c) Chapter 6 - Sedimentary Pyrite. Pp. 233–285 in: *Sulfidic Sediments and Sedimentary Rocks*, (D. Rickard, editor). Elsevier, Oxford, UK.

Rickard D. (1997) Kinetics of pyrite formation by the H_2S oxidation of iron (II) monosulfide in aqueous solutions between 25 and 125°C: The rate equation. *Geochimica et Cosmochimica Acta*, **61**, 115–134.

Rickard D. (2015) *Pyrite: a natural history of fool's gold*,. Oxford University Press, New York.

Rickard D. (2019) How long does it take a pyrite framboid to form? *Earth and Planetary Science Letters*, **513**, 64–68.

Rickard D. (2024) The composition of mackinawite. *American Mineralogist*, **109**, 401–407.

Rickard D., Butler I.B. and Oldroyd A. (2001) A novel iron sulphide mineral switch and its implications for earth and planetary science. *Earth and Planetary Science Letters*, **189**, 85–91.

https://doi.org/10.1180/gbi.2024.9 Published online by Cambridge University Press

Rickard D., Griffith A., Oldroyd A., Butler I.B., Lopez-Capel E., Manning D.A.C. and Apperley D.C. (2006) The composition of nanoparticulate mackinawite, tetragonal iron(II) monosulfide. *Chemical Geology*, **235**, 286–298.

Rickard D., Grimes S., Butler I., Oldroyd A. and Davies K.L. (2007) Botanical constraints on pyrite formation. *Chemical Geology*, **236**, 228–246.

Rickard D. and Luther G.W. (1997) Kinetics of pyrite formation by the H_2S oxidation of iron (II) monosulfide in aqueous solutions between 25 and 125°C: The mechanism. *Geochimica et Cosmochimica Acta*, **61**, 135–147.

Rickard D. and Luther G.W. (2007) Chemistry of iron sulfides. *Chemical Reviews*, **107**, 514–562.

Rickard D. and Morse J.W. (2005) Acid volatile sulfide (AVS). *Marine Chemistry*, **97**, 141–197.

Rickard D., Mussmann M., Steadman J.A. (2017) Sedimentary Sulfides. *Elements*, **13**, 117–122.

Roberts A.P., Chang L., Rowan C.J., Horng C-S. and Florindo F. (2011) Magnetic properties of sedimentary greigite (Fe_3S_4): An update. *Reviews of Geophysics*, **49**, RG1002.

Rolison J.M., Stirling C.H., Middag R., Gault-Ringold M., George E. and Rijkenberg M.J.A. (2018) Iron isotope fractionation during pyrite formation in a sulfidic Precambrian ocean analogue. *Earth and Planetary Science Letters*, **488**, 1–13.

Rothe M., Kleeberg A. and Hupfer M. (2016) The occurrence, identification and environmental relevance of vivianite in waterlogged soils and aquatic sediments. *Earth-Science Reviews*, **158**, 51–64.

Rouxel OJ., Bekker A. and Edwards K.J. (2005) Iron isotope constraints on the Archean and Paleproterozoic ocean redox state. *Science*, **307**, 1088–1091.

Rudnicki M., Elderfield H. and Spiro B. (2001) Fractionation of sulfur isotopes during bacterial sulfate reduction in deep ocean sediments at elevated temperatures. *Geochimica et Cosmochimica Acta*, **65**, 777–789.

Runge E., Mansor M., Chiu T.H., Shuster J., Fischer S., Kappler A. and Duda J-P. (2024) Hydrothermal sulfidation of biogenic magnetite produces framboid-like pyrite. *Communications Earth & Environment*, **5**, 252.

Runge E.A., Mansor M., Shuster J., Fischer S., Liu Y, Lunter D.J., Kappler A. and Duda JP. (2023) Sulfidation of nano-magnetite to pyrite: Implications for interpreting paleoenvironmental proxies and biosignature records in hydrothermal sulfide deposits. *Earth and Planetary Science Letters*, **617**, 118261.

Russell M., Hall A. and Martin W. (2010) Serpentinization as a source of energy at the origin of life. *Geobiology*, **8**, 355–371.

Russell M.J., Barge L.M., Bhartia R., Bocanegra D., Bracher P.J., Branscomb E., Kidd R., McGlynn S., Meier D.H., Nitschke W., Shibuya T., Vance S., White L. and Kanik I. (2014) The Drive to Life on Wet and Icy Worlds. *Astrobiology*, **14**, 308–343.

Russell M.J. and Hall A.J. (1997) The emergence of life from iron monosulphide bubbles at a submarine hydrothermal redox and pH front. *Journal of the Geological Society*, **154**, 377–402.

Ruvalcaba Baroni I., Palastanga V. and Slomp C.P. (2020) Enhanced Organic Carbon Burial in Sediments of Oxygen Minimum Zones Upon Ocean Deoxygenation. *Frontiers in Marine Science*, **6**, 481325.

Sánchez-Andrea I., Knittel K., Amann R., Amils R. and Sanz J.L. (2012) Quantification of Tinto river sediment microbial communities: Importance of sulfate-reducing bacteria and their role in attenuating acid mine drainage. *Applied and Environmental Microbiology*, **78**, 4638–4645.

Sanz-Montero MER-A. and Pablo Pérez-Soba C. (2009) Microbial weathering of Fe-rich phyllosilicates and formation of pyrite in the dolomite precipitating environment of a Miocene lacustrine system. *European Journal of Mineralogy*, **21**, 163–175.

Saunders J.A., Lee M-K., Dhakal P., Ghandehari S.S., Wilson T., Billor M.Z. and Uddin A. (2018) Bioremediation of Arsenic-Contaminated Groundwater by Sequestration of Arsenic in Biogenic Pyrite. *Applied Geochemistry*, **96**, 233–243.

Scholten L., Schmidt C., Lecumberri-Sanchez P., Newville M., Lanzirotti A., Sirbescu M.L.C. and Steele-MacInnis M. (2019) Solubility and speciation of iron in hydrothermal fluids. *Geochimica et Cosmochimica Acta*, **252**, 126–143.

Scholz F., Severmann S., McManus J., Noffke A., Lomnitz U. and Hensen C. (2014) On the isotope composition of reactive iron in marine sediments: Redox shuttle versus early diagenesis. *Chemical Geology*, **389**, 48–59.

Schoonen M.A. (2004) Mechanisms of sedimentary pyrite formation. *Geological Society of America Special Paper*, **379**, 117–134.

Schoonen M.A. and Barnes H.L. (1991) Reactions forming pyrite and marcasite from solution: II. Via FeS precursors below 100°C. *Geochimica et Cosmochimica Acta*, **55**, 1505–1514.

Schreiner E., Nair N.N., Wittekindt C. and Marx D. (2011) Peptide synthesis in aqueous environments: The role of extreme conditions and pyrite mineral surfaces on formation and hydrolysis of peptides. *Journal of the American Chemical Society*, **133**, 8216–8226.

Schütze E., Gypser S. and Freese D. (2020) Kinetics of phosphorus release from vivianite, hydroxyapatite, and bone char influenced by organic and inorganic compounds. *Soil Systems*, **4**, 1–20.

Schwarzenbach G. and Fischer A. (1960) Die Acidität der Sulfane und die Zusammensetzung wässeriger Polysulfidlösungen. *Helvetica Chimica Acta*, **43**, 1365–1390.

Schwertmann U. and Cornell R.M. (2000) *Iron oxides in the laboratory: Preparation and characterization*, 2nd ed. Wiley-VCH, Weinheim.

Senarmont D. (1851) Experience sur la formation des mineraux par voie humide dans lea gites metalliferes coneretionnes. *Annales de Chimie et Physique, Troisième Séries*, 129–175.

Severmann S., Lyons T.W., Anbar A., McManus J. and Gordon G. (2008) Modern iron isotope perspective on the benthic iron shuttle and the redox evolution of ancient oceans. *Geology*, **36**, 487–490.

Sharma V., Yan R., Feng X., Xu J., Pan M., Kong L. and Li L. (2024) Removal of toxic metals using iron sulfide particles: A brief overview of modifications and mechanisms. *Chemosphere*, **346**, 140631.

Shen Y and Buick R. (2004) The antiquity of microbial sulfate reduction. *Earth-Science Reviews*, **64**, 243–272.

Shumway S., Wilson J., Lilova K., Subramani T., Navrotsky A. and Woodfield B. (2022) The low-temperature heat capacity and thermodynamic properties of greigite (Fe_3S_4). *The Journal of Chemical Thermodynamics*, **173**, 106836.

Shuster J., Reith F. and Southam G. (2019) Applications of Transmission Electron Microscopy in Geomicrobiology. Pp. 166–186 in: *Analytical Geomicrobiology: A Handbook of Instrumental Techniques*, (Janice P. L. Kenney, Harish Veeramani, Daniel S, Alessi, editors). Cambridge University Press.

Sievert S.M., Wieringa E.B.A., Wirsen C.O. and Taylor C.D. (2007) Growth and mechanism of filamentous-sulfur formation by *Candidatus* Arcobacter sulfidicus in opposing oxygen-sulfide gradients. *Environmental Microbiology*, **9**, 271–276.

Sim M.S., Bosak T. and Ono S. (2011a) Large sulfur isotope fractionation does not require disproportionation. *Science (New York, N.Y.)*, **333**, 74–77.

Sim M.S., Ono S., Donovan K., Templer S.P. and Bosak T. (2011b) Effect of electron donors on the fractionation of sulfur isotopes by a marine *Desulfovibrio* sp. *Geochimica et Cosmochimica Acta*, **75**, 4244–4259.

Sim M.S., Ono S. and Bosak T. (2012) Effects of iron and nitrogen limitation on sulfur isotope fractionation during microbial sulfate reduction. *Applied and Environmental Microbiology*, **78**, 8368–8376.

Skinner B., Erd R. and Grimaldi F. (1964) Greigite, the thio-spinel of iron; A new mineral. *American Mineralogist: Journal of Earth and Planetary Materials*, **49**, 543–555.

Sklute E.C., Kashyap S., Dyar M.D., Holden J.F., Tague T., Wang P. and Jaret S.J. (2018) Spectral and morphological characteristics of synthetic nanophase iron (oxyhydr)oxides. *Physics and Chemistry of Minerals*, **45**, 1–26.

Slotznick S.P., Sperling E.A., Tosca N.J., Miller A.J., Clayton K.E., van Helmond N.A.G.M, Slomp C.P. and Swanson-Hysell N.L. (2020) Unraveling the mineralogical complexity of sediment iron speciation using sequential extractions. *Geochemistry, Geophysics, Geosystems*, **21**, e2019GC008666.

Smith D.A., Fike D.A., Johnston D.T. and Bradley A.S. (2020) Isotopic fractionation associated with sulfate import and activation by *Desulfovibrio vulgaris* str. Hildenborough. *Frontiers in Microbiology*, **11**, 529317.

Smith P., Evensen N., York D. and Moorbath S. (2005) Oldest reliable terrestrial 40Ar-39Ar age from pyrite crystals at Isua west Greenland. *Geophysical research letters*, **32**, 1–4.

Sojo V., Herschy B., Whicher A., Camprubí E. and Lane N. (2016) The Origin of Life in Alkaline Hydrothermal Vents. *Astrobiology*, **16**, 181–197.

Son S., Hyun S.P., Charlet L. and Kwon K.D. (2022) Thermodynamic stability reversal of iron sulfides at the nanoscale: Insights into the iron sulfide formation in low-temperature aqueous solution. *Geochimica et Cosmochimica Acta*, **338**, 220–228.

https://doi.org/10.1180/gbi.2024.9 Published online by Cambridge University Press

Song H., Wignall P.B., Chu D., Tong J., Sun Y, Song H., He W. and Tian L. (2014) Anoxia/high temperature double whammy during the Permian-Triassic marine crisis and its aftermath. *Scientific Reports*, **4**, 4132.

Stanley W. and Southam G. (2018) The effect of gram-positive (*Desulfosporosinus orientis*) and gram-negative (*Desulfovibrio desulfuricans*) sulfate-reducing bacteria on iron sulfide mineral precipitation. *Canadian Journal of Microbiology*, **64**, 629–637.

Stetter K.O., König H. and Stackebrandt E. (1983) *Pyrodictium* gen. nov., a new genus of submarine disc-shaped sulphur reducing archaebacteria growing optimally at 105°C. *Systematic and Applied Microbiology*, **4**, 535–551.

Steudel R. (2003) *Elemental sulfur and sulfur-rich compounds I and II*, (Ralf Steudel, editor). Springer Science & Business Media, Berlin, Heidelberg.

Subramani T., Lilova K., Abramchuk M., Leinenweber K.D. and Navrotsky A. (2020) Greigite (Fe_3S_4) is thermodynamically stable: Implications for its terrestrial and planetary occurrence. *Proceedings of the National Academy of Sciences*, **117**, 28645–28648.

Sun J., Feng Y, Zheng R., Kong L., Wu X., Zhang K., Zhou J. and Liu S. (2023) Chameleon-like anammox bacteria for surface color change after suffering starvation. *Environmental Science and Technology*,. **57**, 15087–15098.

Swanner E.D., Webb S.M. and Kappler A. (2019) Fate of cobalt and nickel in mackinawite during diagenetic pyrite formation. *American Mineralogist*, **104**, 917–928.

Sweeney R.E. and Kaplan I.R. (1973) Pyrite framboid formation: Laboratory synthesis and marine sediments. *Economic Geology*, **68**, 618–634.

Takai K., Komatsu T., Horikoshi K. (2001) Distribution of archaea in a black smoker chimney structure. *Applied and Environmental Microbiology*, **67**, 3618–3629.

Taylor P., Rummery T.E. and Owen D.G. (1979) Reactions of Iron Monosulfide Solids with Aqueous Hydrogen Sulfide up to 160°C. *Journal of Inorganic and Nuclear Chemistry*, **41**, 1683–1687.

Tétrault A. and Gélinas Y. (2022) Preferential sorption of polysaccharides on mackinawite: A chemometrics approach. *Geochimica et Cosmochimica Acta*, **337**, 61–72.

Thamdrup B., Finster K., Hansen J.W. and Bak F. (1993) Bacterial disproportionation of elemental sulfur coupled to chemical reduction of iron or manganese. *Applied and Environmental Microbiology*, **59**, 101–108.

Thiel J., Byrne J.M., Kappler A., Schink B. and Pester M. (2019) Pyrite formation from FeS and H_2S is mediated through microbial redox activity. *Proceedings of the National Academy of Sciences*, **116**, 6897–6902.

ThomasArrigo L.K., Bouchet S., Kaegi R. and Kretzschmar R. (2020) Organic matter influences transformation products of ferrihydrite exposed to sulfide. *Environmental Science: Nano*, **7**, 3405–3418.

Tivey M. and Delaney J. (1986) Growth of large sulfide structures on the Endeavour Segment of the Juan de Fuca Ridge. *Earth and Planetary Science Letters*, **77**, 303–317.

Tivey M.K. (2007) Generation of seafloor hydrothermal vent fluids and associated mineral deposits. *Source: Oceanography*, **20**, 50–65.

Toner B.M., Rouxel O.J., Santelli C.M., Bach W. and Edwards K.J. (2016) Iron transformation pathways and redox micro-environments in seafloor sulfide-mineral deposits: Spatially resolved Fe XAS and $\delta^{57/54}$Fe observations. *Frontiers in Microbiology*, **7**, 1–17.

Tribovillard N., Algeo T.J., Lyons T. and Riboulleau A. (2006) Trace metals as paleoredox and paleoproductivity proxies: An update. *Chemical Geology*, **232**, 12–32.

Tribovillard N., Bout-Roumazeilles V., Delattre M., Ventalon S. and Bensadok A. (2022) Sedimentary pyrite as a trap of organic matter: preliminary results from large-framboid observation. *European Journal of Mineralogy*, **34**, 77–83.

Truong C., Bernard S., Baudin F., Gorlas A. and Guyot F. (2024) Carbon-containing pyrite spherules: mineral biosignatures in black smokers? *European Journal of Mineralogy*, **36**, 813–830.

Truong C., Bernard S., Le Pape P., Morin G., Baya C., Merrot P., Gorlas A. and Guyot F. (2023) Production of carbon-containing pyrite spherules induced by hyperthermophilic *Thermococcales*: a biosignature? *Frontiers in Microbiology*, **14**, 1145781.

Tsyrenova D.D., Barkhutova D.D., Buryukhaev S.P., Lazareva E.V., Bryanskaya A.V. and Zamana L.V. (2018) Cyanobacterial diversity and the role of cyanobacteria in formation of minerals in the Baunt Group Hydrotherms (Baikal Rift Zone). *Microbiology (Russian Federation)*, **87**, 508–518.

Turney J.N., Weiss D., Muxworthy A.R. and Fraser A. (2023) Greigite formation in aqueous solutions: Critical constraints into the role of iron and sulphur ratios, pH and Eh, and temperature using reaction pathway modelling. *Chemical Geology*, **635**, 121618.

Unruh D.K. and Forbes T.Z. (2019) X-ray Diffraction Techniques. In: *Analytical Geomicrobiology: A Handbook of Instrumental Techniques*, (Janice P. L. Kenney, Harish Veeramani, Daniel S. Alessi, editors), University Press.

Vargas M., Kashefi K., Blunt-Harris E.L. and Lovley D.R. (1998) Microbiological evidence for Fe(III) reduction on early Earth. *Nature*, **395**, 65–67.

Varma S.J., Muchowska K.B., Chatelain P. and Moran J. (2018) Native iron reduces CO_2 to intermediates and end-products of the acetyl-CoA pathway. *Nature Ecology & Evolution*, **2**, 1019–1024.

Wacey D., Kilburn M.R., Saunders M., Cliff J. and Brasier M.D. (2011) Microfossils of sulphur-metabolizing cells in 3.4-billion-year-old rocks of Western Australia. *Nature Geoscience*, **4**, 698–702.

Wächtershäuser G. (1988) Pyrite formation, the first energy source for life: A hypothesis. *Systematic and Applied Microbiology*, **10**, 207–210.

Wächtershäuser G. (1992) Groundworks for an Evolutionary Biochemistry: The Iron-Sulphur World. *Progress in Biophysics and Molecular Biology*, **58**, 85–201.

Wadia C., Alivisatos A.P. and Kammen D.M. (2009) Materials availability expands the opportunity for large-scale photovoltaics deployment. *Environmental Science and Technology*, **43**, 2072–2077.

Wan M., Schröder C. and Peiffer S. (2017) Fe(III):S(-II) concentration ratio controls the pathway and the kinetics of pyrite formation during sulfidation of ferric hydroxides. *Geochimica et Cosmochimica Acta*, **217**, 334–348.

Wang H.Y, Byrne J.M., Perez J.P.H., Thomas A.N., Göttlicher J., Höfer H.E., Mayanna S., Kontny A., Kappler A., Guo H.M., Benning L.G. and Norra S. (2020) Arsenic sequestration in pyrite and greigite in the buried peat of As-contaminated aquifers. *Geochimica et Cosmochimica Acta*, **284**, 107–119.

Wang Q. and Morse J.W. (1996) Pyrite formation under conditions approximating those in anoxic sediments I. *Pathway and morphology.* Marine Chemistry, **52**, 99–121.

Wang Q., Wang J., Wang X., Kumar N., Pan Z., Peiffer S. and Wang Z. (2023) Transformations of ferrihydrite-extracellular polymeric substance coprecipitates driven by dissolved sulfide: interrelated effects of carbon and sulfur loadings. *Environmental Science and Technology*, **57**, 4342–4353.

Wang S., Shen J., Du B., Xu K., Zhang Z. and Liu C. (2021) The relationship between natural pyrite and impurity element semiconductor properties: A case study of vein pyrite from the Zaozigou gold deposit in China. *Minerals*, **11**, 596.

Wang Y, Zhang Z., Han L., Sun K., Jin J., Yang Y, Yang Y, Hao Z., Liu J. and Xing B. (2019) Preferential molecular fractionation of dissolved organic matter by iron minerals with different oxidation states. *Chemical Geology*, **520**, 69–76.

Wei C., Yin S., Kappler A., Tao S. and Zhu D. (2023) A new pathway for pyrite formation in low-sulfate sediments driven by mineralization of reduced organic sulfur. *Fundamental Research*,.

Wei D. and Osseo-Asare K. (1997) Aqueous synthesis of finely divided pyrite particles. *Colloids and Surfaces A: Physicochemical and Engineering Aspects*, **121**, 27–36.

Welch S.A., Beard B.L., Johnson C.M. and Braterman P.S. (2003) Kinetic and equilibrium Fe isotope fractionation between aqueous Fe(II) and Fe(III). *Geochimica et Cosmochimica Acta*, **67**, 4231–4250.

Wikjord A., Rummery T. and Doern F. (1976) Crystallization of pyrite from deoxygenated aqueous sulfide solutions at elevated temperature and pressure. *The Canadian Mineralogist*, **14**, 571–573

Wikjord A.G., Rummery TE., Doern F.E. and Owen D.G. (1980) Corrosion and deposition during the exposure of carbon steel to hydrogen sulphide-water solutions. *Corrosion Science*, **20**, 651–671.

Wilkin R.T. and Barnes H.L. (1996) Pyrite formation by reactions of iron monosulfides with dissolved inorganic and organic sulfur species. *Geochimica et Cosmochimica Acta*, **60**, 4167–4179.

Wilkin R.T. and Barnes H.L. (1997) Formation processes of framboidal pyrite. *Geochimica et Cosmochimica Acta*, **61**, 323–339.

Wing B.A. and Halevy I. (2014) Intracellular metabolite levels shape sulfur isotope fractionation during microbial sulfate respiration. *PNAS*, **111**, 18116–18125.

https://doi.org/10.1180/gbi.2024.9 Published online by Cambridge University Press

Wirsen C.O., Sievert S.M., Cavanaugh C.M., Molyneaux S.J., Ahmad A., Taylor L.T., DeLong E.F. and Taylor C.D. (2002) Characterization of an autotrophic sulfide-oxidizing marine *Arcobacter* sp. that produces filamentous sulfur. *Applied and Environmental Microbiology*, **68**, 316–325.

Wolthers M., Van der Gaast S.J. and Rickard D. (2003) The structure of disordered mackinawite. *American Mineralogist*, **88**, 2007–2015.

Wortmann U., Bernasconi S. and Böttcher M. (2001) Hypersulfidic deep biosphere indicates extreme sulfur isotope fractionation during single-step microbial sulfate reduction. *Geology*, **29**, 647–650.

Wu B., Liu F., Fang W., Yang T., Chen G., He Z. and Wang S. (2021) Microbial sulfur metabolism and environmental implications. *Science of The Total Environment*, **778**, 146085.

Wu L., Druschel G., Findlay A., Beard B.L. and Johnson C.M. (2012) Experimental determination of iron isotope fractionations among Feaq2^{+}–FeSaq–Mackinawite at low temperatures: Implications for the rock record. *Geochimica et Cosmochimica Acta*, **89**, 46–61.

Wu N., Farquhar J., Strauss H., Kim S.T. and Canfield D.E. (2010) Evaluating the S-isotope fractionation associated with Phanerozoic pyrite burial. *Geochimica et Cosmochimica Acta*, **74**, 2053–2071.

Wu Z., Zhang T., Lanson B., Yin H., Cheng D., Liu P. and He F. (2023) Sulfidation of Ni-bearing goethites to pyrite: The effects of Ni and implications for its migration between iron phases. *Geochimica et Cosmochimica Acta*, **353**, 158–170.

Yan R., Kappler A., Muehe E.M., Knorr K-H., Horn M.A., Poser A., Lohmayer R. and Peiffer S. (2019) Effect of reduced sulfur species on chemolithoautotrophic pyrite oxidation with nitrate. *Geomicrobiology Journal*, **36**, 19–29.

Yang Y, Chen T., Sumona M., Gupta B.S., Sun Y., Hu Z. and Zhan X. (2017) Utilization of iron sulfides for wastewater treatment: A critical review. *Reviews in Environmental Science and Bio/Technology 2017*, **16**, 289–308.

Yang Y, Cheng T. and Zhou G. (2023) Effect of Sulfate-Reducing Bacteria on the Production of Iron Sulfides. *Geomicrobiology Journal*, **40**, 247–254.

Ye L. and Jing C. (2022) Iron(III) reducing bacteria immobilise antimonite by respiring elemental sulfur. *Geochemical Perspectives Letters*, **21**, 37–41.

Young E., Galy A. and Nagahara H. (2002) Kinetic and equilibrium mass-dependent isotope fractionation laws in nature and their geochemical and cosmochemical significance. *Geochimica et Cosmochimica Acta*, **66**, 1095–1104.

Zaka A., Alhassan S.M. and Nayfeh A. (2022) Iron pyrite in photovoltaics: A review on recent trends and challenges. *ACS Applied Electronic Materials*, **4**, 4173–4211.

Zerkle A.L., Farquhar J., Johnston D.T., Cox R.P. and Canfield D.E. (2009) Fractionation of multiple sulfur isotopes during phototrophic oxidation of sulfide and elemental sulfur by a green sulfur bacterium. *Geochimica et Cosmochimica Acta*, **73**, 291–306.

Zhang Y, Zhu Z., Liao Y.G., Dang Z. and Guo C. (2021) Effects of Fe(II) source on the formation and reduction rate of biosynthetic mackinawite: Biosynthesis process and removal of Cr(VI). *Chemical Engineering Journal*, **421**, 129723.

Zhou C., Vannela R., Hayes K.F. and Rittmann B.E. (2014) Effect of growth conditions on microbial activity and iron-sulfide production by *Desulfovibrio vulgaris*. *Journal of Hazardous Materials*, **272**, 28–35.

Zhou L., Liu J. and Dong F. (2017) Spectroscopic study on biological mackinawite (FeS) synthesized by ferric reducing bacteria (FRB) and sulfate reducing bacteria (SRB): Implications for in-situ remediation of acid mine drainage. *Spectrochimica Acta Part A: Molecular and Biomolecular Spectroscopy*, **173**, 544–548.

Zhou Y, Gao Y, Xie Q., Wang J., Yue Z., Wei L., Yang Y, Li L. and Chen T. (2019) Reduction and transformation of nanomagnetite and nanomaghemite by a sulfate-reducing bacterium. *Geochimica et Cosmochimica Acta*, **256**, 66–81.

Zhu F., Huang Y, Ni H., Tang J., Zhu Q., Long-er L. and Zou L. (2022) Biogenic iron sulfide functioning as electron-mediating interface to accelerate dissimilatory ferrihydrite reduction by *Shewanella oneidensis* MR-1. *Chemosphere*, **288**, 132661.

Zopfi J., Böttcher M.E. and Jørgensen B.B. (2008) Biogeochemistry of sulfur and iron in *Thioploca*-colonized surface sediments in the upwelling area off central Chile. *Geochimica et Cosmochimica Acta*, **72**, 827–843.

Zopfi J., Ferdelman T.G. and Fossing H. (2004) Distribution and fate of sulfur intermediates - sulfite, tetrathionate, thiosulfate, and elemental sulfur - in marine sediments. *Geological Society of America*, **379**, 97–116.

https://doi.org/10.1180/gbi.2024.9 Published online by Cambridge University Press